UNIVERSITY OF OKLAHOMA

GRADUATE COLLEGE

THERMAL EXPANSION COEFFICIENT INVESTIGATIONS IN OILWELL CEMENTS AND VARIOUS MATERIALS USING A UNIQUE EXPERIMENTAL SETUP

A THESIS

SUBMITTED TO THE GRADUATE FACULTY

in partial fulfillment of the requirements for the

Degree of

MASTER OF SCIENCE

By

ALBERTO TOLEDO VELAZCO

Norman, Oklahoma

2024

Downloaded from SHAREOK. Persistent Handle URL: https://hdl.handle.net/11244/340502

THERMAL EXPANSION COEFFICIENT INVESTIGATIONS IN OILWELL CEMENTS AND VARIOUS MATERIALS USING A UNIQUE EXPERIMENTAL SETUP

A THESIS APPROVED FOR THE

MEWBOURNE SCHOOL OF PETROLEUM AND GEOLOGICAL ENGINEERING

BY THE COMMITTEE CONSISTING OF

Dr. Catalin Teodoriu, Chair

Dr. Ramadan Ahmed

Dr. Ahmad Ghassemi

© Copyright by ALBERTO TOLEDO VELAZCO 2024

All Rights Reserved.

ACKNOWLEDGMENTS

This thesis represents the culmination of one of the most exciting journeys I have experienced in my life. And while I reminisce about the different situations that lead me here, I would like to dedicate a few verses to all the people who supported me and accompanied me throughout this ride.

First of all, I would like to express my deepest gratefulness to my advisor, Dr. Catalin Teodoriu. Nothing of this could have been possible without your help even before coming to OU. Thank you for guidance, your support and example during this past two years. Working and sharing tons of moments with you was something truly especial. I couldn't have asked for a better advisor.

To my parents, Miguel and Mireida. Thank you for being my first teachers, my first advisors, and my forever supporters. There are no words to express how thankful I am for having the best parents in the entire world, and for everything you have done for me. I love you and I will always try to make you proud. This is all yours.

To my siblings, Kristy and Leonardo. Thank you for your unconditional support and love, for always rooting for me and being there since we were born. I love you hermanitos. I feel blessed for having the best siblings on earth. This is also yours.

To my whole family in Mexico. Starting with my grandparents, Miguel and Cedalia and the ones who take care of me from a better place, Juan and Aurora. I hope I made you and our families honored. I would also like to thank all my aunts, uncles and cousins. Your love is everything.

To my friends in Mexico. From San Pedro to JMBP, from my elementary school to my university. To the lloristas. To all the people with whom I've shared minutes in my life. I would

take three pages mentioning all of your names, but you already know who you are. Thank you for your presence even far away.

To my friends here in the US. From my Mexicanos to my internationals. From my buddies in STM to the friends I met at Sarkeys. Thank you to all of you who made my life in Norman easier and funnier. I wish for our friendship to be everlasting.

To all the people I have met here at OU, and have helped me during this journey. My research group, teachers, advisors and staff at MPGE. Special thanks to Mrs. Yoana Walschap, who was, from the beginning, a fundamental person in my entire process here. To Mrs. Katie Shapiro, who always helped me and answered all my questions and coffee requests. To Mr. Derrick Whitney who is always supportive with us as students, to Mr. Eric Powel, who helped me with the hard work. To Dr. Ramadan and Dr. Ghassemi, who were my thesis advisors; and to my brother Khizar, whose support and guidance have been fundamental in my degree. Thank you all for everything.

To Welltec, and all the people who I met during these past two years from that company. To Yosafat, Ricardo, Leonardo. Thank you for trusting in me, and continue doing it with all the opportunities provided. To the Department of Energy and all the people involved. Always grateful.

To Mr. Arcadio Penagos, Mr. Alfredo medina and Ms. Miranda Coss, who believed in me ever since my undergrad. Thank you for introducing me to the exciting world of oil and gas. We are always #teampetro.

Last, but not least, to the reason of everything: **God**. You are the One and Only, the Beginning and the End. You make everything new. I am where I am because of you. I am who I am because of you. Always thankful with You.

Mex I can Boomer Sooner!

TABLE OF CONTENTS

ACKNOWLEDGMENTS IV

LIST OF FIGURES X

LIST OF TABLES XIV

LIST OF EQUATIONS XV

ABSTRACT XVI

CHAPTER 1. INTRODUCTION 1

1.1 PROBLEM STATEMENT 1

1.2 OBJECTIVES 4

1.2.1 Main objective 4

1.2.2 Specific objectives 4

1.3 SCOPE OF WORK 5

CHAPTER 2. LITERATURE REVIEW 6

2.1 GEOTHERMAL 6

2.1.1 Geothermal systems 7

2.1.2 Geothermal uses 7

2.2 WELL INTEGRITY 9

2.3 THERMAL EXPANSION 12

2.3.1 Coefficient of linear thermal expansion (CLTE) 13

2.3.2 Techniques used for measuring CLTE 14

2.3.2.1 Dilatometry 15

2.3.2.2 Thermomechanical analysis 24
2.3.2.3 Interferometry (optical interference) 28
2.3.3 Other techniques used for measuring CLTE 32
2.3.3.1 Diffraction 33
2.3.3.2 Fused-quartz tube 36
2.3.3 Measurements of CLTE 37
CHAPTER 3. EXPERIMENTAL APPARATUS 43
3.1 NOVEL EXPERIMENTAL APPARATUS 43
3.1.1 Micrometer and laser beams 44
3.1.2 Heat controller 45
3.1.3 Aluminum block 47
3.1.4 Sample 48
3.1.5 Thermometer 49
3.1.6 Data acquisition system 50
3.2 APPARATUS OVERVIEW 51
3.2.1 Advantages 51
3.2.2 Limitations 51
CHAPTER 4. METHODOLOGY 53
4.1 CALIBRATION 54
4.1.1 Accuracy of the equipment – Calibration 55
4.1.2 Aluminum – Calibration 57
4.1.3 Brass – Calibration 57
4.2 PLACEMENT OF THE SAMPLE 59

4.3 SETTING THE TEMPERATURE 59
4.4 MEASUREMENTS 61
4.5 CLTE CALCULATIONS 62
4.6 CYCLIC VS NON-CYCLIC TEST 62
CHAPTER 5. RESULTS 65
5.1 METALS AND DIFFERENT MATERIALS 65
5.1.1 Brass 65
5.1.2 Aluminum 66
5.1.3 Steel 67
5.1.4 Titanium 68
5.1.5 Carbon Steel (A36) 69
5.1.6 Stainless Steel (304) 70
5.1.7 Glass Fiber 71
5.2 ROCKS 72
5.2.1 Sandstone 73
5.2.2 Granite 74
5.2.3 Bandera Sandstone 75
5.2.4 Carbonate 76
5.3 CEMENT COMPOSITES 77
5.3.1 Overview 77
5.3.1.1 Class H + 10% Gilsonite 78
5.3.1.2 Class H + 10% Sand 79
5.3.1.3 Class G + 5% Sand 80

5.3.2 No-cyclic test 81

5.3.2.1 Class G (28 days curing + 7 days dry) 81

5.3.2.2 Class H (28 days curing + 7 days dry) 82

5.3.2.3 Class C (28 days curing + 7 days dry) 83

5.3.2.4 Class G + 40% Silica (28 days curing + 7 days dry) 84

5.3.3 One-year curing time versus short curing time 85

5.3.3.1 Class H cement – 14 days curing time 86

5.3.3.2 Class H cement – one-year curing time 87

5.3.3.3 Class G + 10% MB cement – 21 days curing time 88

5.3.3.4 Class G + 10% MB cement – one-year curing time 89

5.3.4 Long-term curing time 90

5.3.4.1 Class C cement – three-years curing time 91

5.3.4.2 Class 50% C + 50% H cement – three-years curing time 91

5.3.4.3 Class C + 10% Bentonite cement – three-years curing time 92

CHAPTER 6. DISCUSSIONS 94

CHAPTER 7. CONCLUSIONS 116

REFERENCES 119

LIST OF FIGURES

Figure 1: Energy consumption predicted by 2050 by end-use sector (AEO by EIA, 2023) ...2

Figure 2: Global energy markets throughout time (BP and Dale, 2022) 3

Figure 3:Schematic of a geothermal well for energy production 7

Figure 4: Range of geothermal temperatures and their applications (Abid et al., 2022, as cited from Dincer and Ezzat, 2018; Shapley, 2011 and Williams et al., 2008).....8

Figure 5: Operational time for geothermal well in Indonesia (Nugroho, 2017) 10

Figure 6: Dilatometers for thermal expansion measurements of different materials. (a) double push rod, (b) tube and a push rod, (c) differential with reference material, R. (James et al., 2001). 15

Figure 7: Silica dilatometer schematic according to ASTM E228. 17

Figure 8: Coefficient of linear thermal expansion process by using a silica dilatometer according to ASTM E228 18

Figure 9: Cross sectional schematic of the absolute dilatometer used in the experiment performed by Kroeger and Swenson (1977) 19

Figure 10: Thermal expansion apparatus according to Nelson and Guillot (2006).....20

Figure 11: Quartz dilatometer by Popov et al (2012), with 1 – temperature controller, 2 – furnace, 3 – vitreous silica specimen holding system and extensometers mounting block; 4 – lifting system 21

Figure 12: AASHTO-type device of the CTE test, according to Yang et al (2003).....23

Figure 13: Modified dilatometer used by Loiseau (2014).....24

Figure 14: Diagram of a thermomechanical analysis apparatus according to Corporation, H.H. (revised in 2024) 25

Figure 15: TMA apparatus probe types depending on the purpose 26

Figure 16: Thermomechanical analyzer according to ASTM E381 28

Figure 17: Typical arrangements of interferometers with their variations (James et al., 2001) 29

Figure 18: Two-fold interferometer by Okaji and Imai (1984) 31

Figure 19: Setup developed by Yogaswara and Eljabbar (2018), including the following: (a) trial set schematic, (b) experimental device arrangement in data collection, (c) video frames using Tracker software. 35

Figure 20: Formula used by Yogaswara and Eljabbar (2018) to calculate the CLTE 36

Figure 21: Fused-quartz tube expansion apparatus 37

Figure 22: Novel experimental apparatus developed at the Well Integrity Laboratory 44

Figure 23: Micrometer and laser beam used for length measurements 45

Figure 24: Heat controller used in the novel apparatus 46

Figure 25: Aluminum block from the experimental apparatus 47

Figure 26: Samples used during this experiment 48

Figure 27: Thermometer used to measure the temperature on the sample 49

Figure 28: Data acquisition system used in this investigation 50

Figure 29: Workflow performed during this investigation 53

Figure 30: CLTE of aluminum with error bars for accuracy – Calibration purposes 56

Figure 31: CLTE values for Aluminum – Calibration purposes 57

Figure 32: CLTE values for Brass – Calibration purposes 58

Figure 33: Temperatures with their distribution along the aluminum block and length of the sample versus time 60

Figure 34: Cyclic testing procedure for oilwell cements 63

Figure 35: Non-cyclic testing procedure for oilwell cements 63

Figure 36: CLTE values measured for Brass 66

Figure 37: CLTE values measured for Aluminum 67

Figure 38: CLTE values measured for Steel 68

Figure 39: CLTE values measured for Titanium 69

Figure 40: CLTE values measured for Carbon Steel 70

Figure 41: CLTE values measured for Stainless Steel 71

Figure 42: CLTE values measured for Glass Fiber 72

Figure 43: CLTE values measured for Sandstone 74

Figure 44: CLTE values measured for Granite 75

Figure 45: CLTE values measured for Bandera Sandstone 76

Figure 46: CLTE values measured for Carbonate 77

Figure 47: CLTE values measured for Class H + 10% Gilsonite 78

Figure 48: CLTE values measured for Class H + 10% Sand 79

Figure 49: CLTE values measured for Class G + 5% Sand 80

Figure 50: CLTE values measured for Class G (28 days curing time) – no cyclic testing 82

Figure 51 : CLTE values measured for Class H (28 days curing time) – no cyclic testing 83

Figure 52: CLTE values measured for Class C (28 days curing time) – no cyclic testing 84

Figure 53: CLTE values measured for Class G + 40% silica (28 days curing time) – no cyclic testing 85

Figure 54: CLTE values measured for Class H (14 days curing time) 87

Figure 55: CLTE values measured for Class H (one-year curing time) 88

Figure 56: CLTE values measured for Class G + 10% MB (21 days curing time) 89

Figure 57: CLTE values measured for Class G + 10% MB (one-year curing time) 90

Figure 58: CLTE values measured for Class C (three-years curing time) 91

Figure 59: CLTE values measured for Class 50% C + 50% H (three-years curing time)... 92

Figure 60: CLTE values measured for Class C + 10% Bentonite (three-years curing time) 93

Figure 61: CLTE comparison of all metallic and non-metallic elements tested with the novel apparatus..... 97

Figure 62: CLTE comparison of rocks tested with the novel apparatus 100

Figure 63: CLTE comparison of short curing time vs long curing time cement tested with the novel apparatus..... 104

Figure 64: CLTE values of samples depending on their curing time..... 105

Figure 65: CLTE values measured for oilwell cements cured for short time..... 106

Figure 66: CLTE values measured for metallic elements, cement and rock 107

Figure 67: Tangential stresses depending on the CLTE value of oilwell cement 112

Figure 68: Radial stresses depending on the CLTE value of oilwell cement 114

LIST OF TABLES

Table 1: Brief summary of CLTE values of different metallic elements found in diverse literature.....37

Table 2: Brief summary of CLTE values of different rocks found in diverse literature.....39

Table 3: Brief summary of CLTE values of different cement samples found in diverse literature.....41

Table 4: Comparison of CLTE values from literature and CLTE values measured with the novel equipment for metallic elements and non-metallic element with % of error.....95

Table 5: Comparison of CLTE values from literature and CLTE values measured with the novel equipment for rocks with % of error 98

Table 6: Comparison of CLTE values from literature and CLTE values measured with the novel equipment for cement composites with % of error.....101

Table 7: Input variables and values for stresses simulation, after Ugwu (2010).....108

LIST OF EQUATIONS

Equation 1: Linear thermal expansion 13

Equation 2: Coefficient of linear thermal expansion 14

Equation 3: Inner contact equation, recovered from Ugwu (2010) 110

Equation 4: Outer contact equation, recovered from Ugwu (2010) 111

Equation 5: Tangential stresses equation, recovered from Ugwu (2010) 111

Equation 6: Radial stresses equation, recovered from Ugwu (2010) 113

ABSTRACT

The energy demand is increasing around the globe, and while oil and gas continue to play a main part in the energy impact, renewables are taking place as important contributors. In addition to this, the net-zero policy by 2050 developed in the United States is leaning the efforts towards cleaner energies. In that respect, geothermal will play an important function due to the untapped resources and presence around the world. Geothermal, as well as oil and gas operations, comes with different operational challenges, such as depth, which makes subsurface conditions very aggressive with respect to temperature and pressure. Therefore, to successfully perform geothermal operations, the integrity of the well needs to be assured.

Casing and cement play a crucial role in terms of well integrity, as many studies have suggested. Moreover, the elevated temperatures in geothermal operations make thermal properties on these components a parameter of utmost importance, something not widely investigated in comparison with mechanical properties. Thermal expansion is a thermal property with an important impact in the integrity of the wells, which might be jeopardized due to the constant thermal loads effected in such operations. Effects in casing go up to the collapse of the tubular, while cement can suffer from micro-annuli, cracks or debonding.

This investigation focuses on the measurements of the coefficient of linear thermal expansion for oilwell cements, as well as other reference materials and rocks, with novel equipment developed in the Well Integrity Laboratory at The University of Oklahoma. This equipment, which uses an

optical shadowing technique, provides faster coefficient of linear thermal expansion calculations in contrast to other equipment or techniques.

More than 300 measurements were performed in this investigation, which includes diverse materials and rocks, are performed not just to corroborate the reliability on the equipment, but also to create a comparison between the coefficient of linear thermal expansions found in diverse literature. The experiments are performed at high temperatures up to 200 ºC (400 ºF), which simulate the extreme temperature conditions encountered in deeper downhole conditions for oil and gas, as well as in geothermal processes. Additionally, characterization of this thermal property is performed for oilwell cement composites, creating a unique database for different mixtures in which different recipes, including neat Class C, G and H cement, as well as other recipes with added additives are comprised. Moreover, other aspects such as cyclic tests or curing times, which go from 14 days to 3 years, are varied.

In conclusion, the results generated by this novel equipment provide reliable coefficient of linear thermal expansion values, when associating them with the values found in different studies. Additionally, the comparison in the coefficient of linear thermal expansion values performed for the different cement composites shows the effects of curing time and cyclic loading for the coefficient in linear thermal expansion on oilwell cements. Several discussions are made based on the experiments conducted in this research.

Chapter 1. INTRODUCTION

1.1 Problem statement

The population on earth is increasing and with it, the needs of meeting the energy requirements. Dudley (2017) has suggested that the expected population by 2035 will be around 8.8 billion, with energy demand increasing by 30%. United Nations, (2023), suggested that the population could increase up to 9.7. billion by 2050, reaching a peak of 10.4 billion in the mid-2080's.

Due to this reason, the energy demand is on the rise. AEO by EIA (2023) predicts an increment in energy consumption as shown in Figure 1, in which industrial section increases as much as 32%, whereas transportation sector increases 8%. According to some investigations, energy demand will not be shared equally as expected by 2040. This comes from the increase in the search of renewable energies.

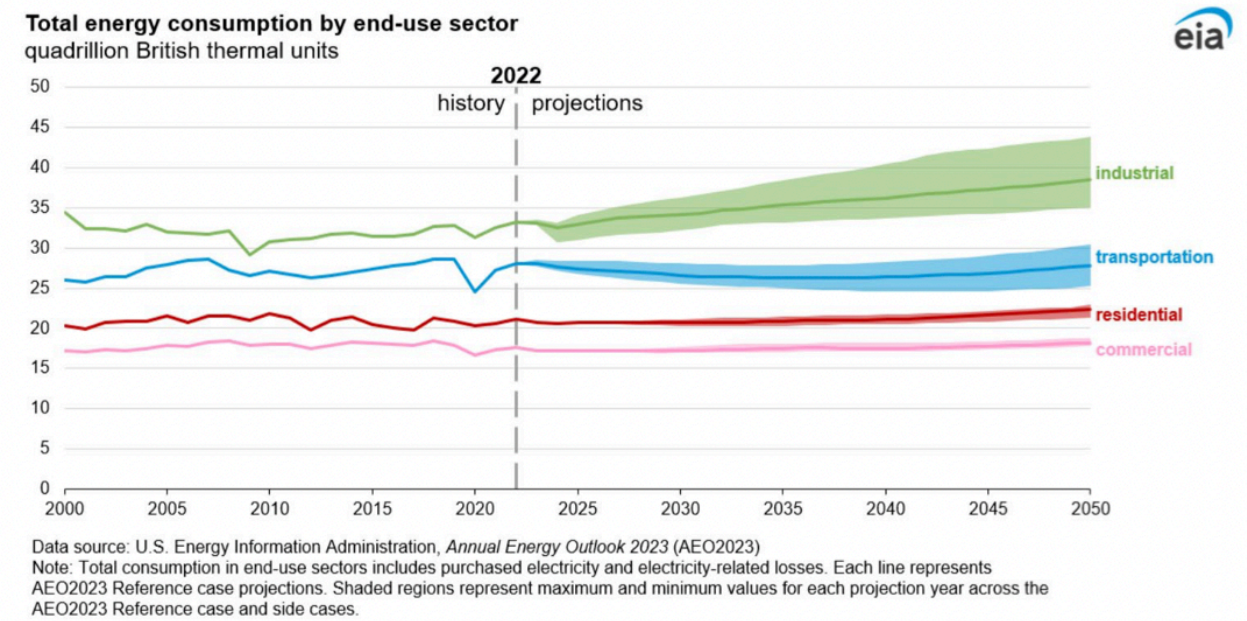

Figure 1: Energy consumption predicted by 2050 by end-use sector (AEO by EIA, 2023)

BP performed a forecast in which is shown the importance of renewable energies in the upcoming future, which is displayed in Figure 2. The investigation performed by BP underlines the importance oil and gas have shared in the previous century, having a participation in the energy contribution as high as 45% of all the energy sources. However, starting by 2030, the energy participation provided by renewables will outstrip the contribution oil and gas generate. In this aspect, different types of renewables, such as solar, wind, hydropower and geothermal are becoming more attractive.

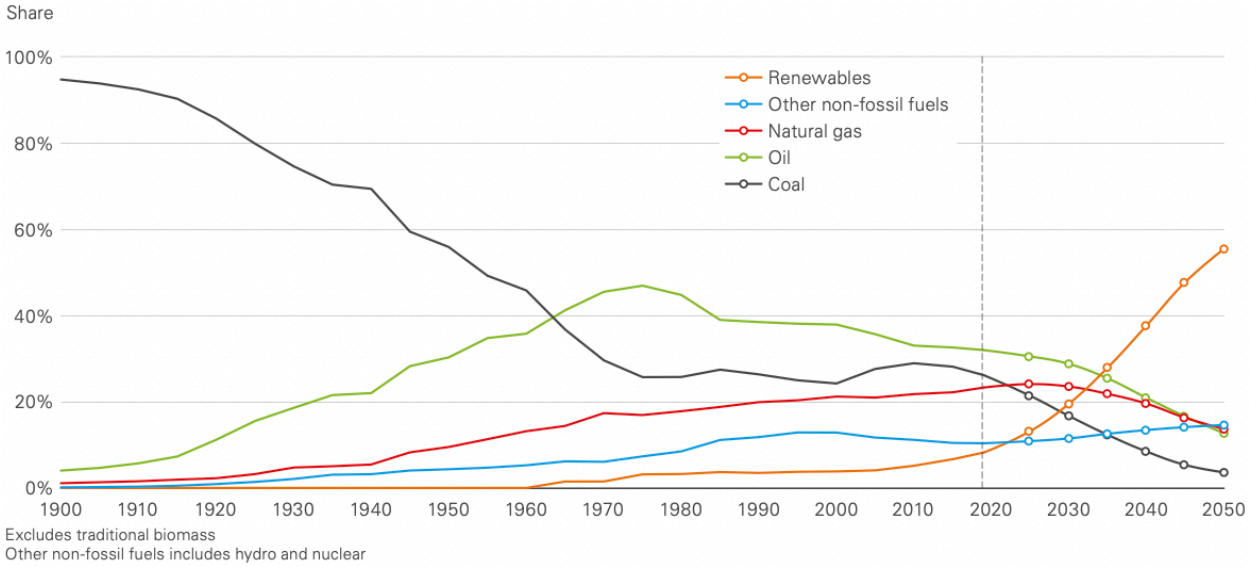

Figure 2: Global energy markets throughout time (BP and Dale, 2022)

Although the current geothermal contribution for renewable energies is less than 1%, which is on the lower side when compared to other renewables such as hydropower with 71% (Abid et al. 2023, as cited from WEC, 2016), it has different advantages, which makes this energy eye-catching for future developments. However, geothermal comes with different challenges, in which the subsurface environment conditions is of the utmost importance.

Temperatures of some developed geothermal wells ranges between 150 – 300 ºC, with some wells under supercritical conditions where temperature and pressure exceed values of 374 ºC and 221 bar for pure water, and 406 ºC and 298 bar for seawater (Reinsch et al., 2017). In order to be able to enable an effective production of the working fluid, the integrity of the wells have to be assured despite these extreme HPHT conditions. Two main components control the integrity of the well during the operations: casing and cement. Due to the high temperature exposure, thermal properties must be investigated, which can affect these components and hence jeopardize the well integrity.

While some thermal properties, such as thermal diffusivity, thermal effectivity, heat capacity, should be carefully reviewed, the most critical is thermal expansion, which affects casing and especially cement. Therefore, it is of highest importance to understand this property and the effects it may have in both casing and cement sheath, especially when facing extreme conditions of temperature and pressure. The objectives for this investigation that uses a novel equipment to determine the thermal expansion and coefficient of linear thermal expansion, in addition to the scope of work, are detailed as follows.

1.2 Objectives

1.2.1 Main objective

The main objective of this investigation is to determine the coefficient of thermal expansion from different materials, rocks and oilwell cements, demonstrating the reliability performed of the novel apparatus by comparing the results with previous studies of this property. In addition, to develop a unique database for this thermal property on cements, which are not widely studied and hence, developed.

1.2.2 Specific objectives

- Conduct research focused on the coefficient of linear thermal expansion for different materials, proving the functioning and reliability of the equipment.
- Observe the coefficient of linear thermal expansion for metallic elements and the different trends followed on the by these materials when comparing them with previous studies.
- Perform some studies on rocks, providing the coefficient of linear thermal expansion results for each one of the rocks tested.

- Create a database of coefficient linear thermal expansion for different cement composites in a systematic investigation, analyzing the difference in each one of the values depending on the mixture.
- Demonstrate the effects, if encountered, of curing time as well as cyclic testing in the oilwell cements tested for this thermal property.

1.3 Scope of work

This work encompasses the experimental study and determination of the coefficient of linear thermal expansion in different materials, which include metals, non-metallic elements, rocks and oilwell cements. The experimentation aims to perform thermal expansion studies for these materials under elevated temperatures in the range of 100 ºC, 150 ºC and 200 ºC, to later calculate their coefficient of thermal expansion. Metallic and non-metallic elements, whose coefficients of linear thermal expansion values are widely encountered in different literature, are used as reference and to demonstrate the trustworthiness of the measurements performed by the novel equipment developed. Additionally, some metallic materials serve as reference as they are used for casing. Furthermore, the experimentations conducted on the oilwell cement, which includes different mixtures, curing times and processes, are used to determine their coefficient of linear thermal expansion, and characterize the property, performing a comprehensive analysis between their values.

Chapter 2. LITERATURE REVIEW

2.1 Geothermal

Geothermal comes from the Greek word gê and thêrm, which refers to earth and energy, respectively (Abid et al., 2022). This energy, which is also defined as the heat from the earth (Kagel et al., 2005), can be used in small scales by heating buildings and large commercial scales, by generating electricity. Some of the advantages of this source of energy in contrast with other energies are the large amount of untapped resources, consistency, a wide range of applications, and availability in different parts of the world at certain depths (Lund, 2000). Additionally, geothermal's low impact on the environment, technology availability, and reduced emission of greenhouse gases, candidate this energy as an important renewable energy (Moya et al., 2018 and Shortall et al., 2015).

The heat that comes from geothermal is extracted by the circulation of fluid produced in the geothermal reservoir, which is mostly brine, from the bottom to the surface. In some scenarios, no fluid is encountered (dry rock), or the permeability is low, so a stimulation must be performed to increase the transfer properties in the formation (Abid et al., 2022). The stimulation is conducted by injecting water from an injection well, which is later recovered from a production well (Walters et al., 212). The water collected from the production wells comes under high-temperature conditions, as illustrated in Figure 3.

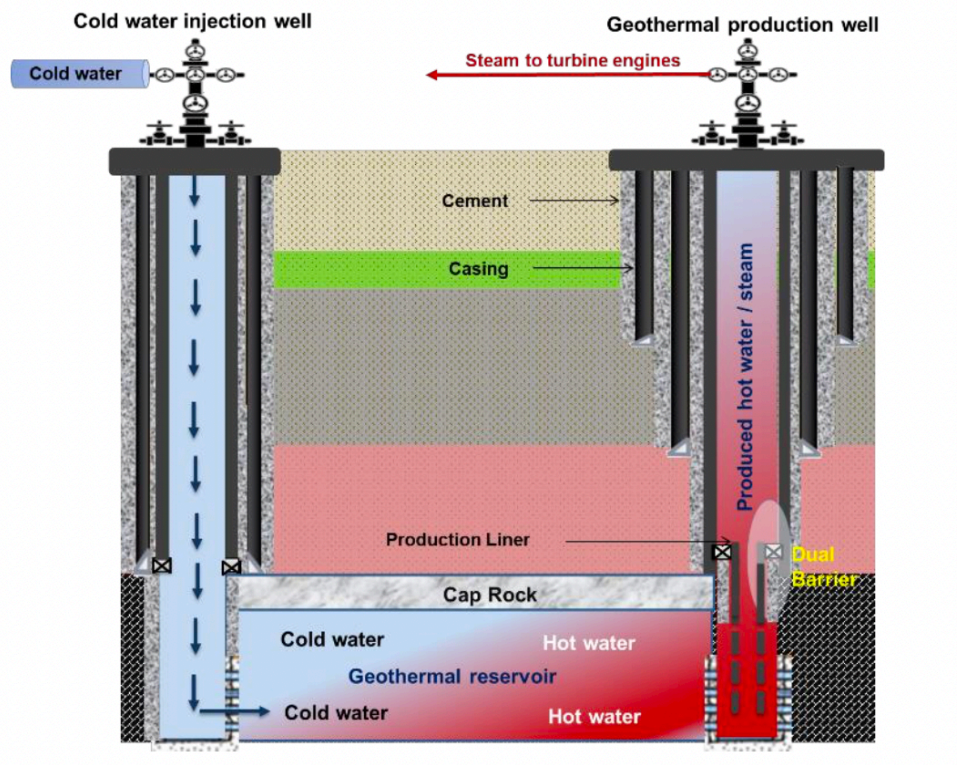

Figure 3:Schematic of a geothermal well for energy production

2.1.1 Geothermal systems

Different geothermal systems are used in geothermal energy, in which energy production can be possible. The systems are listed as follows:

- Hydrothermal
- Geopressured system
- Magmatic system
- Hot dry rock (HDR)
- EGS

2.1.2 Geothermal uses

The use of geothermal energy depends on the source, temperature, as shown in Figure 4.

Range	Temperature	Dominated Fluid	Application
High temperature	Above 150 °C	Vapor and liquid	Fuel and power generation
Medium temperature	Around 95 °C	Mostly liquid	Electricity production by utilizing binary plant
	From 90 °C to 150 °C		Drying of timber, refrigeration, cooling, or heating of buildings
Low Temperature	From 90 °C to 30 °C	Liquid	Aquaculture, processing of food, and heating of the greenhouse
	Below 30 °C		Warming of soil

Figure 4: Range of geothermal temperatures and their applications (Abid et al., 2022, as cited from Dincer and Ezzat, 2018; Shapley, 2011 and Williams et al., 2008)

From Figure 4 above, it can be noticed that the different uses of geothermal can go from warming the soil, to power generation depending on the temperatures. Moreover, the uses for geothermal are delimited in two, which are power generation and direct use.

For power generation, the temperature of either the steam or water recovered should exceed 100 ºC and go up to ~370 ºC (Abid et al., 2022). The plants, which are in charge of the power generation, are generally located in areas where the existence of the geothermal reservoir is within a depth of up to two miles (Zoet, 2011). Abid et al. (2022) also mention that there are three different categories of electricity-producing geothermal plants, which include direct steam power plants, flash steam power plants, and binary cycle power plant. The first one needs higher temperatures up to 235 ºC in which the steam feeds a turbine, hence allowing energy generation (Abid et al., 2022, as cited from Hulen and Wright, 2001). The second one uses hot liquid whose pressure is reduce to transform it into flash steam, which is later removed from the liquid and fed to an electric

generator through turbines. Meanwhile, the liquid is injected back into the subsurface (Abid et al., 2022, as cited from Zoet, 2011). Lastly, the binary cycle can happen under lower temperatures (as low as 85 ºC), in which the transfer of heat in the plants occurs from hot subsurface fluid to working fluid (with low boiling hydrocarbon), vaporizing and driving the generator turbines (Abid et al., 2022, as cited from DOE, 2010). For direct use, geothermal energy has been used as a district. heating system, in which one of many buildings are heated. This practice is almost 80% cheaper than the heat obtained by regular fossil fuels (Abid et al., 2022, as cited from Zoet, 2011).

However, different challenges are present in order to develop a geothermal operation. These challenges go from the extreme conditions encountered in the geothermal wells, to different well integrity issues, as mentioned in the next section of the chapter.

2.2 Well integrity

Different challenges are present within geothermal energy. Some of the challenges described by Abid et al. (2022) are listed below:

- Subsurface environment
- Corrosion and scaling
- Wellbore instability
- Circulation loss
- Wellbore cementing challenges

From the list above, it can be seen that these challenges are especially related to drilling and completion. Drilling and completion are a critical part when developing a geothermal or

hydrocarbon well, accounting for approximately 50% of the cost when setting a geothermal well (DiPippo, 2016). Nugroho et al. (2017), performed a geothermal well operation in Indonesia, in which 30% of the operational time was used to combat losses on the well. The author also mentions that loss circulation also creates problems in casing and cement, which as seen in Figure 5 were also taking >30% of the same operational time.

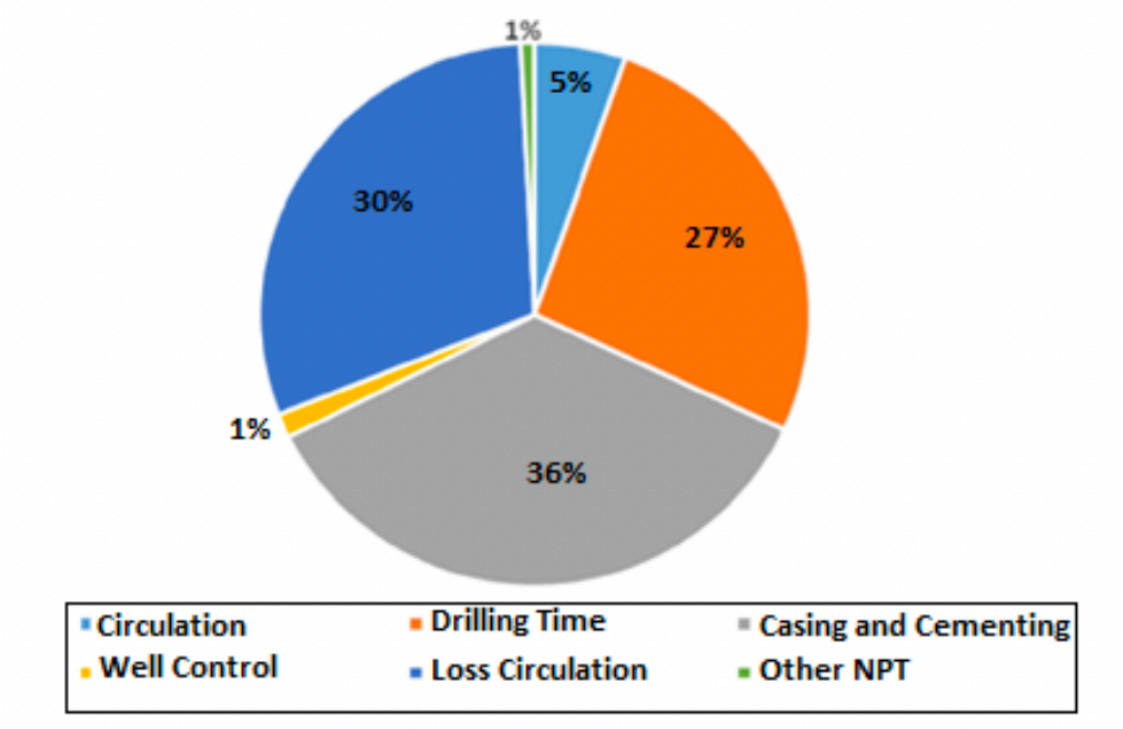

Figure 5: Operational time for geothermal well in Indonesia (Nugroho, 2017)

Moreover, a challenge that is encountered in geothermal wells, as well as in oil and gas operations is the well integrity.

Well integrity can be defined as the ability that a well possesses to produce or inject fluids in a controlled manner while preventing any unwanted fluids migration outside the well system (Teodoriu et al., 2021, as cited from Torbergsen et al., 2012). The NORSOK standard D-010 defines the well integrity as the "*application of technical, operational, and organizational solutions to reduce the risk of uncontrolled release of formation fluids throughout the entire life cycle of the well*" (Norsok, 2013). Then American Petroleum Institute also provides a definition for well integrity, describing it as "*the design and installation of well equipment to a standard that protects and isolates useable quality groundwater, delivers and executes a hydraulic fracture treatment, and contains and isolates the produced fluids*" (American Petroleum Institute, 2016).

A loss in the well integrity can happen due to several reasons; some of them related with the deficient understanding of the downhole conditions, inappropriate well construction practices, inadequate design verification and validation of downhole specimen, poor selection of casing and cement and temperature changes in casing fluid, which includes the expansion and contraction of the casing which leads to stresses on the casing-cement interface (Teodoriu et. al, 2021; as cited from Phi et al., 2019; Bachu and Bennion, 2009; Lavrov et al., 2016 and Zhang and Bachu, 2011).

It is noticeable that the two main components highly associated with well integrity issues are casing and cement. In geothermal operations, cement and casing may take up to 30-35% of the total well cost (Pierce et al., 1996). These components have to be designed to withstand the extreme conditions of temperature and pressure, as well as corrosive fluids, that might be present in geothermal operations. Cementing operation holds the casing in place, preventing undesired formation fluids from entering the wellbore, which is part of the well integrity. This is performed by creating an annular barrier between the formation and casing. Also, it provides structural

support and helps prevent corrosion on the casing from corrosive fluids (Abid et al., 2022). Therefore, while mechanical properties have been deeply investigated for cementing operations, thermal properties, such as thermal expansion, have not. This thermal property is better described in the following section of this chapter.

2.3 Thermal expansion

Thermal expansion can be defined as the dimensional change, such as length, area or volume of a material, when exposed to temperature variations (Bajpai, 2018). This expansion is generated with the increase in the kinetic energy present in the atoms of the material, allowing their movement, excitation and later separation (Liu et al., 2017). Thermal expansion is a property present in different areas, including oil and gas and geothermal operations, in which high temperatures can be found.

The effects of thermal expansion can be noticed in both the casing and the cement sheath. In the casing, thermal expansion can induce stresses that might exceed the yield strength of the casing with respect to compression, thus developing a plastic strain that may end up in the collapse of the casing (Kaldal and Thorbjornsson, 2016). Moreover, thermal expansion can also create axial loads in the casing, that may cause casing buckling where lateral support is not provided, which could happen if there is a void in the cement sheath, for example. Casing string can buckle under high temperature conditions due to large compressive forces caused by the effect of thermal expansion (Xie and Liu, 2008). The effects generated by this thermal property on the cement sheath are related to thermal stresses on the cement sheath. Moreover, cracks, micro annuli, and debonding from the casing and formation can happen (Bu et al., 2017). Therefore, it is indispensable to

understand this thermal property which is present under high temperature conditions, expected not just in oil and gas but also in geothermal operations.

2.3.1 Coefficient of linear thermal expansion (CLTE)

All experiments with novel equipment were conducted to measure linear thermal expansion, which was analyzed in this investigation. Linear thermal expansion is based in the change of length of the material, and is represented by the following Equation 1:

Equation 1: Linear thermal expansion

$$\Delta L = L_0 * \alpha * (T_1 - T_0)$$

Where, $\Delta L, L_0, T_1, T_0$, and α, are change of the length, initial length, initial temperature, final temperature and coefficient of linear thermal expansion, correspondingly.

The coefficient of linear thermal expansion, α, is defined by Cverna and ASM (2002) as the increase in length per unit rise in temperature, and the mathematical expression is defined in Equation 2:

Equation 2: Coefficient of linear thermal expansion

$$\alpha = \frac{\Delta L}{L_0 * (T_1 - T_0)}$$

From Equation 2 above, it can be noticed that this coefficient is dependent on two physical properties which are the length and the temperature. Once measured, the coefficient of linear thermal expansion (CLTE) can be calculated. There have been different techniques used to measure these two properties and calculate CLTE, which are described in the following section of this investigation.

2.3.2 Techniques used for measuring CLTE

Coefficient of linear thermal expansion has been presented in different studies, especially for metallic elements. In order to calculate this property, different techniques have been used. These techniques allow the measurement of the length, and temperature of the samples, which are later used for CLTE calculations. The main techniques used for CLTE measurements are listed below:

- Dilatometry
- Interferometry
- Thermomechanical analysis

2.3.2.1 Dilatometry

For dilatometry, the common procedure consists of heating a material placed in a furnace and then measuring the displacement of the material through a sensor by means of push rods (Cverna and ASM, 2002). The apparatus used with this technique is called a dilatometer, in which the mechanical dilatometer is one of the oldest and most used methods.

Mechanical dilatometry works by measuring the displacement of the material while increasing the temperature. This displacement is mechanically transmitted to a sensor positioned away from the heat, generating a plot of the temperature versus displacement from which the coefficient of thermal expansion can be calculated and obtained (James et al., 2001). The arrangements for mechanical dilatometers can vary as shown in the following Figure 6:

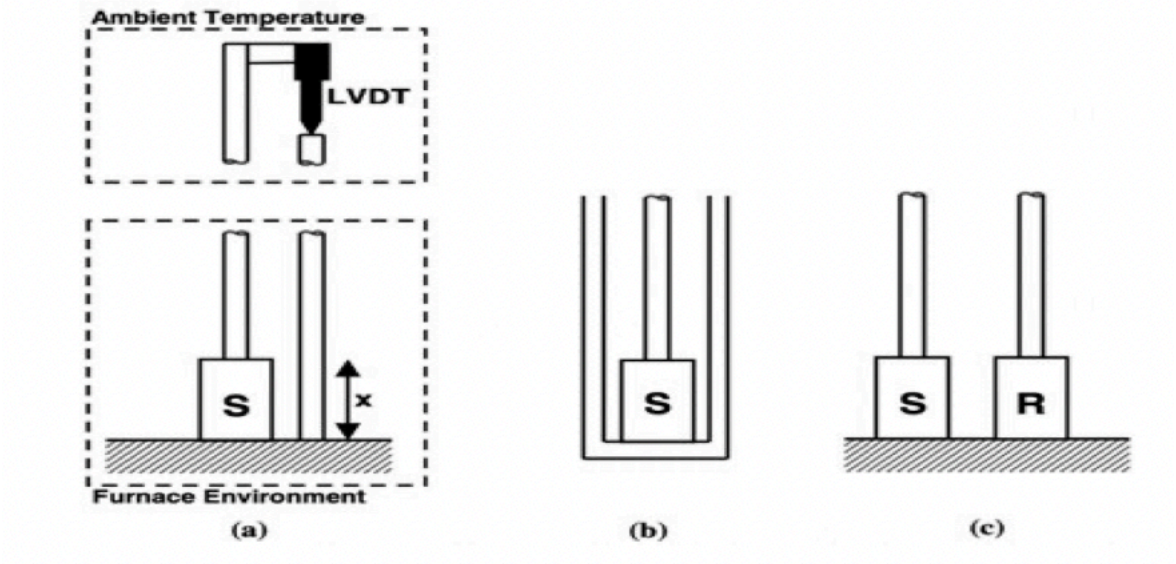

Figure 6: Dilatometers for thermal expansion measurements of different materials. (a) double push rod, (b) tube and a push rod, (c) differential with reference material, R. (James et al., 2001).

From Figure 6, three variations of the pushrod dilatometer are illustrated. First, the double push rod, is in which the selected material is enclosed in a furnace or other environment with a controlled temperature in which two rods, aligned side by side, are in contact with opposite faces of the material. The alignment is parallel to the direction of expansion. The rods protrude out from the temperature environment to a linear variable differential transformer (LVDT), which is a linear sensor and remains at room temperature, where the relative displacement of the rods when changing the temperature is measured (James et al., 2001).

The other arrangement is using one of the rods as a closed tube, in which the material is located. The other rod runs down the axis of this tube, leading to resting against the opposite surface of the material. Therefore, the material expands, pushing the central rod along the axis of the tube, allowing the measurement of the relative movement. And the last one, the differential dilatometer, employs two specimens, one as a reference with a reference material to which the material under research is compared. The procedure refers to both materials having a push rod attached to them and the difference in displacement for both the two rods is recorded while heating them up (James et al., 2001).

The push rods are important in dilatometers, and can be made from different materials, such as aluminum, graphite, or vitreous silica. The material is selected dependent on the temperature in which the test is to be performed. The standard that deals with the dilatometry with different push rods is given in ASTM E228-95 and ASTM D696 (Cverna and ASM, 2002).

The silica dilatometer shown in the ASTM E228 standard and described in Prospector (revised in 2024), works by placing the material inside of the silica tube and then a silica rod is inserted into the tube. This rod has a dial gage attached to it, as illustrated in Figure 7.

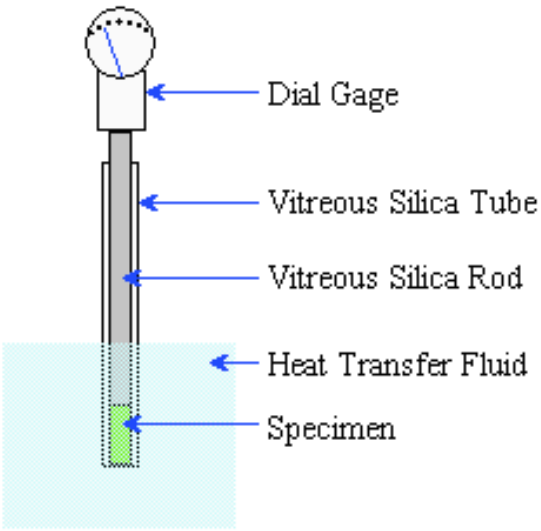

Figure 7: Silica dilatometer schematic according to ASTM E228.

The material is contained in the end of the tube, which is placed in a constant low-temperature bath under low temperature conditions. Once the material has reached a low temperature indicated by the no-movement in the dial gage, the bath is replaced with a high-temperature bath until the material reaches the high temperature. The process of changing baths is again repeated by changing the high-temperature bath with a low-temperature bath once the material reaches high-temperature conditions and, once the material reaches the low temperature, the material is removed and measured at room temperature. The temperatures used with this standard go from -180 ºC to 900 ºC. Figure 8 illustrates the process described above.

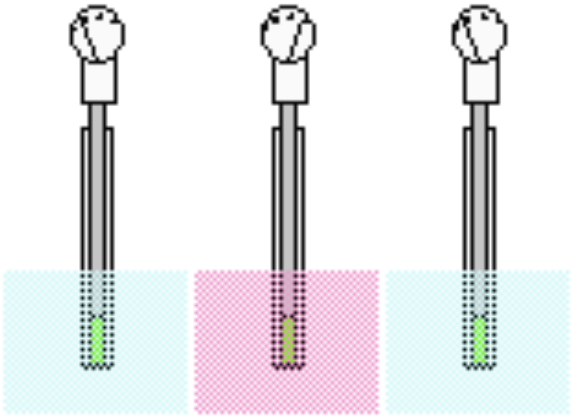

Figure 8: Coefficient of linear thermal expansion process by using a silica dilatometer according to ASTM E228

The calculation of the coefficient of linear thermal expansion is then performed by using the Equation 2, described above in this research.

There exist other apparatuses that use dilatometry for the measurement of linear thermal expansion. These devices have similarities but some of them have some changes in the device depending on their need. For example, Kroeger and Swenson (1977) used a dilatometer with some modifications as shown in the following Figure 9.

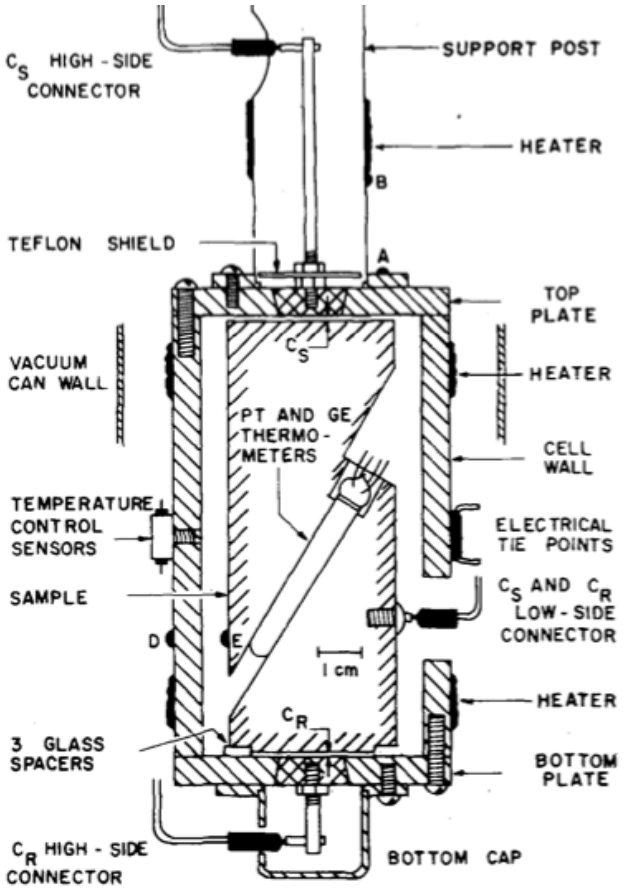

Figure 9: Cross sectional schematic of the absolute dilatometer used in the experiment performed by Kroeger and Swenson (1977)

As shown in the Figure 9, the dilatometer is constituted by some cell walls and vacuum can walls, in which the linear thermal expansion of metals can be measured.

Nelson and Guillot (2006) from SLB describe a much simpler typical thermal expansion apparatus for cement samples, with a quartz rod and a digital micrometer positioned on a stand made of a thick stainless-steel plate, as shown in Figure 10.

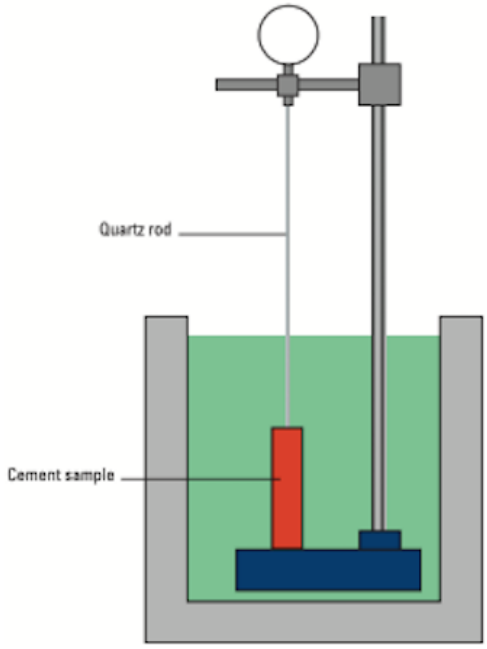

Figure 10: Thermal expansion apparatus according to Nelson and Guillot (2006)

The stand is sited inside a water bath while the measuring tip of the digital indicator, extended with a thin quartz rod, is in contact with the top of the cement sample bar. The temperature of the water bath is then increased to a temperature lower than the cement curing temperature in many steps. At the same time, and throughout the test, the temperature and sample deformation values are recorded. The coefficient of linear thermal expansion is then calculated from the temperature increment and the dilatation of the material. This dilatometer has also similarities with other dilatometers used by Yang (2003) and Loiseau (2014) which will be described later in this investigation.

Other modifications have been performed in the dilatometers to obtain better results depending on the material measured. For example, Popov et al (2012) used a quartz dilatometer using an early dilatometer developed by the Ural Electrode Institute as prototype, as shown in Figure 11.

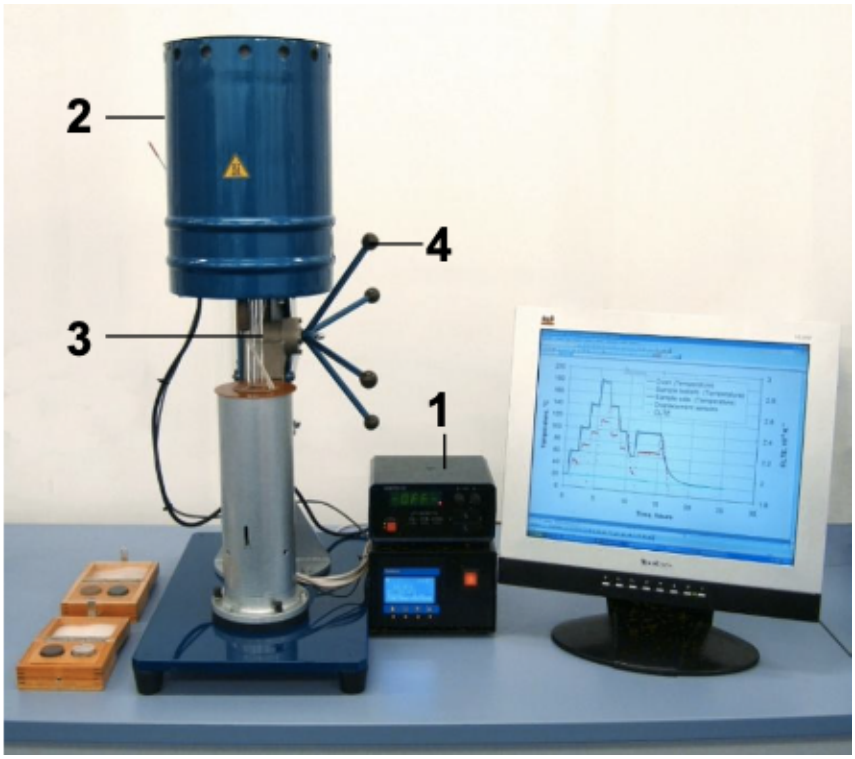

Figure 11: Quartz dilatometer by Popov et al (2012), with 1 – temperature controller, 2 – furnace, 3 – vitreous silica specimen holding system and extensometers mounting block; 4 – lifting system

This dilatometer has to achieve certain specifications such as the possibility of CLTE measurements on core plugs used for measurements of other petrophysical properties, the determination of CLTE tensor components on one rock sample placed in the instrument in three different directions, measurement of sample surface temperature in two different points during CLTE determination, the extension of the CLTE measurement range to the range of rock-forming minerals and has to have adherence to the basic ASTM standards (Popov et al., 2012).

Dilatometry has also been used to measure the thermal expansion of cement concrete. Yang et al (2003) describe the dilatometer used following the AASHTO standard. This is a methodology

adopted by the American Association of State Highway and Transportation Officials, to determine the coefficient of thermal expansion for Portland-cement concretes.

An important part of the equipment is the extensometer, which is mounted in a rigid invar frame, whereas the materials are mounted on three pins set in the base plate of the frame and are transmitted to the extensometer throughout an invar rod (Yang et al., 2003). The determination of the thermal expansion is provided by measuring the length change of the cylindrical or prism concrete specimens. This is measured by strain gauges mounted on the surface or inside the specimen. According to Yang et al (2003) each beam specimen, with shape of 150 x 150 x 500 mm, was instrumented with the aid of two embedded electrical wire strain gauges. The strain gauges are made of two types and fixed in the concrete: TML KM100B (transducer type) and PML 60. Additionally, there is another testing method, although is more complex to install. This testing method uses fiber-optic sensors. These sensors are embedded into a cement sample. Figure 12 shows the equipment described by Yang et al. (2003).



Figure 12: AASHTO-type device of the CTE test, according to Yang et al (2003).

Based on the set-up mentioned above, and taking the dilatometer used by Nelson and Guillot (2006), Loiseau (2014) developed another setup to measure thermal expansion of cement composited used in HT applications via dilatometry at the SRWI laboratory. The device follows the same principle as the one described above by Yang et al. (2003). However, some modifications are made in this equipment.

In this setup, some quartz rods were used to fix the digital micrometer on the top of the sample, this was performed to decrease the dilation impact from the extensometer. Another modification was the implementation of a thin metallic plate on the top of the cement sample. Every 10 seconds, the extension of the sample and the temperature are simultaneously monitored. Figure 13 illustrates the modified dilatometer used by Loiseau (2014).

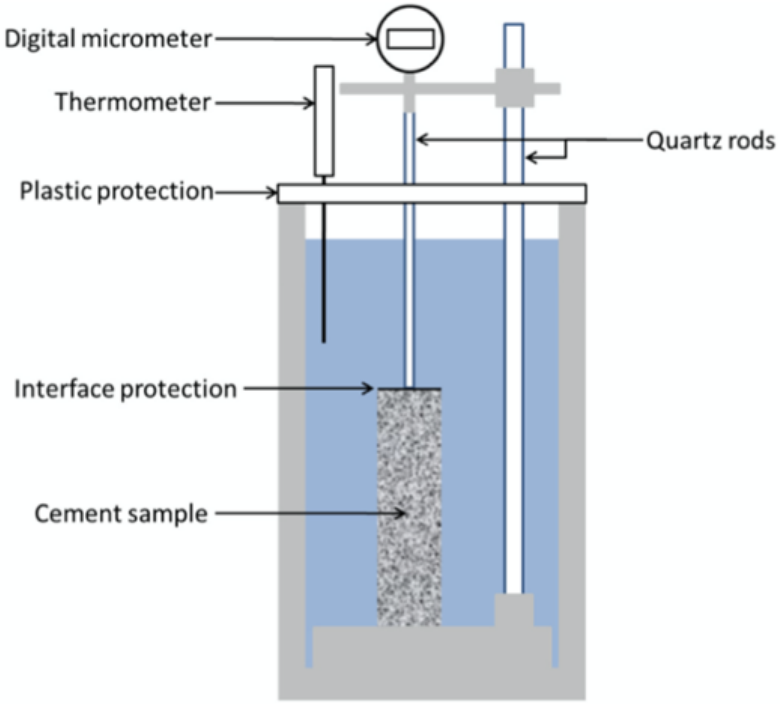

Figure 13: Modified dilatometer used by Loiseau (2014)

Despite being the most used technique for thermal expansion measurements, one of the cons of this method is its accuracy which is less compared to the interferometry technique.

2.3.2.2 Thermomechanical analysis

For thermomechanical analysis the measurements are performed by using a thermomechanical analyzer which consists of a probe and a specimen holder. The probe transmits the changes in the length to a transducer, which transforms the movement of the probe into an electrical signal (Cverna and ASM, 2002). Some analyzers can have additional parts, such as furnaces and sensors for temperature while others, such as the one described by Corporation Hitachi High- Tech (revised in 2024), have thermocouples and force generators. The apparatus described by ISO in the 11359

standards has a cooling device and a gas supply. The temperature range usually goes from -120 to 600 ºC and besides the ISO 11359 standard, ASTM has its own reference for thermomechanical analysis in ASTM E831 (Cverna and ASM, 2002).

Thermomechanical analysis is used to measure thermal expansion in cement concrete according to the AASHTO T336-15 (2015) and the apparatus used is illustrated in the following Figure 14.

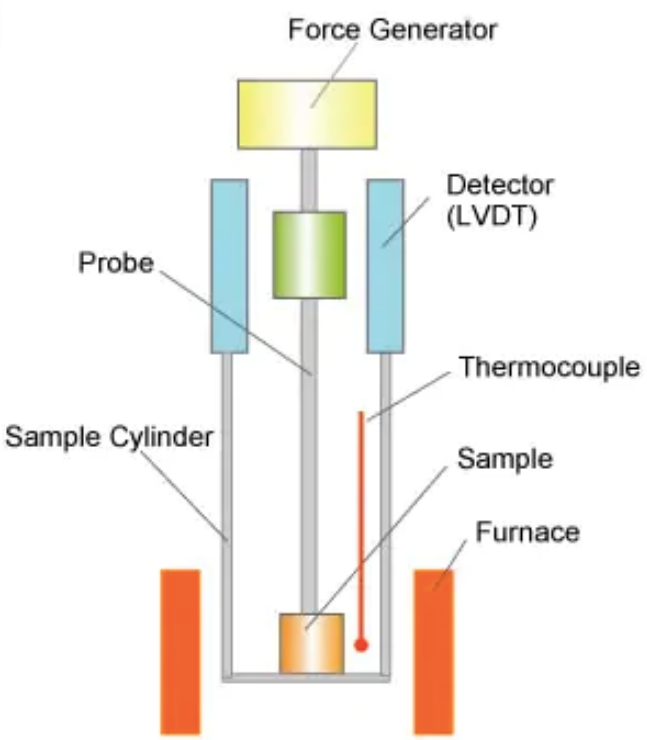

Figure 14: Diagram of a thermomechanical analysis apparatus according to Corporation, H.H. (revised in 2024)

For the measurement of the thermal expansion with this apparatus, the sample is inserted into the furnace and gets in contact with the probe that is connected to a length detector and the force generator. The temperature is measured with a thermocouple, close to the sample, and it changes

in the furnace by applying force onto the sample from the force generator via the probe. The thermal expansion is then measured as the probe displacement with the length detector. For the sensor in the length detector, the Linear Variable Differential Transformer (LVDT) is used (Corporation, H.H., revised in 2024).

This apparatus uses different types of probes depending on the measurement purpose as the following Figure 15 shows.

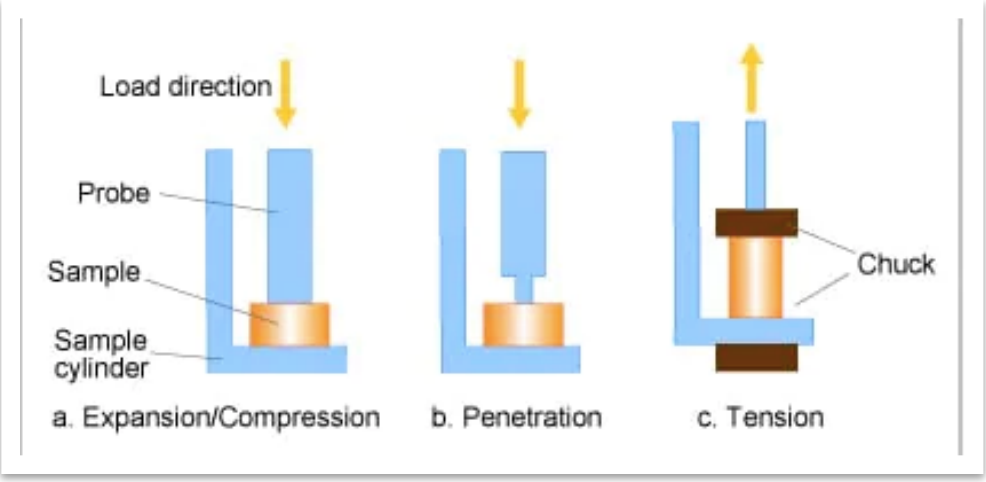

Figure 15: TMA apparatus probe types depending on the purpose

First, there is the expansion/compression probe which is used for the measurement of the deformation generated by the thermal expansion of the material while applying the transition of the sample under the compressed force. The penetration probe refers to the probe used to measure of the softening temperature. Lastly, the tension probe is used to measure the thermal expansion and shrinkage of different samples such as the film and fiber. These probes can be made of quartz

glass, alumina, and metals and, and, same with the dilatometers, the selection relies on the temperature range or the measurement process (Corporation, H.H., revised in 2024).

ISO 11359 standard describes another TMA apparatus with some changes from the apparatus described above. The apparatus still has a temperature-programmable furnace with a capacity of generating constant heating or cooling for the intended measurements and covering this temperature range. It also has the capacity to maintain a controlled pure gas atmosphere. The apparatus also contains a probe and other components such as a displacement transducer, load application device, a cooling device, an inert or oxidizing gas supply, and micrometers/calipers. These micrometers have an accuracy of ±2 μm or better and one of the advantages of using this apparatus is that the material can have any shape although it has to have a suitable thickness for the intended measurement (ISO 11359, revised 2023).

For the ASTM E831 standard, in the thermomechanical analyzer the material is held and contacted by a probe which leads to a displacement sensor while applying a small force, in the range of 1 to 100 mN, to provide contact between the probe and the material (ASTM E381, revised 2024). Figure 16 shows the thermomechanical analyzer used in this standard.

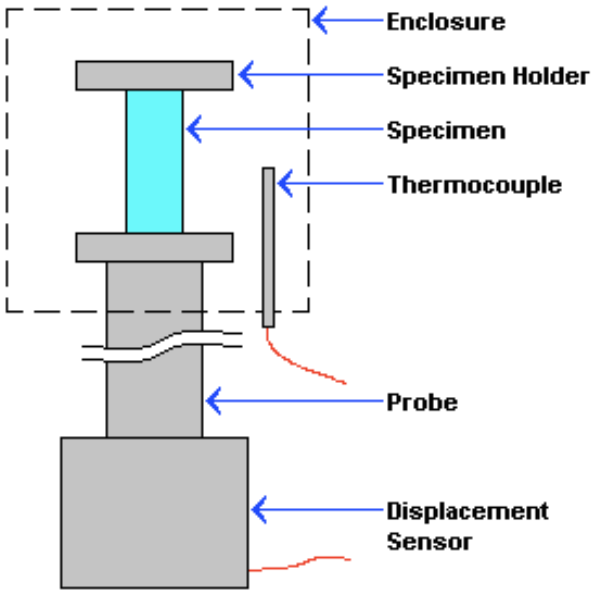

Figure 16: Thermomechanical analyzer according to ASTM E381

The procedure consists in bringing the enclosure to a starting temperature. This temperature is increased at a rate of 5ºC/min and the expansion of the material is then measured by the sensor over the temperature range of interest. It should be remembered that according to the standard, the temperatures covered goes from -120 and 600 ºC (ASTM E381, revised 2024). The coefficient of thermal expansion is then obtained from the Equation 2, described above in this investigation.

2.3.2.3 Interferometry (optical interference)

Interferometry, also called optical interference, is an optical interference technique in which the displacement of the material is measured through the wavelengths of light. The wavelengths travel parallel to the displacement direction (James et al., 2001). These techniques can be Fizeau, Fabry-Pérot, or some other laser-based polarizing interferometers (James et al., 2001 as cited from

Touloukian et al., 1975; Hahn, 1988 and Ruffino, 1994). For this technique, the temperature range is usually from -150 to 700 ºC. ASTM has a standard for optical interferometry which is the ASTM E28-99 (Cverna and ASM, 2002).

There are two typical arrangements for the optical interference. Frist, the typical arrangement for an interferometer consists of the material placed between two optical flats, which move apart as the material expands. Monochromatic light is reflected from the bottom of the surface of the upper flat and the top surface of the lower flat. The two rays interfere depending on the separation, this can be constructive or destructive (James et al, 2001). The second and alternative arrangement contains a reference sample, acting as the lower reflection surface. The optical flat is supported either by a ring-shaped specimen or three separated specimens of the material under research. In this case and also similar to the reference techniques in dilatometry, the value for the distance change is the difference between the expansion of the material in relation to the reference used (James et al., 2001). Both arrangements are shown in the following Figure 17.

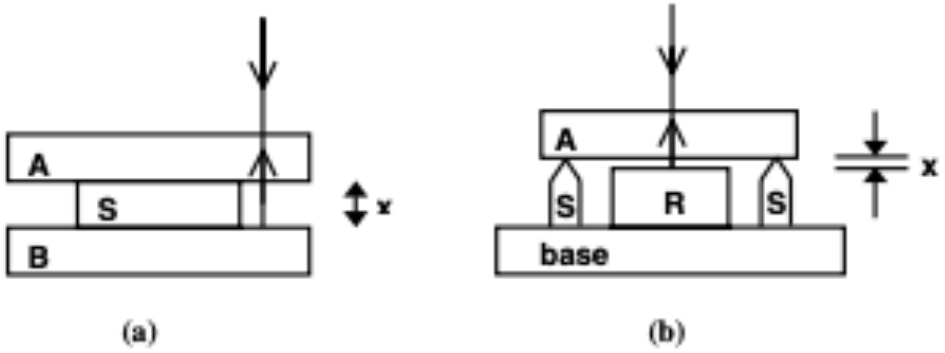

Figure 17: Typical arrangements of interferometers with their variations (James et al., 2001)

From Figure 17, a) the main used and the arrangement b) alternative arrangement. A and B act as the flats, S as the material, and R as the reference specimen in the second type of arrangement.

As mentioned above, optical interference techniques for the measurement of thermal expansion include Fizeau, Fabry–Pérot and laser-based polarizing interferometers and the geometry of the optical system may vary. For example, Fizeau interferometer, a point source of light is collimated by a lens, in order to give rays to the reflecting surfaces. The Fabry-Pérot interferometer, on the other hand, uses optical flats that have high reflective coatings, resulting in sharper fringes hence improving the accuracy of measurement. Nonetheless, this interferometer works better for low temperatures rather than high temperatures due to the deterioration of the special optical coating (James et al., 2001).

Another apparatus using interferometry technique was described by Okaji and Imai (1984) who used a two-fold path interferometer to measure the linear thermal expansion coefficient, as illustrated in Figure 18. The apparatus involves a self-compensation of optical misalignment and a wide tolerance of non-parallelism between two mirrors. The construction, nonetheless, is simpler and with fewer optical elements than the version presented by the authors in a previous work (Okaji and Imai, 1983).

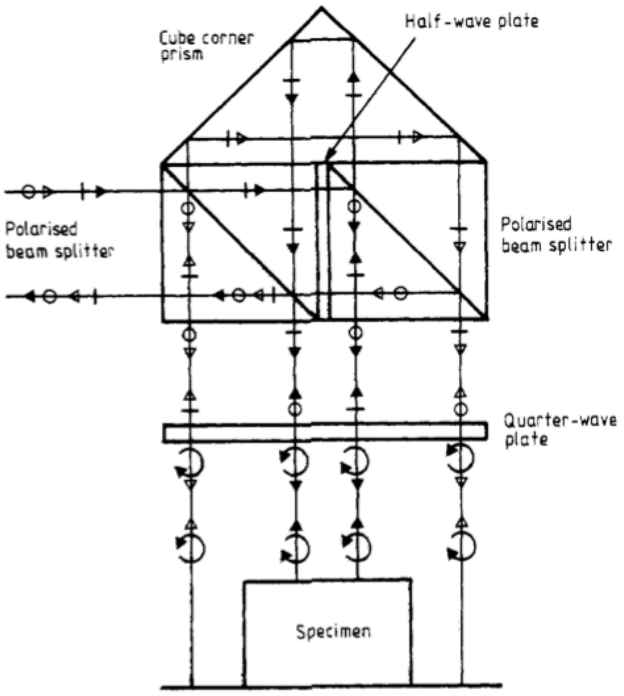

Figure 18: Two-fold interferometer by Okaji and Imai (1984)

One of the conditions of this system is the requirement of a very strict parallelism between two polarizing planes of the double-beam splitter. The condition can be achieved by using a stable precision rotating and tilting table, which functions as a mechanical holder of one of the polarizing beam splitters (Okaji and Imai, 1984). The detection system of the apparatus is the same as Okaji and Imai described in their previous work (Okaji and Imai, 1983).

Okaji and Yamada (1999) have also used the interferometer technique with a double beam for the range of 0-50 ºC leading to a sub-nanometer accuracy for the path length. The equipment used was formed by a vacuum thermal bath with resistance thermometers. The equipment was also used in a following research to measure the expansion of gauge blocks of steel within a similar temperature

range (Okaji and Yamada, 2000). The uncertainty of the measured CTE values was $\pm 0.007 \times 10^{-6}$ K^{-1}.

Another approach involving the interferometry technique is the speckle pattern interferometry. The speckle effect is described as the pattern generated on the surface in which two coherent collimated laser beams are directed (James et al., 2001). This pattern may suffer changes with the deformation of the surface in its own plane (James et al., 2001, as cited from Leendertz, 1970). The methodology was used by Kim et al. (1997) to determine the coefficient of thermal expansion and by Lokberg et al. (1985) to study the deformation on materials in a temperature up to 1700 ºC. Kim recorded the pattern formed in the work using a CCD camera whereas Lokberg et al. used a TV camera. In the work done by Kim et al. the fringes in the resulting patterns, obtained from the subtraction of the patterns at the different measurement temperatures to the initial reference pattern, were used to determine the thermal expansion. Lokberg et al. subtracted the patterns obtained at different temperatures from the original patter obtained at room temperature.

2.3.3 Other techniques used for measuring CLTE

In addition to the techniques presented above, other methods for measuring the linear thermal expansion can be found in the literature, although they are not as used as the previous. These methods adopt optical or another specialized techniques that will be discussed briefly.

2.3.3.1 Diffraction

Calculations of thermal expansion coefficient can be performed via diffraction when measuring the crystal lattice parameters of a material in different exposure temperatures (James et al., 2001). Diffraction refers to phenomena that occur when a wave of light passes through a barrier or gap where it will be spread out, creating a dark-bright pattern on a screen (Yogaswara and Eljabbar, 2018). Diffraction can be done by x-rays (McKinstry, 1988 and Touloukian, 1975), including measurements done at temperatures close to 1200 ºC (Antii, 1999), electron diffraction (Zeng, 1999), or neutron diffraction (Bowman et al., 1972 and Bittorf et al., 1999).

The diffraction by x-ray has the specimen in form of powder, polycrystalline wire, or rotating crystal which is enclosed in a furnace where monochromatic x-rays are directed, and the angles at which the beam is scattered are recorded via measuring the intensity of the beam as a function of the angle using a diffractometer or by means of a cylindrical film surrounding the specimen. Using the Bragg relation, the spacing of the crystal planes from the angle and wavelength can be calculated (James et al., 2001). The thermal expansion of the crystal lattices can be calculated by repeating this process at different temperatures. Electron diffraction has been used and performed to study the thermal expansion in the same crystalline materials (James et al., 2001 as cited from Zeng, 1999). Two techniques have been deployed with the use of electron diffraction, depending on the direction of thermal expansion in accordance to the surface. First, the RHEED which stands for reflection high-energy electron diffraction, and refers to the employment of an electron beam with a glancing angle of 3º to the surface.In this, the thermal expansion is given perpendicular to that surface(James et al., 2001 as cited from Zeng, 1999). The second, which gives the expansion measurements parallel to that surface comes from helium atom scattering (Miyake et al., 1999).

Yogaswara and Eljabbar (2018) developed a setup in which they used a metal rod to create a narrow gap where a beam of light passes, creating the diffraction pattern. The gap that increases is related to the linear expansion of the metal length. In this method the authors used a digital video-based single-slit diffraction to determine the linear thermal expansion coefficient of metal. This expansion can be measured by analyzing the diffraction pattern generated. The measurement was also performed with the help of video analysis using Tracker, which is a software used for motion and optical phenomena. In this setup, the temperature was recorded via a thermocouple temperature sensor, Figure 19 illustrates the setup developed by the authors.

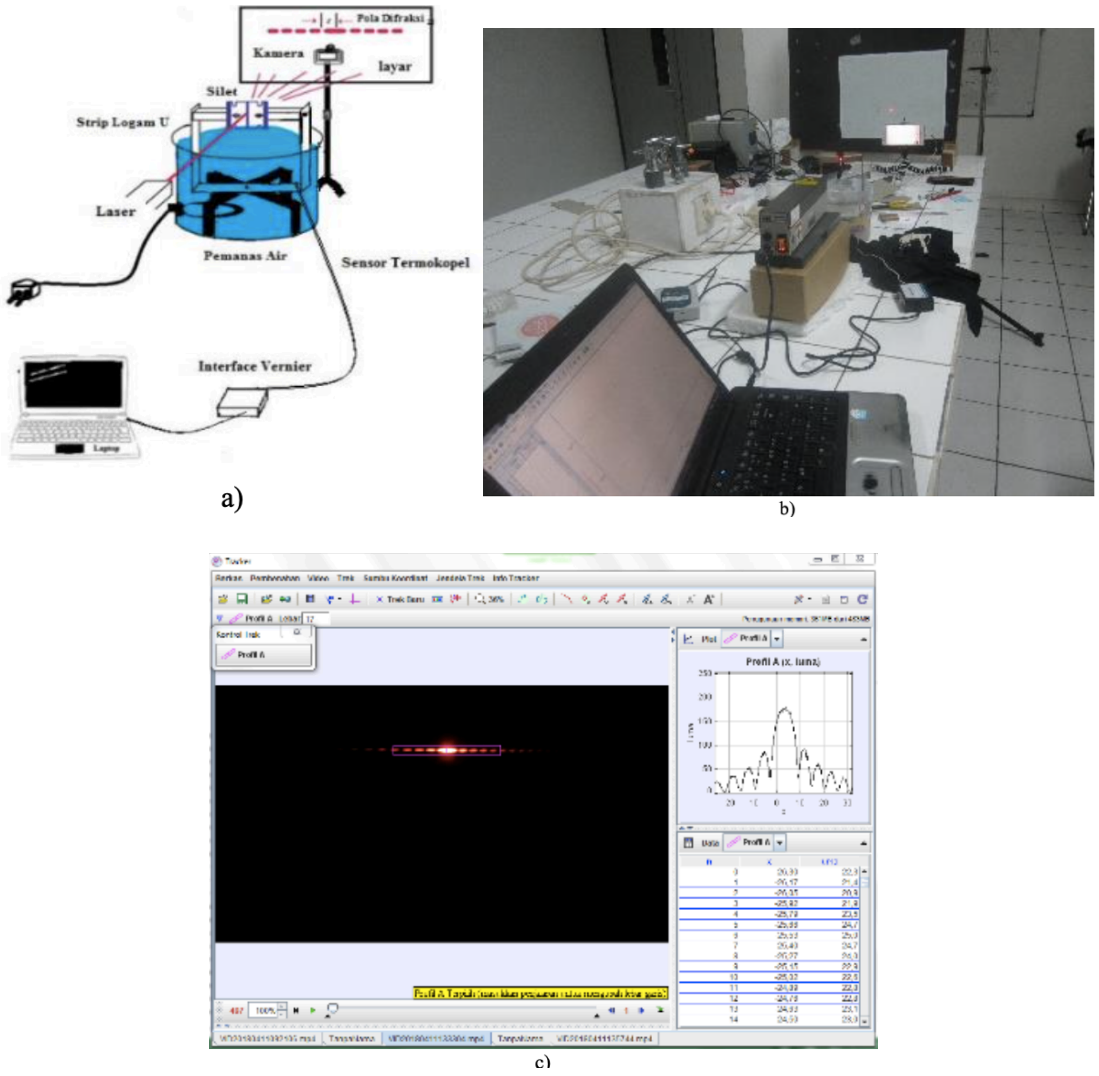

Figure 19: Setup developed by Yogaswara and Eljabbar (2018), including the following: (a) trial set schematic, (b) experimental device arrangement in data collection, (c) video frames using Tracker software.

The calculation of the linear thermal coefficient includes a digital image processing method and the slope of the curve generated from the relationship, analyzed by linear regression, between temperature and 1/y (y= distance of the first order of dark diffraction pattern to center pattern). Once this is obtained, the coefficient of thermal expansion is obtained via the formula shown in Figure 20.

$$\frac{1}{y} = \frac{\alpha L_0}{D\lambda} T + \left(\frac{1}{y_0} - \frac{\alpha L_0 T_0}{D\lambda} \right)$$

Figure 20: Formula used by Yogaswara and Eljabbar (2018) to calculate the CLTE

2.3.3.2 Fused-quartz tube

A fused-quartz tube was employed for the measurement of the thermal expansion of magnesium by Hidnert and Sweeney (1928) and later for other materials (Hidnert and Souder 1950, and Hidnert and Krider, 1952). The apparatus was determined to work for temperatures between -190 ºC and +1000 ºC. However, the experimentations performed by Hidnert and Sweeney (1928) were done between -183 ºC and +500 ºC. The fused-quartz tube is closed at one end with a sample ready to be heated or cooled, and a movable fused-quartz rod resting on top of the sample, which extends above the open end of the tube (Hindert and Souder, 1950). The sample can be of 20 cm long. The heating process is performed by placing the tube with the sample in a water / oil bath or electrical furnace; the temperature is indicated by a thermocouple placed inside the tube near the center of the sample. The expansion is therefore determined by an indicator gauge which registers the differential expansion between the sample and the equivalent length of the fused quartz (20 cm), the indicator is attached near the top of the tube (Hindnert and Souder, 1950). Figure 21 shows the fused-quartz tube apparatus.

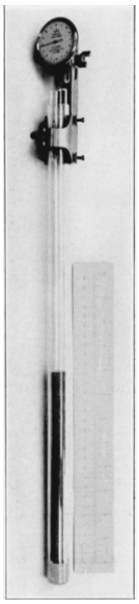

Figure 21: Fused-quartz tube expansion apparatus

2.3.3 Measurements of CLTE

As discussed previously, different researches have been performed CLTE calculations using different techniques. For metallic elements, the values of CLTE can be found in diverse literature but also in manufacturers websites and books, such as the Metals Handbook provided by the ASM (1998). However, CLTE values from these sources rarely specify the technique or apparatus used to obtain those values. Table 1 provides a brief summary of CLTE values obtained in some investigations for different metallic elements and the techniques used for their determination.

Table 1: Brief summary of CLTE values of different metallic elements found in diverse literature

Author	Equipment and Technique	Material	CLTE value (1/ºC)

Hidnert and Krider (1952)	Fused-Quartz Tube	Aluminum	2.38 $x10^{-05}$ to 2.67 $x10^{-05}$
Popov et al. (2012)	Quartz dilatometer	Aluminum	2.3 $x10^{-05}$ to 2.49 $x10^{-05}$
Shrivastava et. al (2020)	Push rod dilatometry	Aluminum	2.32 $x10^{-05}$ to 2.55 $x10^{-05}$
Yogaswara and Eljabbar (2018)	Diffraction	Aluminum	2.29 $x10^{-05}$ to 2.30 $x10^{-05}$
Okaji and Imai (1984)	Interferometer	Aluminum	2.31 $x10^{-05}$
Lewis (1994)	Interferometer	Tool Steel	1.06 $x10^{-05}$ to 1.14 $x10^{-05}$
Martelli et al. (2013)	Interferometric dilatometer	SS 304	5 $x10^{-06}$ to 1.5 $x10^{-05}$
Okaji and Imai (1984)	Interferometer	Carbon Steel (bar gauge)	1.09 $x10^{-05}$
Shrivastava et. al (2020)	Push rod dilatometry	Brass	1.86 $x10^{-05}$ to 21.1 $x10^{-05}$

In the case of rocks, the Table 2 summarizes some selected investigations performed to determine CLTE values. It is important to mention that most of the investigations are performed with the objective to obtain the volumetric thermal expansion rather than a linear thermal expansion; this related to the rock's properties. In addition, the experiments might be also performed under

different conditions, not only of temperature but also of pressure, which can be also applied on the rock, depending on the author's scope of investigation. For example, the results shown by Myer and Rachiele (1981) are results from experiments performed at low confined pressure, whereas the results provided by Somerton et al (1981) are results from an investigation performed under liquid saturation, confining stress and fluid pressure applied on the rock. However, the Somerton et al. (1981) claim that the results obtained are similar to results obtained in dry, unstressed samples. Moreover, CLTE values for rocks found in specific literature are shown in the Table 2. Additionally, the temperature in which the sample was tested is also described in the Table.

Table 2: Brief summary of CLTE values of different rocks found in diverse literature

Author	Equipment and Technique	Rock	CLTE value (1/ºC)	T (ºC) of test
Feng et al. (2020)	HT machine for rock mechanics	Mudstone	1.11×10^{-06} – 3.74×10^{-06} and 2.5×10^{-06} – 4.5×10^{-05}	Up to 400 ºC
Popov et al. (2012)	Quartz dilatometer	Quartz-feldspar sandstone	8.7×10^{-06} and 1.11×10^{-05}	Up to 110 ºC
Luo and Hu (2021)	Dilatometry	Calcareous shale	Max of 3.66×10^{-05}	Up to 1000 ºC

Somerton et al. (1981)	Strain gauges	Sandstone (Berea, Bandera and Boise)	1.3 $x10^{-05}$, 2 $x10^{-05}$ and 1.7 $x10^{-05}$	Up to 200 ºC
Popov et al. (2012)	Quartz dilatometer	Carbonaceous	4.8 $x10^{-06}$ and 6.3 $x10^{-06}$	Up to 110 ºC
Myer and Rachiele (1981)	Thermomechanical analysis	Granite	8.75 $X10^{-06}$ to 1.6 $X10^{-05}$	Up to 200 ºC
Dwivedi et al. (2008)	Push-rod dilatometer	Granite	$1.3E^{-05}$, $1.4E^{-05}$ and $7E^{-06}$	30 – 200 ºC
Popov et al. (2012)	Quartz dilatometer	Quartz sandstone	1.09 $x10^{-05}$ and 1.22 $x10^{-05}$	Up to 110 ºC

Some investigations about the coefficient of linear thermal expansion in some cement composites have also been performed. The literature, however, is not extensive as compared to metallic elements or even rocks. Table 3 summarizes some CLTE values found in specific literature. It is important to highlight that, in the case of cement composites, different factors such as curing time and temperatures may vary depending on the research purpose by each author. Additionally, some experiments such as the ones performed by Ghabezloo et al. (2012) were performed applying pressure, leading to a difference in results.

Table 3: Brief summary of CLTE values of different cement samples found in diverse literature

Author	Equipment and Technique	Cement sample	CLTE value (1/ºC)
Jimenez et al. (2017)	Dilatometer	Class H cured at 60 ºC for 7 days	~4.3 x10^{-06} to 1.1 x10^{-05}
Tomilina et al. (2012)	Dilatometer	Class G + silica and thixotropic cement and thermally responsive cement cured at different pressures and temperatures	9 x10^{-06} and 1.3 x10^{-05}
Loiseau (2014)	Dilatometer	Class G + 40% Silica cured at 20.7 MPa and HT	8.8 x10^{-06}
Loiseau (2014)	Dilatometer	Neat Class H	9.1 x10^{-06}
Meyers (1951)	Not provided	Class A with some relative humidity	~1 x10^{-05}
Ghabezloo et al. (2009)	Triaxial cell	Class G at HT (drained and undrained when heating and cooling)	2x10^{-05}, 3.2 x10^{-05} and 4 x10^{-05}

From Table 3 above, it can be seen how most of the experiments were carried out using dilatometry, which is not as effective as other techniques for thermal expansion measurements such as interferometry. In addition, the data in the literature for cement composites is still very limited. This, with some experiments performed under different circumstances, lead to a narrower database of CLTE values in the literature. For this reason, a unique equipment is designed to measure the CLTE of thermal expansion of cement composites in similar conditions, leading to the creation of a unique CLTE database for oilwell cements. The equipment also involves an innovate and accurate technique, which differs from the common dilatometry used by previous authors. An explanation of the equipment, and the results obtained are presented in the following chapter.

Chapter 3. EXPERIMENTAL APPARATUS

In this investigation, a novel equipment was designed in order to measure the length and temperature of different materials, such as metals, non-metallic elements, rocks and oilwell cements and then calculate their CLTE. The equipment, in contrast with the techniques and apparatus described in the literature review, uses a shadowing technique. The equipment used, its parts and the optical shadowing technique are described as follows.

3.1 Novel Experimental Apparatus

The coefficient of linear thermal expansion (CLTE), as mentioned in the previous chapter, is related with two physical properties, which are the length and the temperature. In this aspect, the novel experimental set-up, developed in the Well Integrity Laboratory at The University of Oklahoma has the capability of measuring them in order to obtain the CLTE of various materials. The equipment, as shown in previous publications (Velazco et al., 2023) is integrated by the components listed below:

- Micrometer
- Heat controller
- Aluminum block
- Thermometer
- Cylindrical sample
- Data acquisition system

Figure 22 shows the novel experimental apparatus presented in this investigation and in previous publications (Velazco et al., 2023; Velazco et al., 2024 and Velazco et al., 2024). A better description of each one of the components of the apparatus will be provided in the following sections.

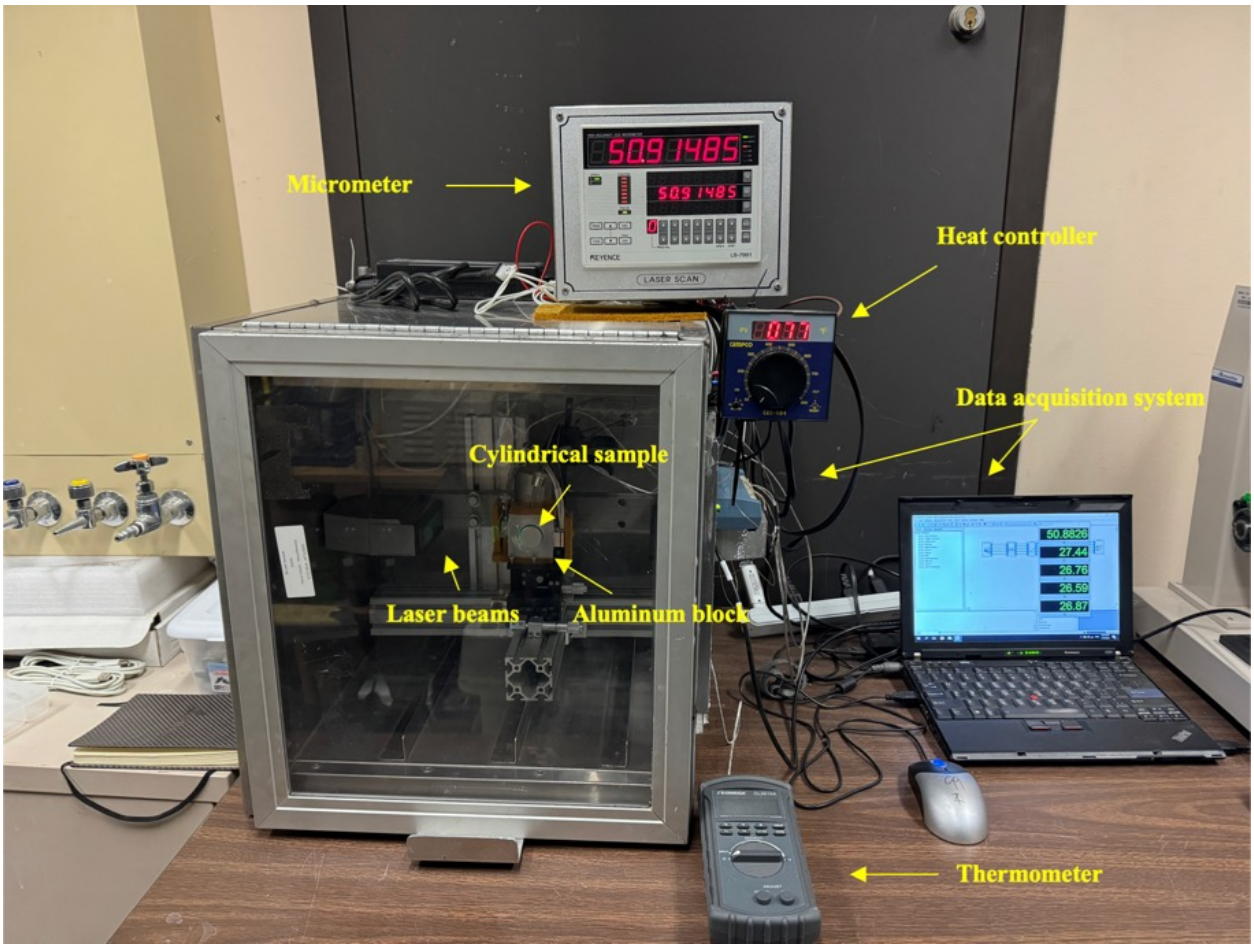

Figure 22: Novel experimental apparatus developed at the Well Integrity Laboratory

3.1.1 Micrometer and laser beams

The micrometer is a device which provides the length of the samples tested, and measured by laser beams using an optical shadowing technique. The length of the sample is measured throughout the

whole experiment, hence both the initial length and the final length, needed to determine the coefficient of linear thermal expansion, can be obtained. Additionally, the micrometer allows the length of the samples to be monitored during the whole experiment. Figure 23 provides a closer look to the micrometer and the laser beams, used to obtain the physical property of length.



Figure 23: Micrometer and laser beam used for length measurements

3.1.2 Heat controller

The heat controller is a device which allows the increment of the temperature of the set-up. This is performed by setting the desired temperature in the heat controller, which transmits the heat through some resistors, connected to the aluminum block. The heat controller has the capability of provide high temperatures up to 315 ºC (~600 ºF). The tests performed during this investigation, where performed in the range between 93ºC (~200 ºF) to 205 ºC (~400 ºF). Moore (2020) mentions that the temperature range for the field in Utah FORGE, in which geothermal projects are currently

ongoing in the United States, is between 175 ºC and 225 ºC, hence the temperatures of exposure in these experiments performed with this equipment are effective for geothermal purposes.

Moreover, the heat controller also visible displays the temperature transmitted to the aluminum block and the sample during the whole test, including the starting point at room temperature, in which the initial length is recorded, and the point in which the sample reaches its maximum length. Figure 24 shows the heat controller used in this investigation.

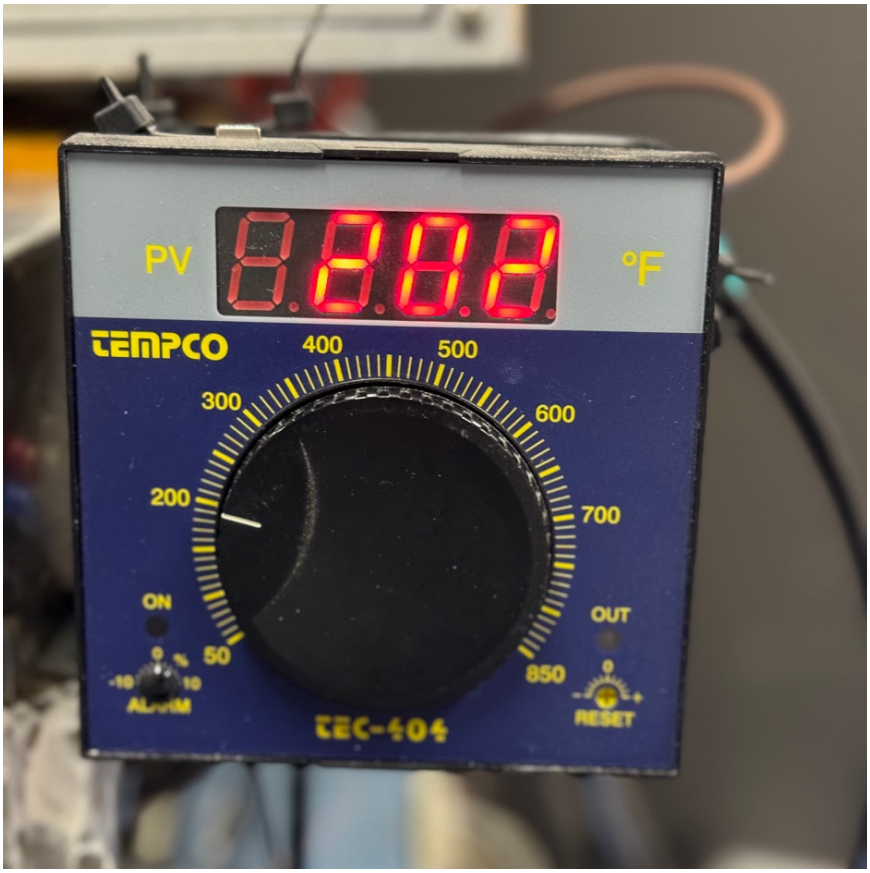

Figure 24: Heat controller used in the novel apparatus

3.1.3 Aluminum block

The aluminum block is the component of the set-up in which the sample is placed during the tests. It has a cylindrical hole in the middle, which is where the sample is positioned to be tested. Moreover, the aluminum block obtains the heat transferred from the heat controller through the resistors, and allows the sample to be heated up to the desired temperature. To effectively perform this, the aluminum block is isolated to avoid any heat losses. Figure 25 shows a closer look to the aluminum block and the cylindrical hole.

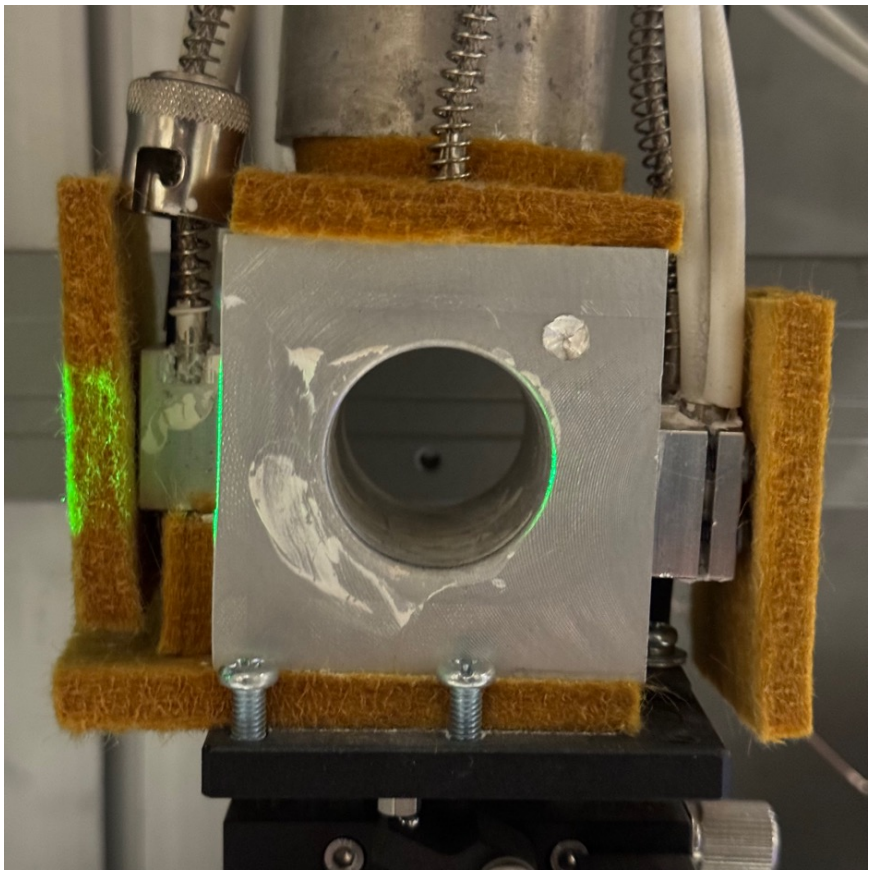

Figure 25: Aluminum block from the experimental apparatus

3.1.4 Sample

The sample is described as any material which is tested using this set-up. The shape of the sample must be cylindrical and there are two main reasons for this. First, since the coefficient of linear thermal expansion is the scope of this investigation, the shape of the sample allows a better determination of the elongation in the linear dimension. Secondly, the samples may be later used for other geomechanical investigations, such as UCS or triaxial testing. In addition, the length of the sample should lay in the range between 53 to 67 mm. Different materials, rocks and oilwell cements were tested during these investigations, and they will be described in the following chapter. Figure 26 shows one of the many samples tested in this investigation.



Figure 26: Samples used during this experiment

3.1.5 Thermometer

The thermometer is the device which displays the values of the temperature measured in the sample while the testing is ongoing. The purpose of this is to demonstrate that the sample reaches the target temperature set in the heat controller for the test. The thermometer measures the temperature in ºC degrees and is shown in Figure 27.

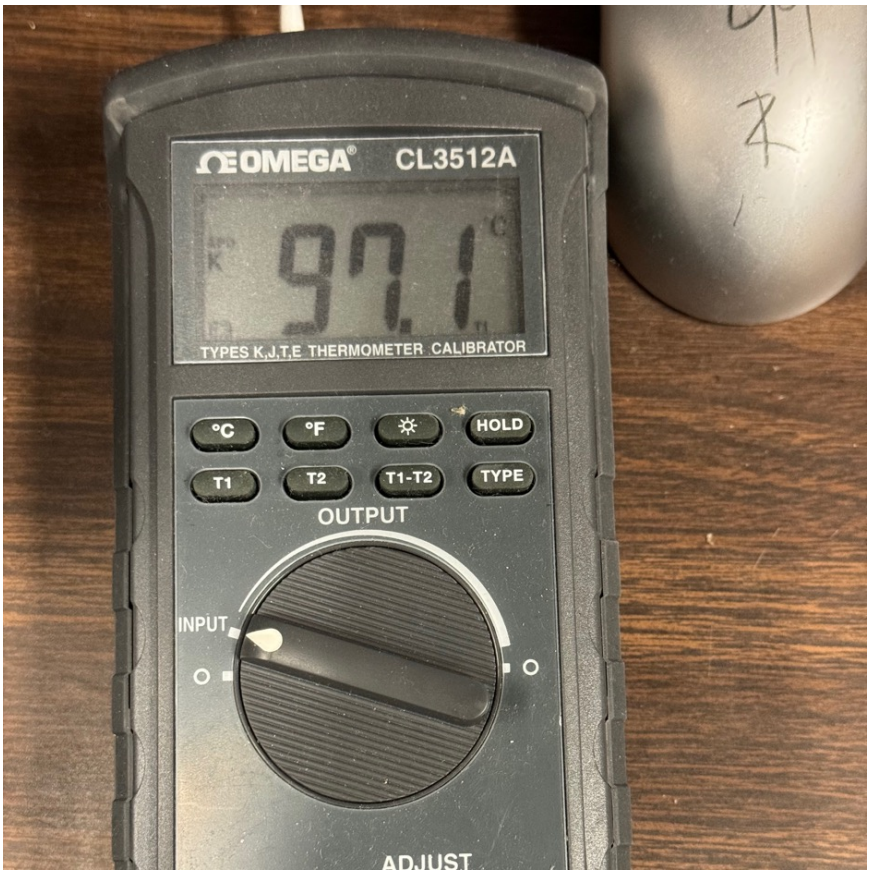

Figure 27: Thermometer used to measure the temperature on the sample

3.1.6 Data acquisition system

A data acquisition system was also adapted to this set-up to provide a data recollection. The software used with this data acquisition system is DasyLAB, and it records the length and four different temperatures along the aluminum block. The four different temperatures are recorded by using four different thermocouples, which are placed in different spots of the aluminum block. A better description of this will be provided in the methodology found in the next chapter. The main purpose of measuring these four different temperatures is to demonstrate a uniformly distributed temperature in the whole aluminum block, hence, in the sample tested. Figure 28 shows the data acquisition system used in this investigation.

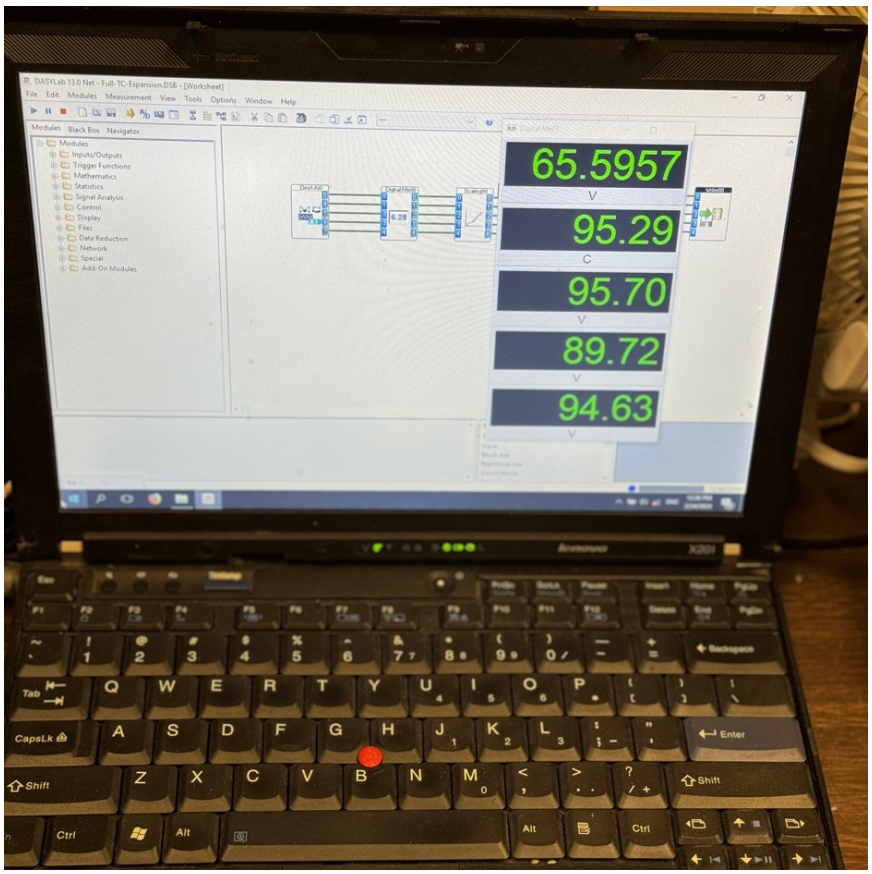

Figure 28: Data acquisition system used in this investigation

3.2 Apparatus overview

This apparatus, designed to measure the coefficient of linear thermal expansion (CLTE) by measuring the physical properties of length and temperature. The equipment has advantages as well some limitations in comparison with other equipments used to measure this thermal property. This is listed as follows.

3.2.1 Advantages

- Fast measurement
- Temperatures up to 600 ºF
- Cyclic testing is possible
- High accuracy
- Allows measurement of other properties afterwards due to the shape of the sample
- Non-destructive test

3.2.2 Limitations

- Cylindrical shaped samples
- Limitation in the length of the sample – range goes from 51 mm to 67 mm
- Tests only performed at atmospheric pressure

Despite the limitations, this apparatus has shown reliability in measurements performed in different materials, in accordance to the literature. It is important to mention that some of the values

obtained and present in the literature are resultant of experiments that take place for hours, making this set-up really convenient for such measurements. The methodology of work is described in the next chapter of this investigation.

Chapter 4. METHODOLOGY

To effectively measure the coefficient of linear thermal expansion, by using this novel apparatus, there is a sequence of steps which have to be followed before testing. These steps are described in the workflow shown in Figure 29.

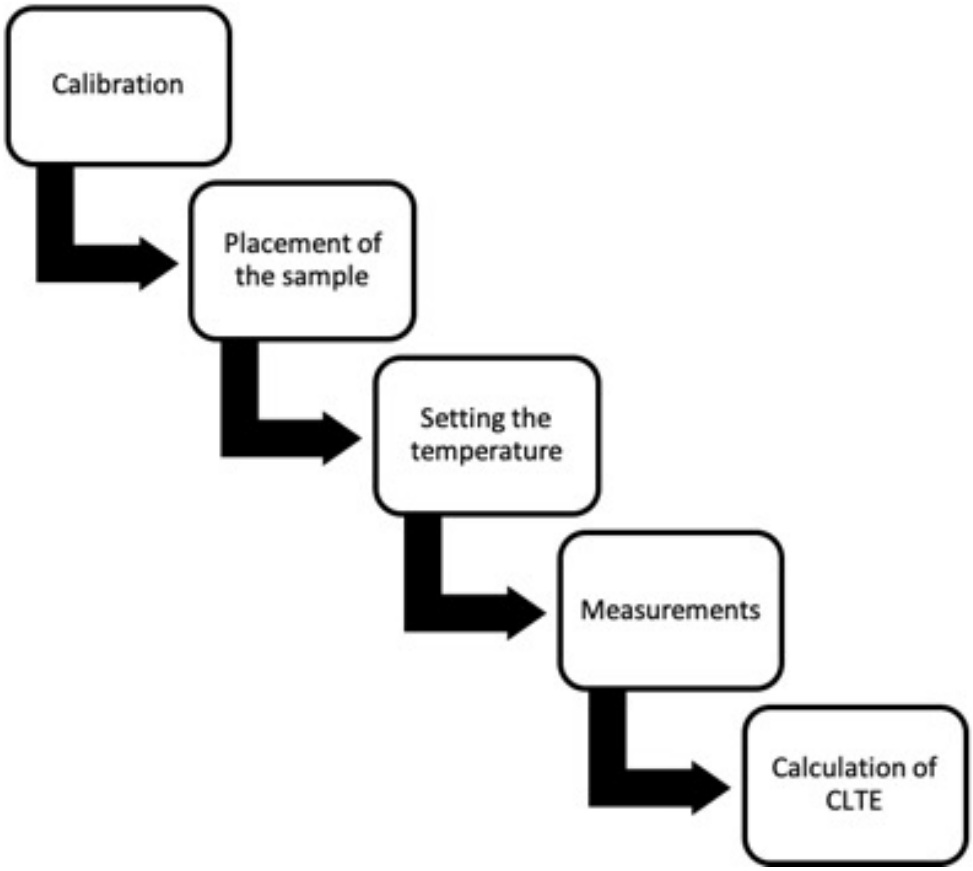

Figure 29: Workflow performed during this investigation

It is important to mention that the placement of the sample, setting of temperature, measurements and calculation of CLTE are performed in the same way when calibrating the apparatus and when experimenting with other different materials. The process, however, requires for the apparatus to

be first calibrated in order to provide accurate results for the other tested materials. Additionally, all the experiments were conducted in a cyclical way, with the exception of cement composites which were tested both in a cyclical way and in a non-cyclical way; which will be later described in this investigation. The individual explanation of each one of the steps is described as follows.

4.1 Calibration

The first step in the procedure performed to calculate the coefficient of linear thermal expansion of different materials, is to calibrate the apparatus. The calibration is fundamental since will provide accurate results out of the experiments, as well as the different coefficients of linear thermal expansion (CLTE) measured for each individual sample. The calibration uses a reference material, with a known coefficient of linear thermal expansion, found in different literature. Once the sample is tested, these CLTE values are compared with the CLTE values measured by the apparatus. If the results are similar, the set-up is said to be calibrated and ready to perform experiments with other materials. Additionally, the accuracy of both the micrometer and the heat controller is taken into consideration when calibrating the system and therefore in all the measurements performed afterwards.

The calibration starts by placing the sample in the aluminum block. The micrometer, with the help of the laser beams, measures the initial length of the sample at room temperature and atmospheric pressure conditions. Once this has been measured, the temperature is set with the heat controller and is constantly applied. The system starts being heated up to the set temperature for one hour, and it reaches a steady-state within this time frame. Under these high temperature exposures, the length and temperature are continuously monitored and measured by the micrometer, heat

controller and data acquisition system, which gathers the data of the experiments. The initial length and temperature, measured at the beginning of the exposure; the final length, which is the maximum length measured during the one hour, and final temperature which is the temperature measured when the maximum length occurs, are then used for CLTE calculations. Further explanations of the calibration procedure are found in a previous study (Toledo Velazco et al., 2023).

In this investigation, two different materials were used to calibrate the system, which are aluminum and brass. The reason behind the utilization of two materials, is to fully corroborate the calibration of the apparatus, by having two references, instead of just one. In addition, the materials selected to calibrate the system are metallic materials. Metallic materials are homogenous and provide good thermal conductivity; hence the measured values of coefficient of linear thermal expansion are going to be more effective when comparing them with values found in the literature. The CLTE values obtained for both the aluminum and brass are shown as follows.

4.1.1 Accuracy of the equipment – Calibration

Initially, the accuracy of both the micrometer and the heat controller need to be taken into consideration when calibrating the equipment for reliable CLTE values. The % of measurement accuracy provided by the micrometer, which reads the length, is of ±0.0030 mm whereas the heat controller has an accuracy of ±2% at the temperature setpoint, therefore, the accuracy of the coefficient of linear thermal expansion (α) measured via this equipment is ±1.2%. Figure 30 displays an error plot for CLTE values of an aluminum bar used for calibration with the % of error obtained from the equipment for CLTE and temperature.

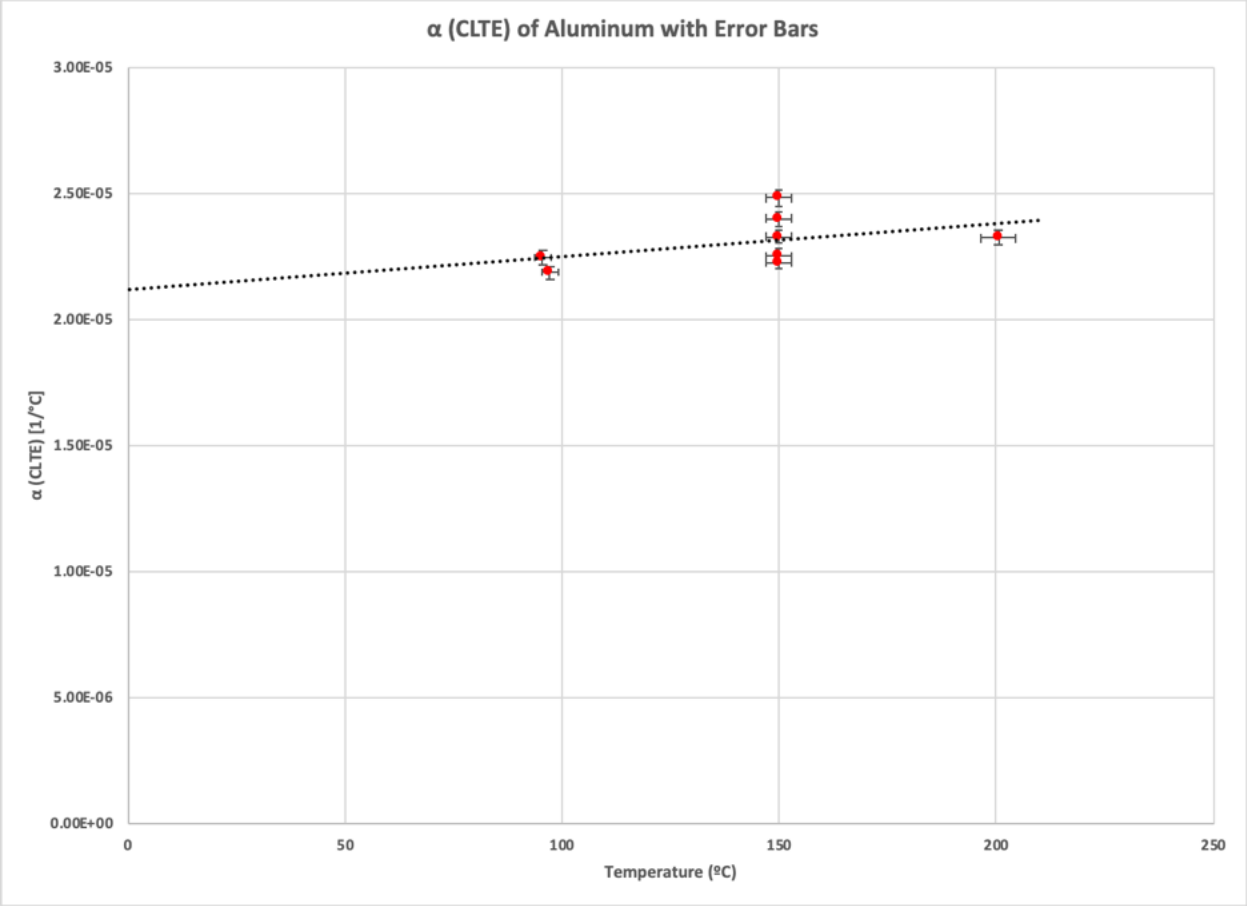

Figure 30: CLTE of aluminum with error bars for accuracy – Calibration purposes

From the Figure above, it can be seen that the measurements from temperature and, especially the CLTE, which are also discussed in the following section, are in a close range from the values present in the literature. Moreover, the error provided by the equipment is minimum, hence the measurements gathered from the samples are highly accurate. Therefore, to fully calibrate the equipment, the next step is to compare the measured CLTE values from the reference samples with the values from the same materials, found in the literature.

4.1.2 Aluminum – Calibration

The CLTE values previously obtained from the aluminum sample, which was used as reference material for calibration purposes, are compared with the values in the literature. As mentioned in previous publications (Toledo Velazco et al., 2023; Toledo Velazco et al., 2024, Toledo Velazco et al., 2024), and shown in the Figure 31, the CLTE values were in the range between 2.1 to 2.5E-05 [1/ºC]. These values are in accordance with values of 2.3E-05 [1/ºC] provided by ASM and Davies (1998) and the range of values between 2.1 to 2.5E-05 [1/ºC] provided by The Engineering Toolbox (2023).

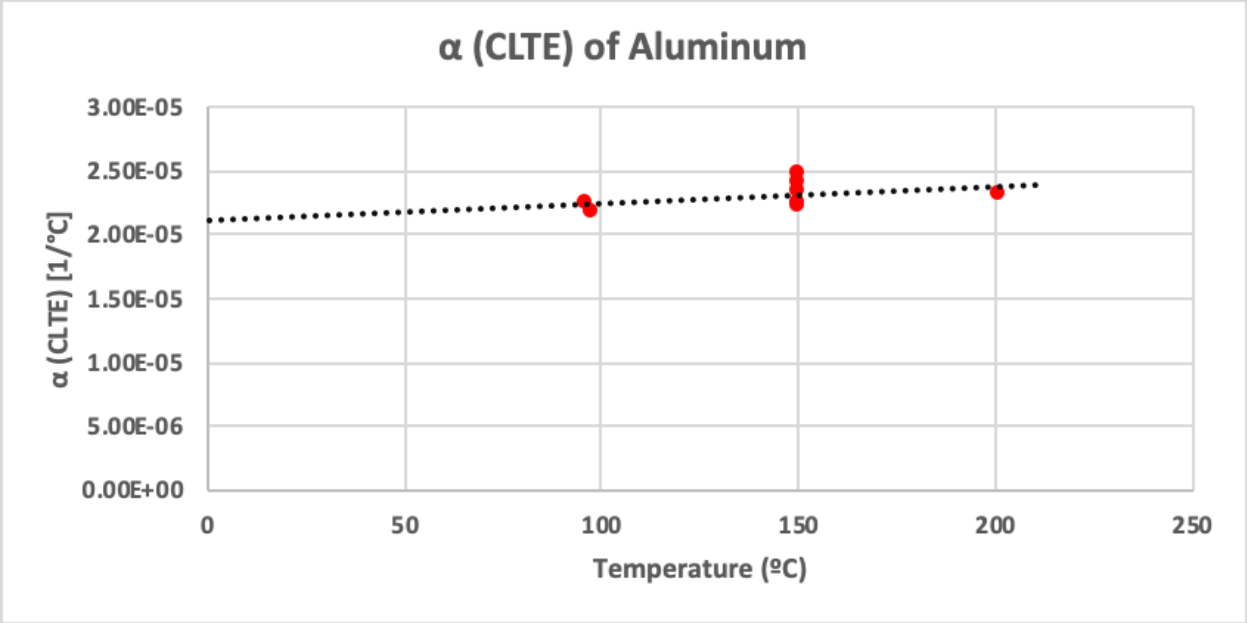

Figure 31: CLTE values for Aluminum – Calibration purposes

4.1.3 Brass – Calibration

The second reference material which was used to calibrate the set-up was brass. Brass, according to The Engineering Toolbox (2023) has values of CLTE in the range between 1.8 to 1.9E-05 [1/ºC].

ASM and Davies (1998) provided CLTE values of 2.03E-05 [1/ºC]. Figure 32 shows the results obtained with the novel experimental set-up. It can be seen that the CLTE values lay in the range between 1.8E-05 [1/ºC] to 2.0 E-05 [1/ºC].

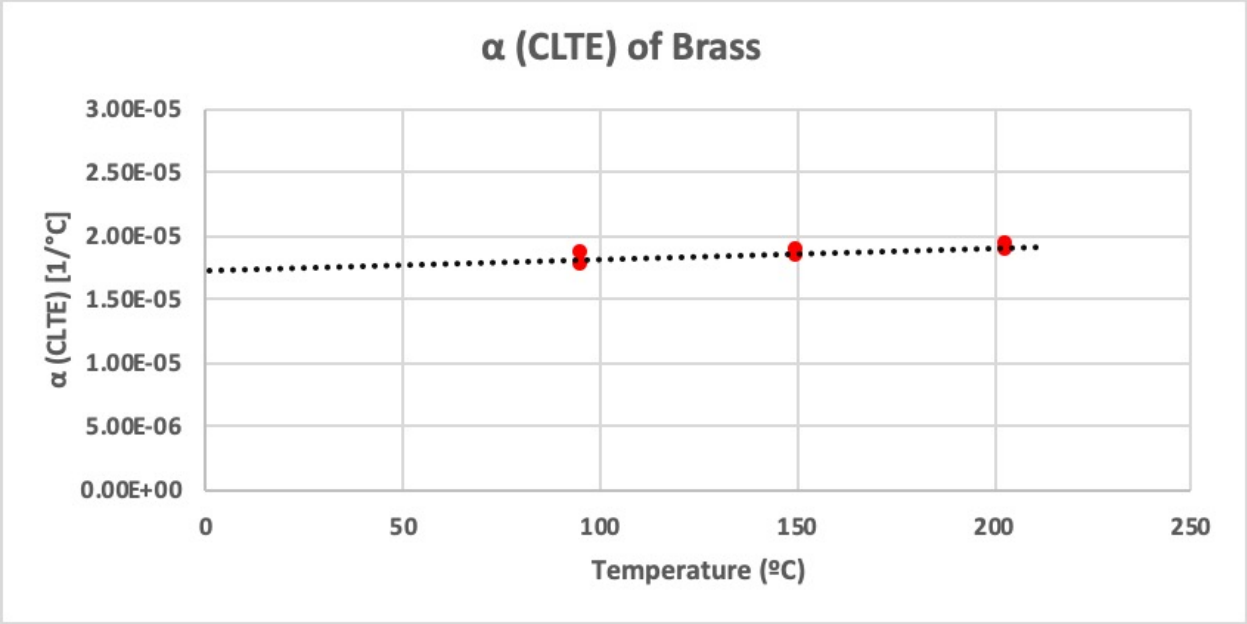

Figure 32: CLTE values for Brass – Calibration purposes

The coefficient of linear thermal expansion results obtained while calibrating, for both aluminum and brass, have shown a strong relationship with the different values present in various literature. This, while also taking the low percentage of error when measuring both the length and temperature into consideration, allows us to gather reliable and accurate results.

4.2 Placement of the sample

The next step in the methodology is to place the sample in the aluminum block, which is a step also performed in the calibration of the apparatus. Once the sample is placed, the length, which has to be in the range between 51 to 67 mm, is measured by the micrometer and the laser beams.

4.3 Setting the temperature

The setting of the temperature occurs right after the placement of the sample and the initial measurements in the system. In this investigation, the temperature is set in the range between 150 ºC to 200 ºC (200 ºF – 400 ºF) although higher temperatures are possible. The temperature is transferred to the aluminum block, via some resistors and is constantly applied during the whole experiment. Once the hour of testing has passed, the temperature is turned down, and the system is cooled down to room temperature.

To verify an effective heat transfer, some thermocouples were placed in the aluminum block as described previously in this investigation. Figure 33 shows four different plots with the measurement and the distribution of the four different temperatures measured with the thermocouples on the aluminum block, with one plot referring to the length of the sample. This was recorded by the data acquisition system.

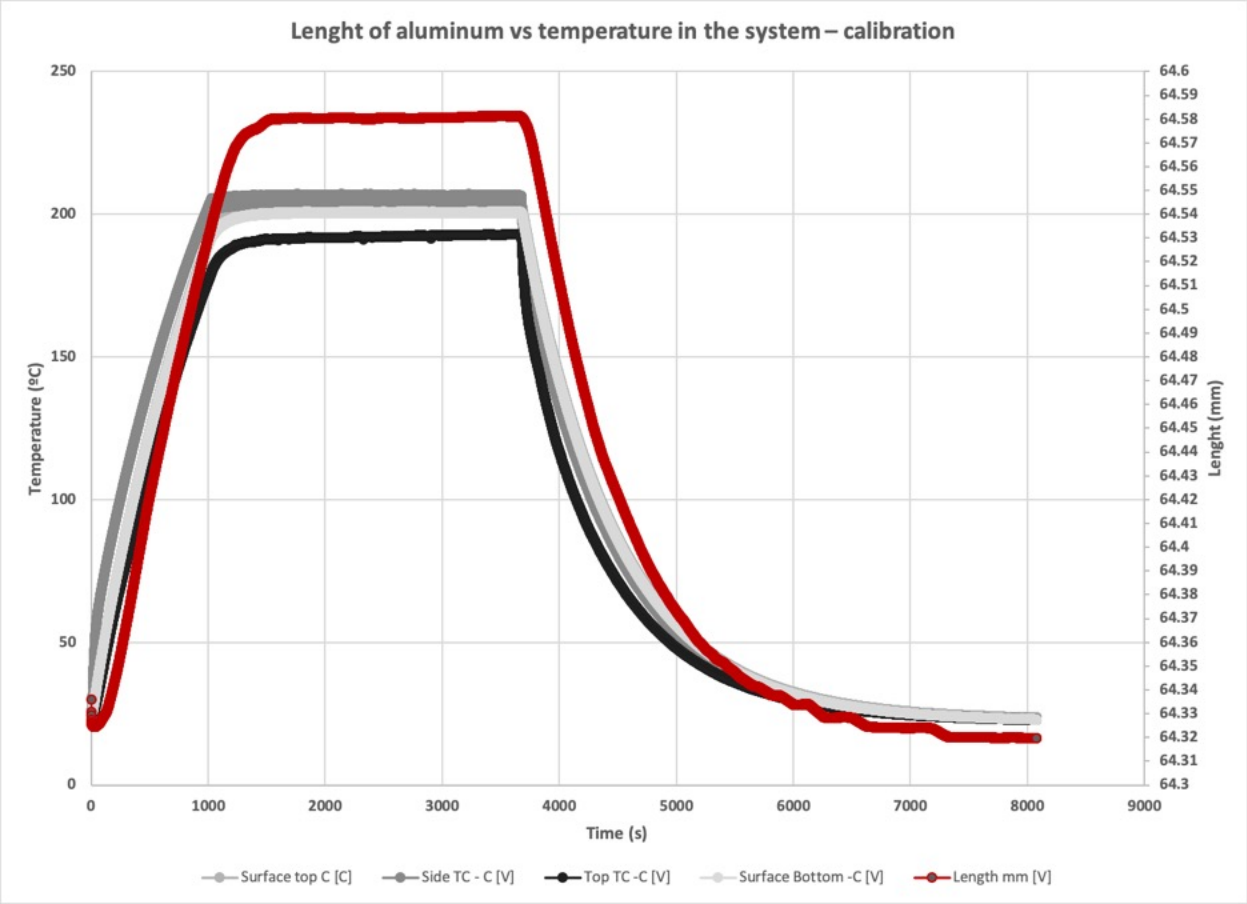

Figure 33: Temperatures with their distribution along the aluminum block and length of the sample versus time

It can be seen how the temperatures are in the same range, hence the temperature exposure is effective towards the block during the entire experiment. The description of each one of the plots is the following:

- Silver plot shows the temperature on the surface top of the aluminum block
- Gray plot shows the temperature on one of the sides of the aluminum block.
- White plot shows the temperature on the surface bottom of the aluminum block.
- Black plot shows the temperature at the top of the aluminum block.

- Red plot shows the length of the sample, during the experiment, in this case the sample was aluminum.

From Figure 32 above, which is from one of the calibrations performed, it can be noticed how the heat is effectively transferred towards the sample. In this calibration, an aluminum sample was heated up to 200 ºC (400 ºF), for one hour, with the aluminum block reaching that temperature within that time. The sample expanded along the increment in temperature, and reached a steady-state point, as described previously in the methodology. Once the hour passed, the system was cooled down and the aluminum block went back to its initial length. These steps are also applied in the other samples tested in this investigation.

4.4 Measurements

After calibrating the system, placing the sample in the aluminum block, and setting the temperature, the measurements take place. Based on the Equation 2, initial and final length, as well as initial and final temperature are needed for CLTE calculations. This are obtained as described now:

- Initial length is the length measured by the micrometer right after placing the sample in the aluminum block, and before the test
- Initial temperature is the temperature in the system micrometer right after placing the sample in the aluminum block, and before the test
- Final length is the maximum length measured during the test, which normally occurs at the same time when the maximum temperature is reached

- Final temperature is the temperature measured when the final length is achieved. Final temperature usually corresponds to the temperature set (target high-temperature) by the heat controller once the sample is placed in the aluminum block

The measurements occur within the time-lapse of one hour, in which the system reaches the set and desired high-temperature and hence the final length is acquired. This is followed by a stabilization of the system, in which, as described previously, a steady-state momentum, where the temperature and length stop increasing, takes place. When it comes to cement composites the length of the sample will also remain constant once the maximum temperature is achieved. However, and due to their properties, if any shrinkage is present, a reverse calculation is performed; in which the final length would still be the length measured after the one-hour time lapse, but the initial length would now be the length of the sample after the system is cooled down.

4.5 CLTE calculations

After performing the measurements, the CLTE is calculated by using the Equation 2. These values need to be validated with the CLTE presented in the different literature, especially for metals which have widely measured this thermal property.

4.6 Cyclic vs Non-cyclic test

As previously mentioned in the investigation, all the experiments conducted with this novel equipment were performed in a cyclical way. This means that, once the sample cools down, another experimentation takes place, hence the system is again heated up and the process described above is repeated for the material tested. However, and only for cement samples, two different approaches of testing were followed due to the interest on the impact the cyclic and no-cyclic test

may have. Figure 34 displays what the cyclic testing procedure is for cement composites, whereas Figure 35 illustrates the non-cyclic testing procedure.

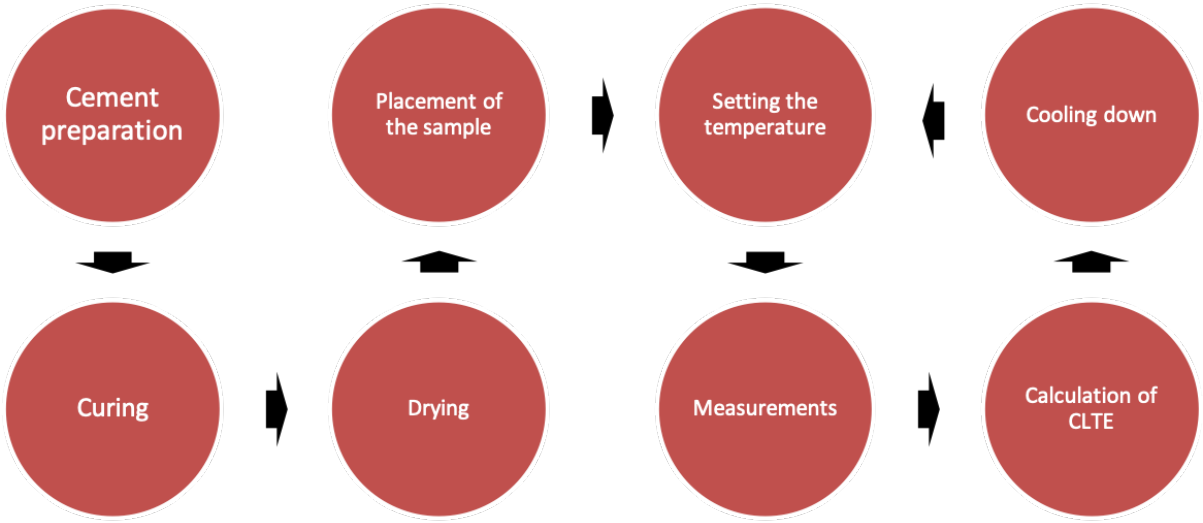

Figure 34: Cyclic testing procedure for oilwell cements

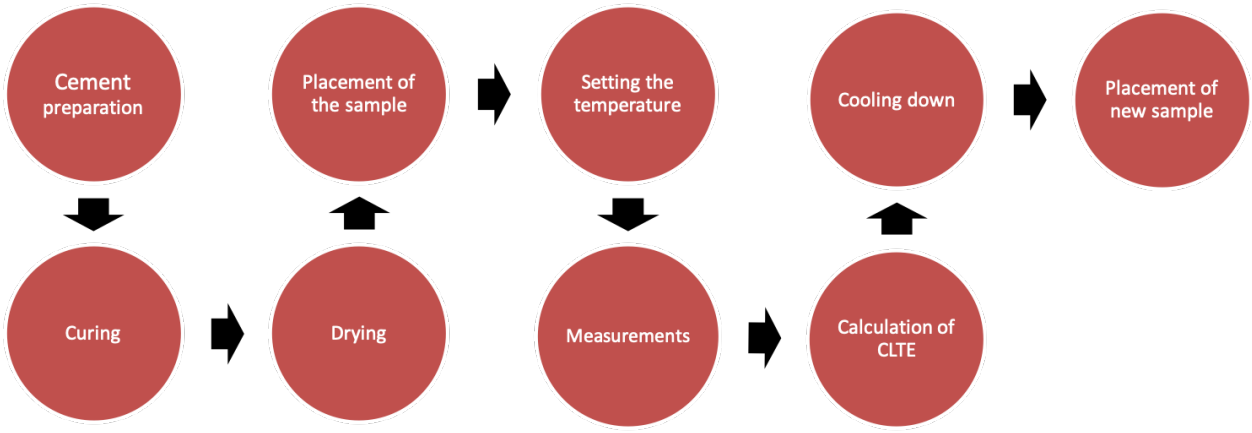

Figure 35: Non-cyclic testing procedure for oilwell cements

The results of the experiments performed throughout these investigations are fully described in the next chapter.

Chapter 5. RESULTS

Different materials were tested via this novel apparatus. After calibrating the equipment, the experiments were conducted. In this investigation, CLTE measurements of metals, other materials, rocks and cement composites are presented.

5.1 Metals and different materials

Metallics materials, as well as glass fiber, were measured with this novel equipment. The results will be described in the following sections and compared with the CLTE values present in the literature, which will allow to demonstrate the reliability of the equipment when measuring this property.

5.1.1 Brass

Brass, which was used for calibration purposes, and is also described in a previous study (Velazco et al.; 2023), was tested again to demonstrate the reliability of the equipment, and to observe if there are any variations in the values of CLTE. Figure 36 shows the CLTE values measured for Brass which lay in the range between 1.6 to 1.9E-05 [1/ºC]. In addition to the CLTE values of 2.03E-05 [1/ºC] provided by ASM and Davies (1998). Dunn (2016) provided CLTE values for Brass of 1.8E-05 [1/ºC], whereas The Engineering Toolbox (2023) has values of CLTE in the range between 1.8 to 1.9E-05 [1/ºC].

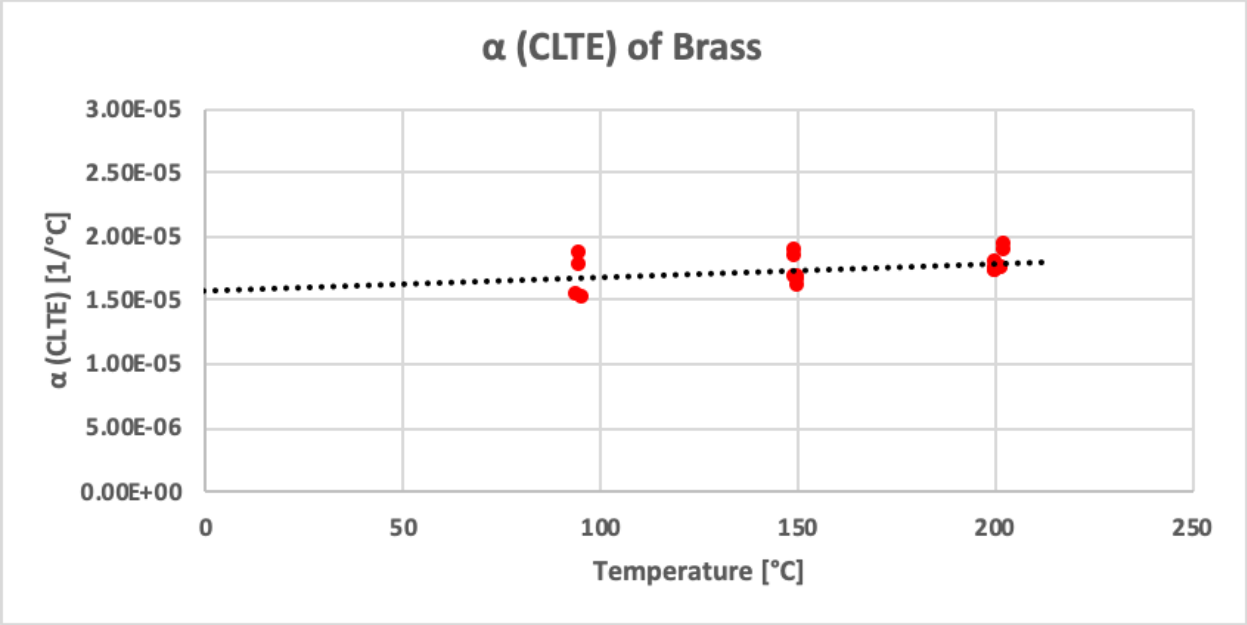

Figure 36: CLTE values measured for Brass

From the plot above, it can be seen how the CLTE values calculated for brass show a good relationship with the values in the literature.

5.1.2 Aluminum

Aluminum was another material which was used for calibration purposes. However, with the same objective when testing brass, measuring the CLTE for this material was intended to demonstrate the reliability of the equipment and to observe the variations in CLTE values. As described above and in previous studies (Velazco et al., 2023, and Velazco et al., 2024), some CLTE values for aluminum of 2.3E-05 [1/ºC] were provided by ASM and Davies (1998), whereas by The Engineering Toolbox (2023) provided values of 2.1 to 2.5E-05 [1/ºC]. In addition to these, Dunn (2016) stated CLTE values of 2.5E-05 [1/ºC].

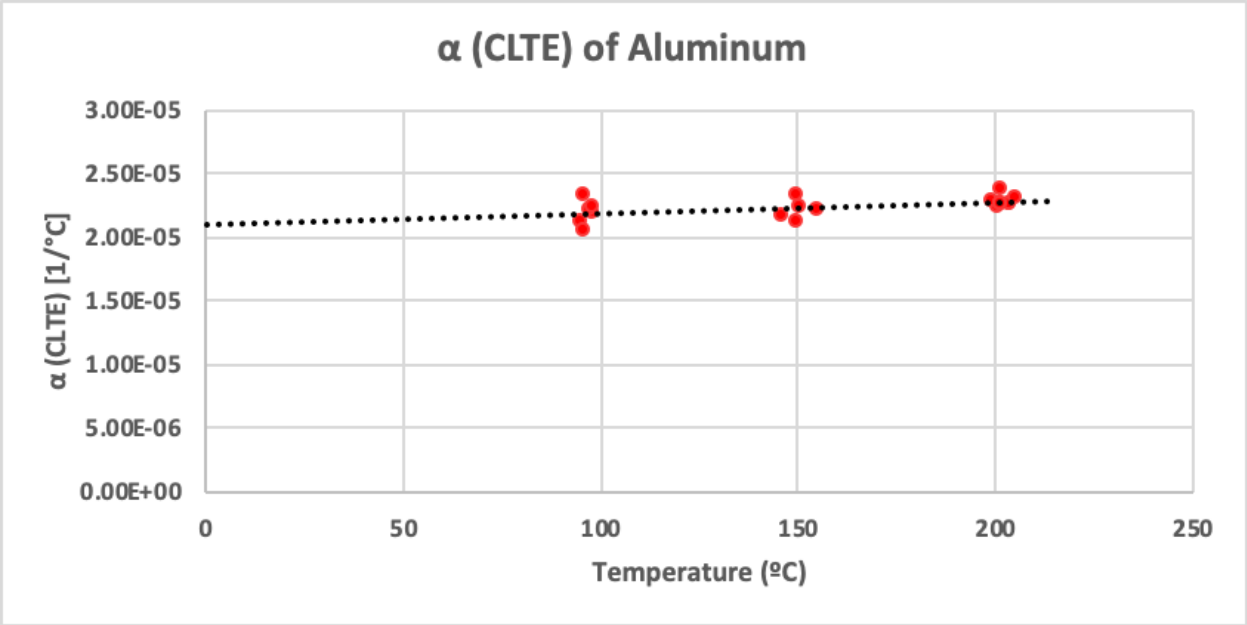

Figure 37: CLTE values measured for Aluminum

From the Figure 37 above, CLTE values for aluminum where in the range of 2.1 to 2.4E-05 [1/ºC], which is aligned with the values present in the literature.

5.1.3 Steel

For steel the CLTE values measured were in the range between 1 to 1.2E-05 [1/ºC], as shown in Figure 38. According to Tomilina et al. (2012), casing steel has a CLTE of 1.3E-05 [1/ºC], hence the results obtained are in accordance with the literature. In addition, Lewis (1994) measured steel tool with CLTE of 1.06 to 1.14 E-05 [1/ºC].

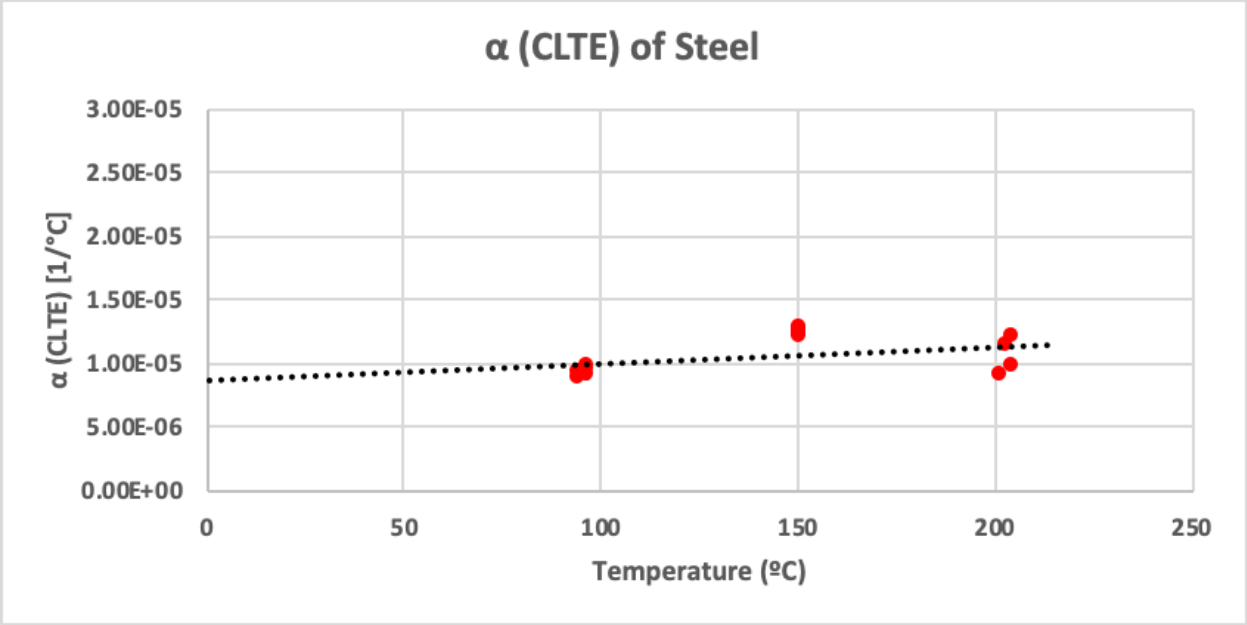

Figure 38: CLTE values measured for Steel

5.1.4 Titanium

Titanium showed CLTE values between 5E-06 [1/ºC]. to 8.5E-06 [1/ºC] as displayed in Figure 39. These values are lower than the values showed for the other metallic materials, presented previously in this investigation.

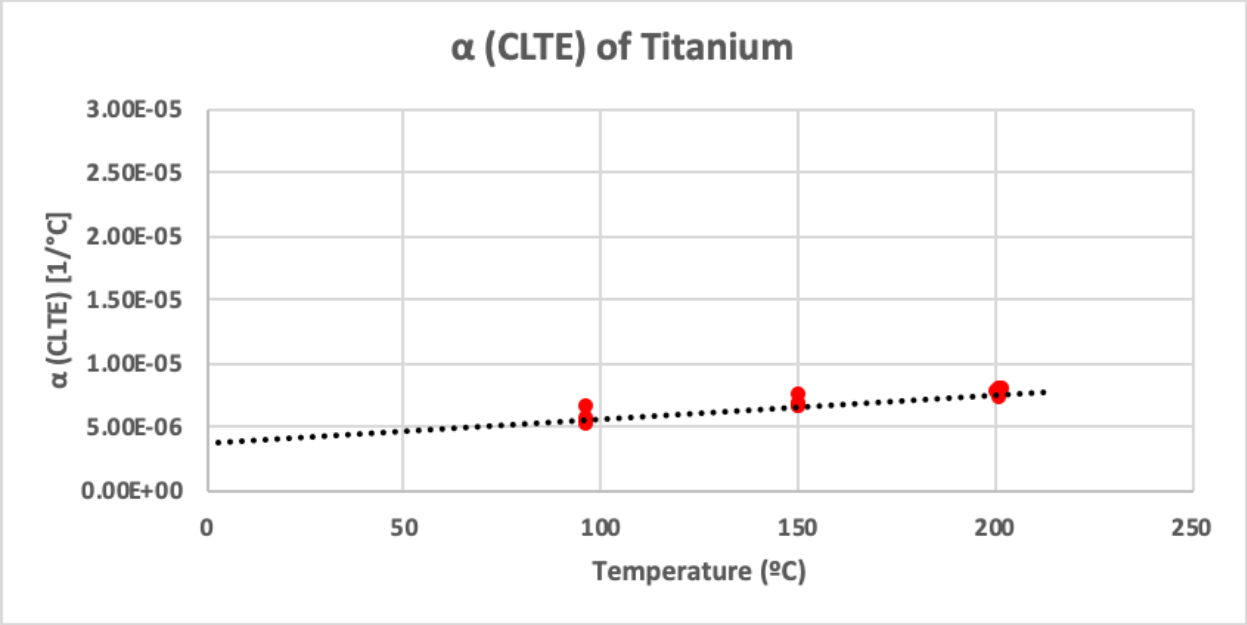

Figure 39: CLTE values measured for Titanium

5.1.5 Carbon Steel (A36)

Carbon steel was also measured. The carbon steel used was the A36, and the CLTE values measured where in the range of 1 to 1.3E-05 [1/ºC]. Figure 40 shows the plot with the measurements.

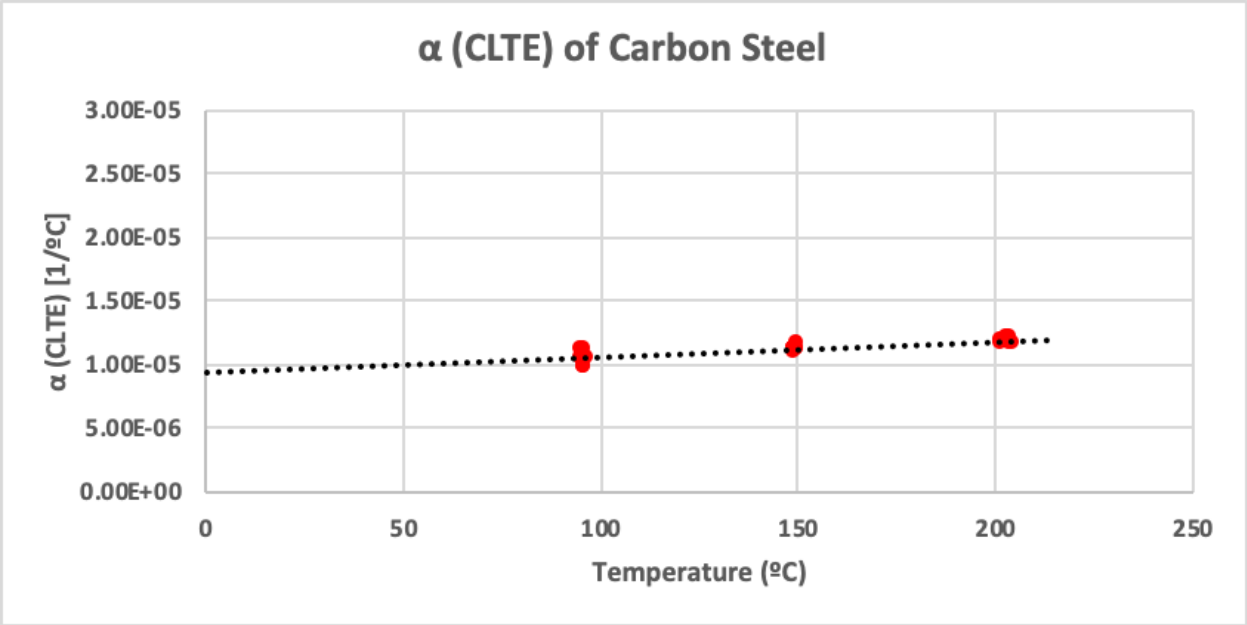

Figure 40: CLTE values measured for Carbon Steel

Depending on the type of carbon steel, Industrial Metal Supply Co. (2022) provides CLTE values for A36 Carbon Steel between 1.08 and 1.25E–05 [1/ºC]. Fatima et al. (2016), as cited from Kahraman (2007), provided CLTE values of 1.17E–05 [1/ºC]. The values obtained in this research are in accordance to the literature.

5.1.6 Stainless Steel (304)

Stainless Steel was also measured with the novel apparatus. However, there are different types of stainless steel and the CLTE varies for each one of them. In this investigation, 304 Stainless Steel was used, and the CLTE values obtained, which are also displayed in Figure 41, where in the range between 1.3 to 1.6E-05 [1/ºC]. Shrivastava et. al (2020), provided CLTE values of 1.3 to 1.6E-05 [1/ºC], and The Nickel Institute (revised in 2024), showed values around 1.26 to 1.6E-05 [1/ºC].

Martelli et al. (2013) also provided similar values with the displayed in this investigation, in the range from 5E-06 [1/ºC]. to 1.5E-05 [1/ºC].

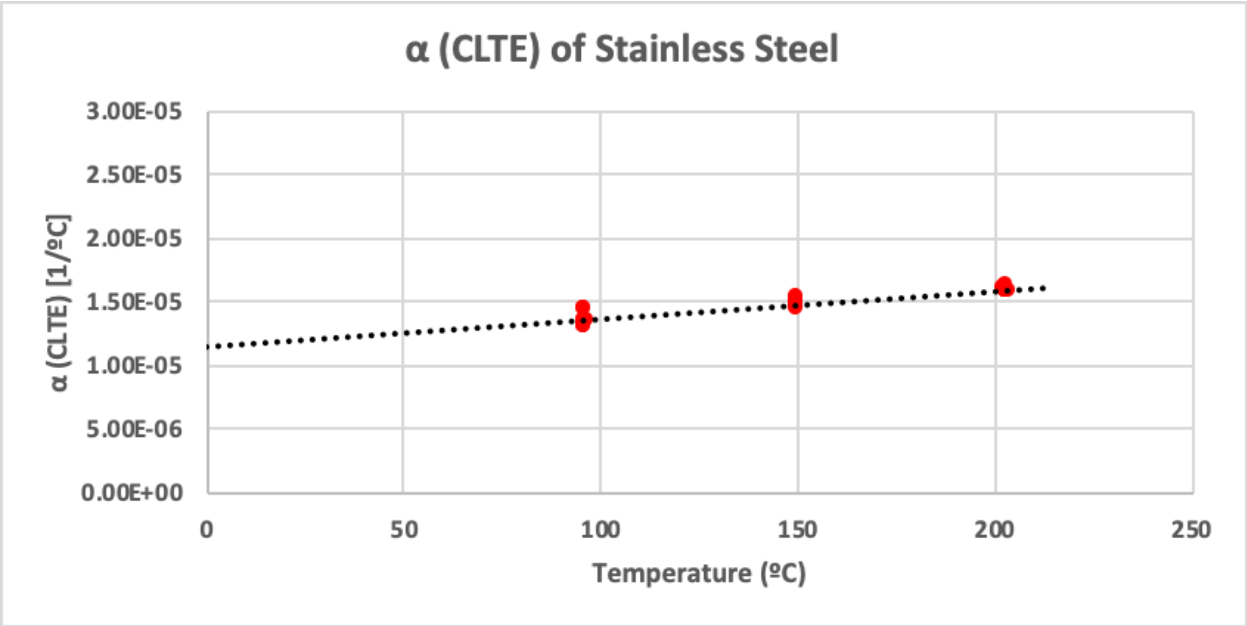

Figure 41: CLTE values measured for Stainless Steel

5.1.7 Glass Fiber

Lastly, CLTE measurements for glass fiber, which is a non-metallic element, were also performed. The flexibility provided by the apparatus allowed the CLTE calculations, which showed values in a range of 4.5 to 5E-06 [1/ºC] and are presented in Figure 42. The values are in accordance with the values provided by JPS Composite Materials (Wpengine, 2022), in which they provide an average CLTE of 5.4E-06 [1/ºC].

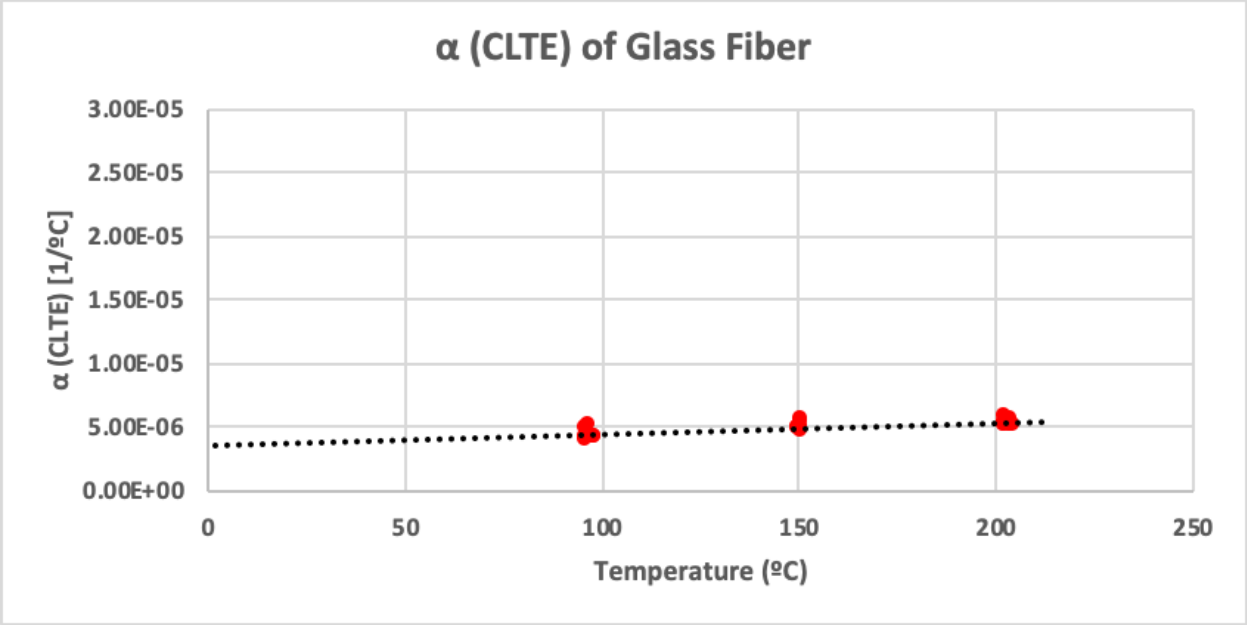

Figure 42: CLTE values measured for Glass Fiber

5.2 Rocks

The following step was to measure the CLTE for some rocks. The apparatus allows to perform some tests on rocks. However, there are some limitations to take into consideration when it comes to calculating this thermal property in rocks for this equipment. First, and as stated in the limitations, the apparatus works just under atmospheric pressure. Some investigations in the literature are performed applying confined pressure. Additionally, most of the investigations of thermal expansion are performed volumetrically, whereas the equipment is designed to measure linear thermal expansion and calculate the coefficient of linear thermal expansion.

Moreover, it is important to mention that the thermal expansion of rocks is the result of mineral thermal expansion and rock thermal fracture (Cooper and Simmons, 1977), and this equipment also doesn't allow the measurement of the expansion of the rock's minerals.

Therefore, and as mentioned previously, the research conducted determined the linear thermal expansion in a macro-scale, and as a reference, without considering the rock's minerals expansion or applying pressure on the rock. Additionally, other factors regarding the rock's properties are not also considered for this investigation.

5.2.1 Sandstone

The first rock to be measured was the sandstone. The measurements performed were quite simple, following the same procedure as before. The results, which were also shown in a previous study (Velazco et al., 2023) and are displayed in Figure 43, provided CLTE values in the range of 8.5E-06 [1/ºC] to 1E-05 [1/ºC]. The values were getting higher and constant while the temperature was being increased. The Engineering Toolbox provides a CLTE value of 1.16E-05 [1/ºC], which aligns with some of the values obtained in this investigation. A study conducted by Feng et al. (2020), provided CLTE values of 1.84E-05 [1/ºC] in a temperature range of room temperature to 600 ºC.

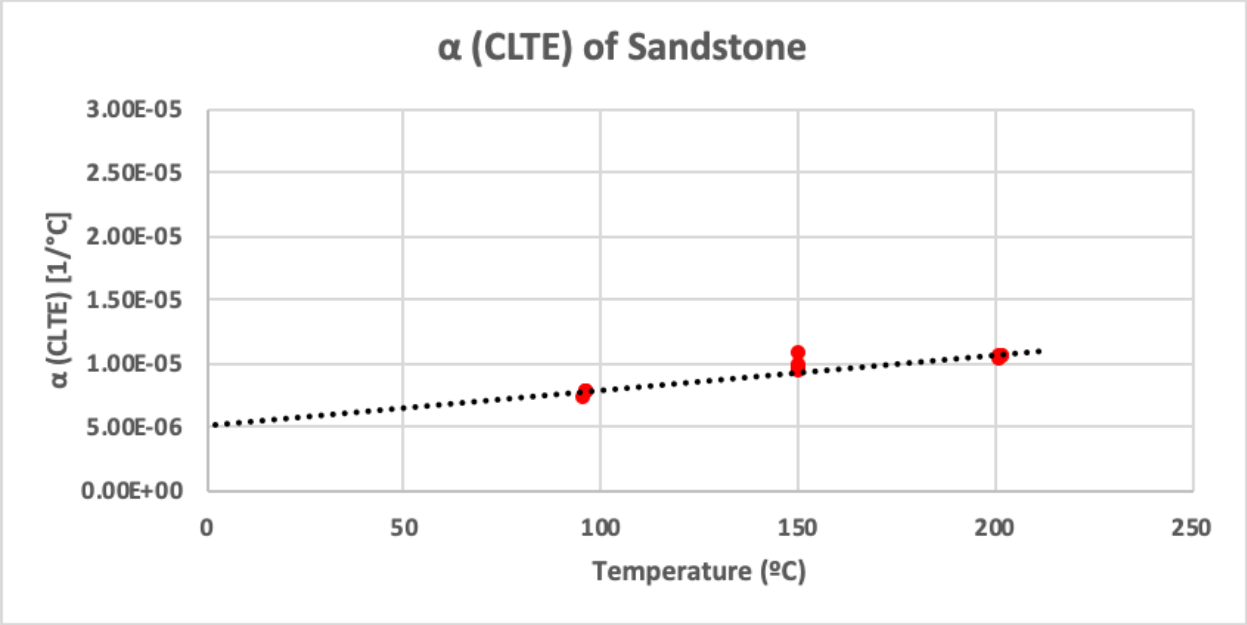

Figure 43: CLTE values measured for Sandstone

However, Feng et al. (2020) also mentions that the CLTE values may differ and are subject to different factors, such as anisotropy, size of the grains, degree of bonding, etc.

5.2.2 Granite

Granite was the second rock to be tested with this apparatus, and the results obtained are shown in Figure 44. Granite is an important rock which is present in geothermal wells, and for this reason measuring a thermal property such as thermal expansion is important. The CLTE values were in the range between 5E-06 [1/ºC] to 1E-05 [1/ºC]. The distribution showed a linear performance, in which the highest the temperature, the highest values of CLTE were measured. A review study on the CLTE value of Granite was performed by Dwivedi et al. (2008), in which they provided CLTE values of Indian Granite in the range of 1.3E–05[1/ºC], 1.4E–05 [1/ºC] and 7E–0 6[1/ºC] to 1.4E–

05 [1/ºC]. Myer and Rachiele (1981) presented CLTE values of Stripa granites in the range from 8.75E–0 6[1/ºC] to ~1.6E–05 [1/ºC] (at low confining pressure).

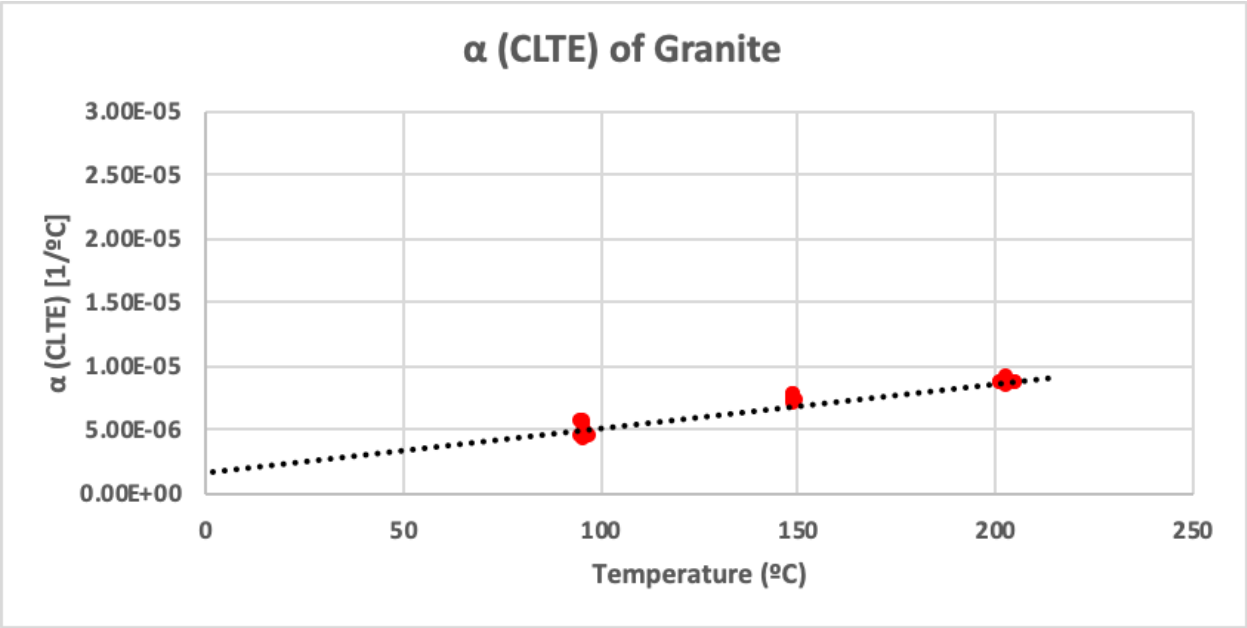

Figure 44: CLTE values measured for Granite

It can be seen how the values obtained in this investigation are similar to the values present in the literature.

5.2.3 Bandera Sandstone

Bandera sandstone was another rock measured with this apparatus. The CLTE values obtained are in the range between 7E-06 [1/ºC] and 1E-05 [1/ºC] as shown in Figure 45. Similar to the granite, the values increased when higher temperatures were applied. However, it can be seen that, similar to the sandstone measured before, a consistency in CLTE values was noticed for temperatures between 150 ºC and 200 ºC.

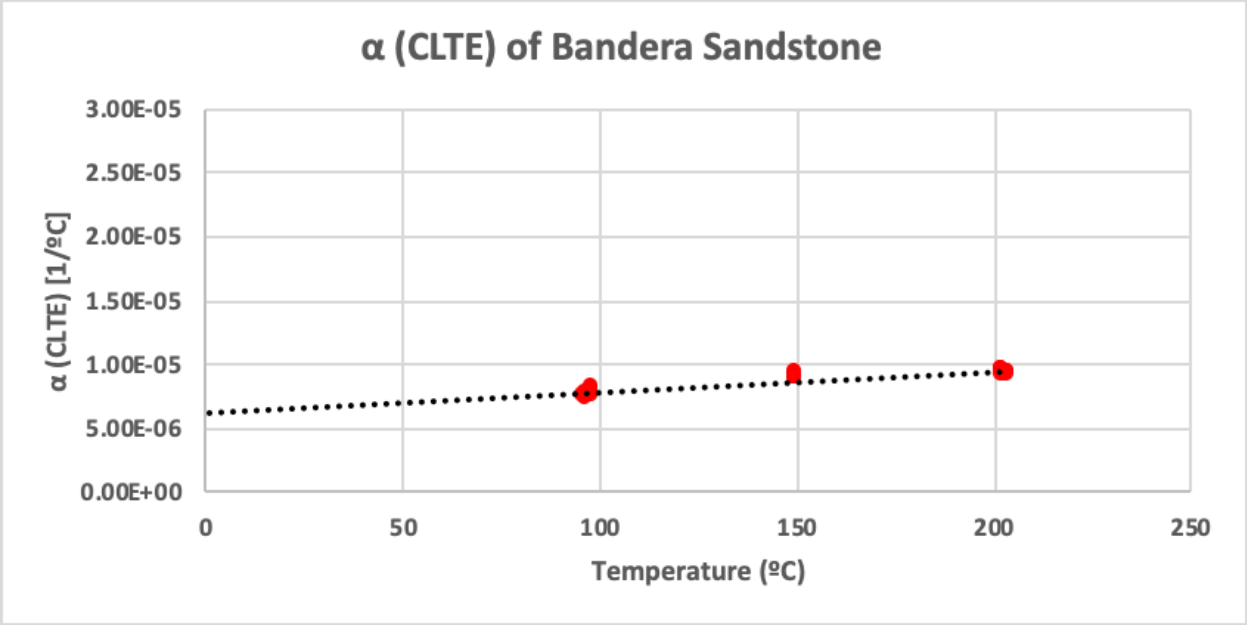

Figure 45: CLTE values measured for Bandera Sandstone

5.2.4 Carbonate

Carbonate was the last rock measured using the experimental apparatus. The CLTE values obtained are between 3.5E-06 [1/ºC] to 5E-06 [1/ºC]. Figure 46 shows how there is a linear trend in the carbonate, in which higher CLTE values are obtained when the rock was exposed to higher temperatures. The most variance can be visualized around 100 ºC (200 ºF), which were the first heating cycles of the test.

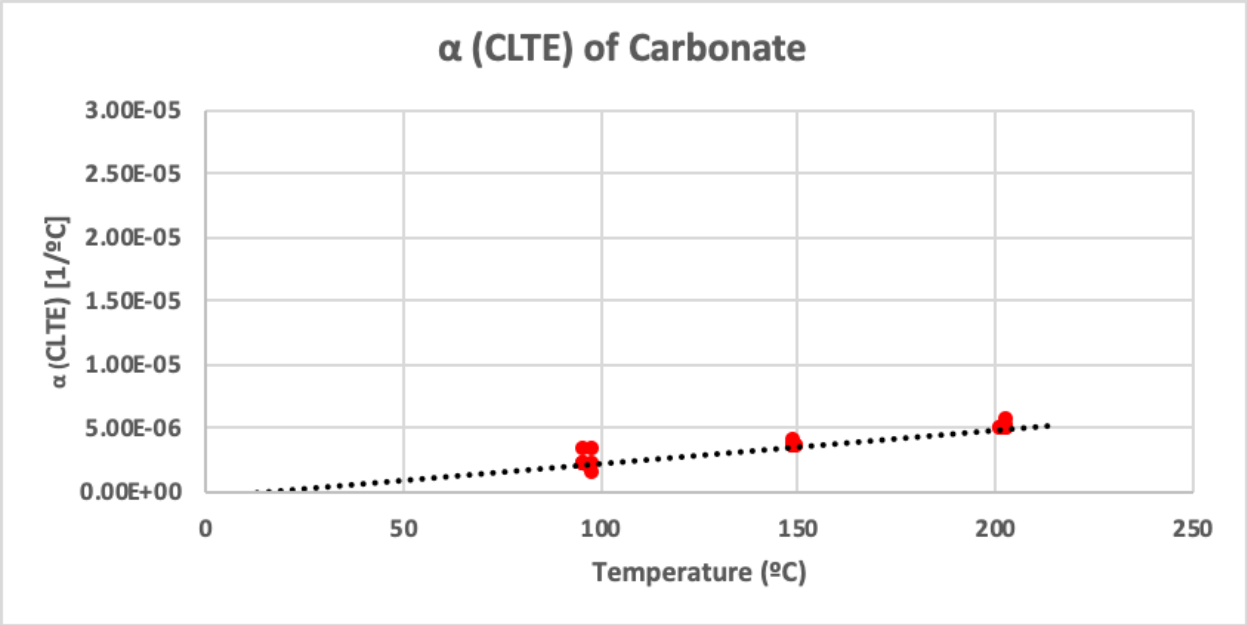

Figure 46: CLTE values measured for Carbonate

5.3 Cement composites

In addition to metallic materials, no-metallic materials and rocks, cement composites are also measured to calculate their CLTE. The measurements are performed according to the scopes, which are generated by previous analysis in the cement composites. Therefore, different analysis depending on different factors are developed when calculating the CLTE for cement composites, as described as follows.

5.3.1 Overview

First, some cement composites from different mixtures are tested and then the CLTE calculated. In this overview, Class H + 10% Gilsonite, Class H + 10% Sand and Class G + 5% Sand were analyzed. Since this were the first mixtures tested with the equipment, the curing time was

neglected and cyclic test was performed A better description of the results is shown in the following.

5.3.1.1 Class H + 10% Gilsonite

Class H + 10% Gilsonite was first measured with the novel apparatus. CLTE values showed a lot of inconsistency during the whole experiment, as displayed in Figure 47. One thing that could be noticed was the reduction in the CLTE when higher temperatures were applied in the experiment. The values were as low as 5E-06 [1/ºC] and as high as 3.5E-05 [1/ºC], with some consistent values around 1E-05 [1/ºC].

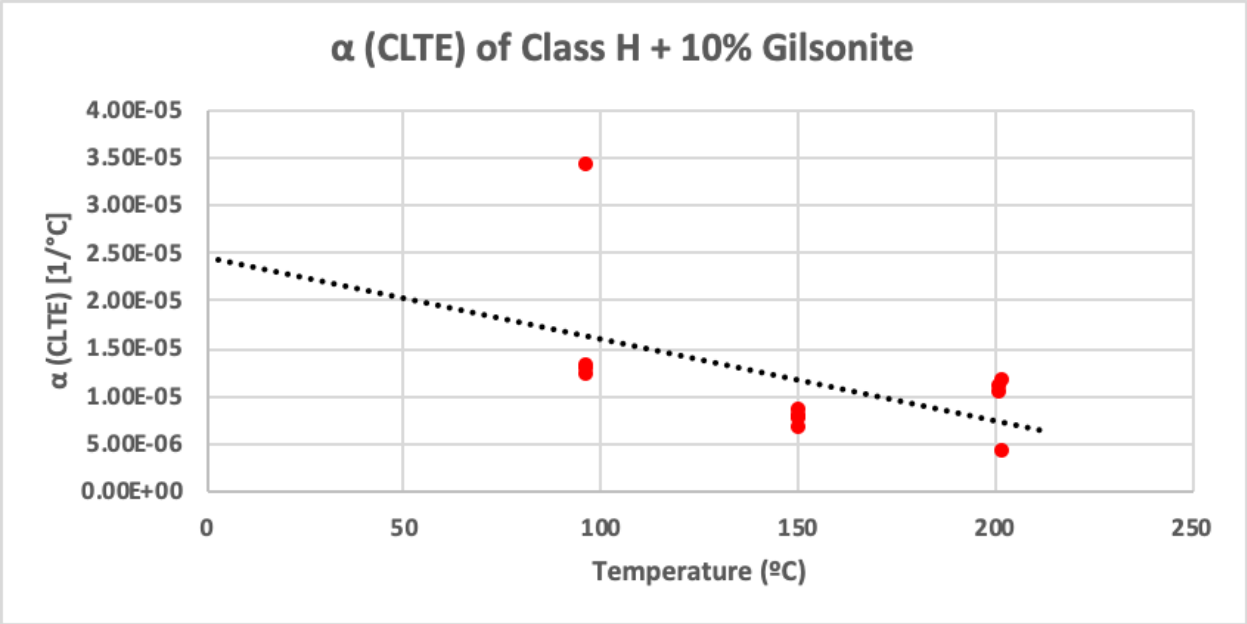

Figure 47: CLTE values measured for Class H + 10% Gilsonite

5.3.1.2 Class H + 10% Sand

Class H + 10% Sand was the second mixture tested. As shown in Figure 48, and also presented in a previous study (Velazco et al., 2023), the CLTE values measured for this mixture were in the range of 4.8E-06 [1/ºC] to 9E-06 [1/ºC], with more consistency around 7E-06 [1/ºC] to 9E-06 [1/ºC].

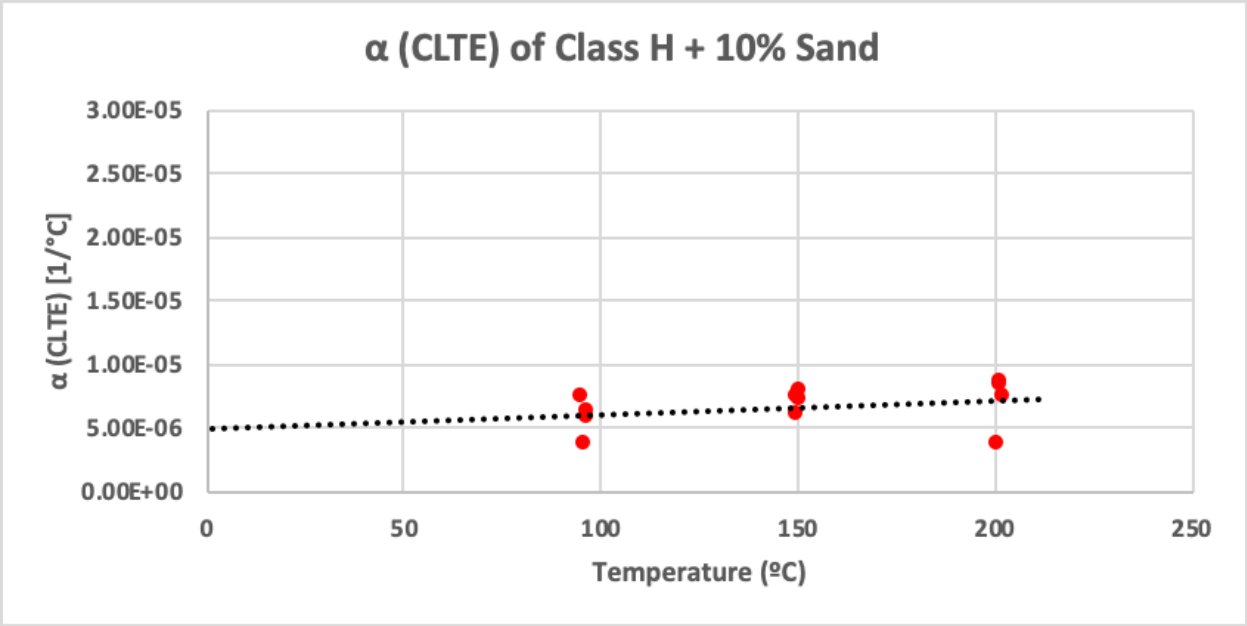

Figure 48: CLTE values measured for Class H + 10% Sand

From the results shown above, it can be perceived how the CLTE results outperformed the inconsistent values found in the previous cement mixture. Although some lower values around 4.8E-06 [1/ºC] are noticed, these are found in two different exposure temperatures.

5.3.1.3 Class G + 5% Sand

After having the difference in behavior from the first two samples, a third sample is prepared for CLTE calculations. Although it was stated above that the curing time was neglected for these measurements, the sample is known to be cured for one-year in contrast with the other two, which were cured for shorter period of time. The results are presented in Figure 49.

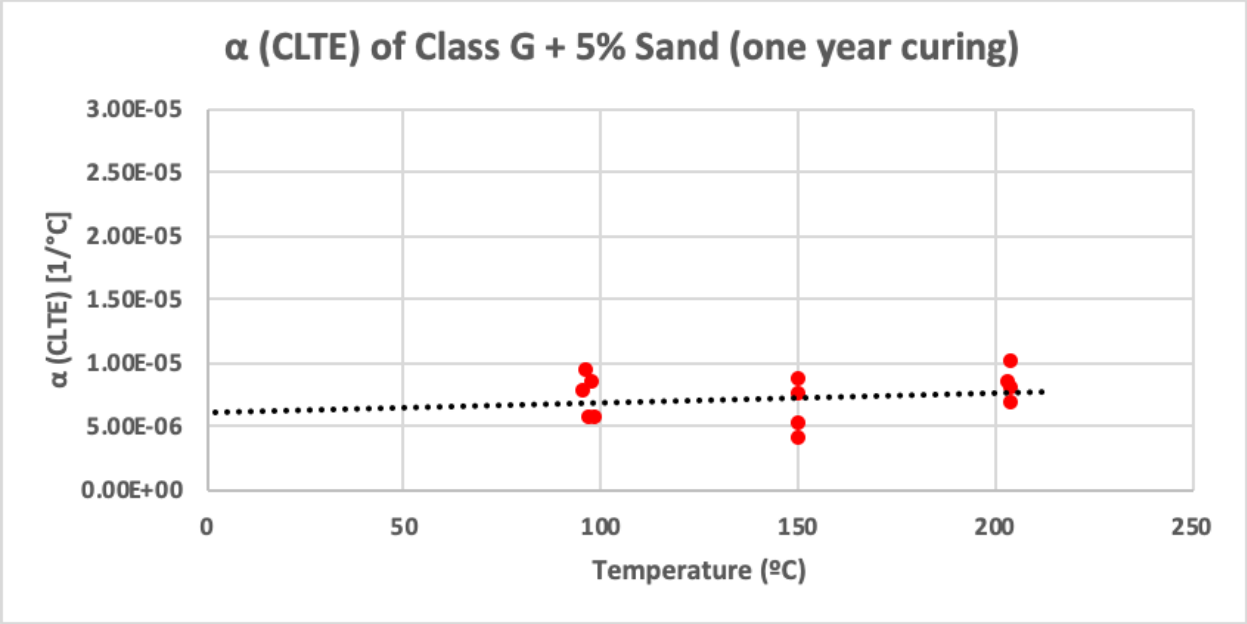

Figure 49: CLTE values measured for Class G + 5% Sand

CLTE values in the range of 5E-06 [1/ºC] to 1E-05 [1/ºC] can be noticed. The values however, show a better consistency despite the changes in temperature, laying in the same range even when temperatures where increased.

The consistent values found for this mixture, as well as Class H + 10% Sand were mostly around 8 to 9E-06 [1/ºC]. These values are in accordance to some values provided by Loiseau (2014) for

cement used in HPHT applications. Loiseau used a cement mixture of Class G + 40% silica by weight of cement, and got CLTE values around 8.8E-06 [1/ºC]. He also developed some CLTE calculations for a neat class G mixture in which he obtained values around 9E-06 [1/ºC]. Additionally, Loiseau put a lot of focus on factors such as curing time for the cement composites, hence is something which is also performed in this investigation and described in following sections.

5.3.2 No-cyclic test

After the initial CLTE measurements for cement composites, a deeper insight is needed to better comprehend the behavior of these samples when measuring this thermal property. For this reason, samples of four different cement mixtures are prepared and cured for a same period of time. The curing time used for the samples was 28 days, at atmospheric pressure and room temperature, with 7 days of drying at the same conditions. In these tests, a non-cyclic procedure was followed, meaning that each sample was tested just once. This is important to mention since the expectation is to obtain constant results, based on the procedure followed, which is the same for each one of the samples tested for each mixture.

The results, which were also discussed in a previous study (Velazco et al., 2024) are described in the following sections.

5.3.2.1 Class G (28 days curing + 7 days dry)

The first sample tested is a neat Class G. The CLTE values obtained are shown in the Figure 50.

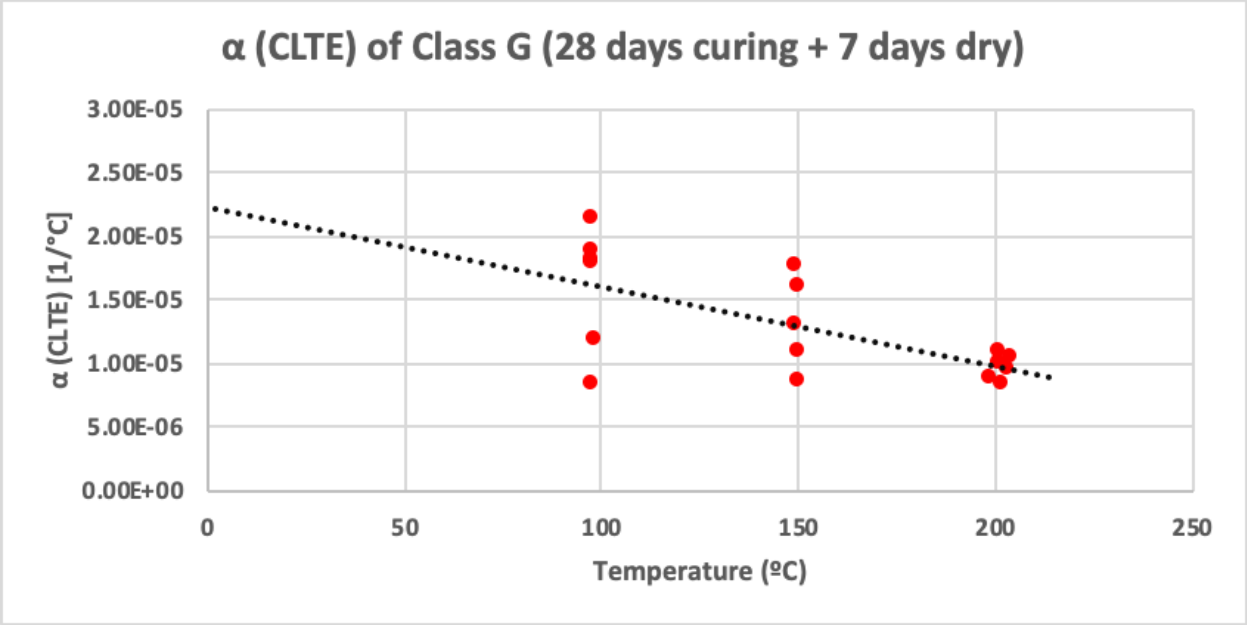

Figure 50: CLTE values measured for Class G (28 days curing time) – no cyclic testing

From the figure above, it can be noticed how CLTE values were dependent of the temperature. Values between a wide range of 5E-06 [1/ºC] to 2E-05 [1/ºC] were noticed when the exposure was at ~95 ºC (200 ºF) and ~150 ºC (300 ºF). However, when the samples were exposed at 200 ºC (400 ºF), the CLTE values were more consistent, around 1E-05 [1/ºC]. Something that can be noticed is how the wide range of values was decreasing when increasing the temperature, reaching a constant value at the highest temperature tested.

5.3.2.2 Class H (28 days curing + 7 days dry)

Neat Class H is the second mixture tested. The sample displays two different ranges of CLTE values when measured. CLTE values in a range between 1.2E-05 [1/ºC] and 1.6E-05 [1/ºC] are present when the samples are exposed to 100, 150 and 200 ºC (200, 300 and 400 ºF), as shown in Figure 51. In addition, some values range from 6E-06 [1/ºC] to 9E-06 [1/ºC].

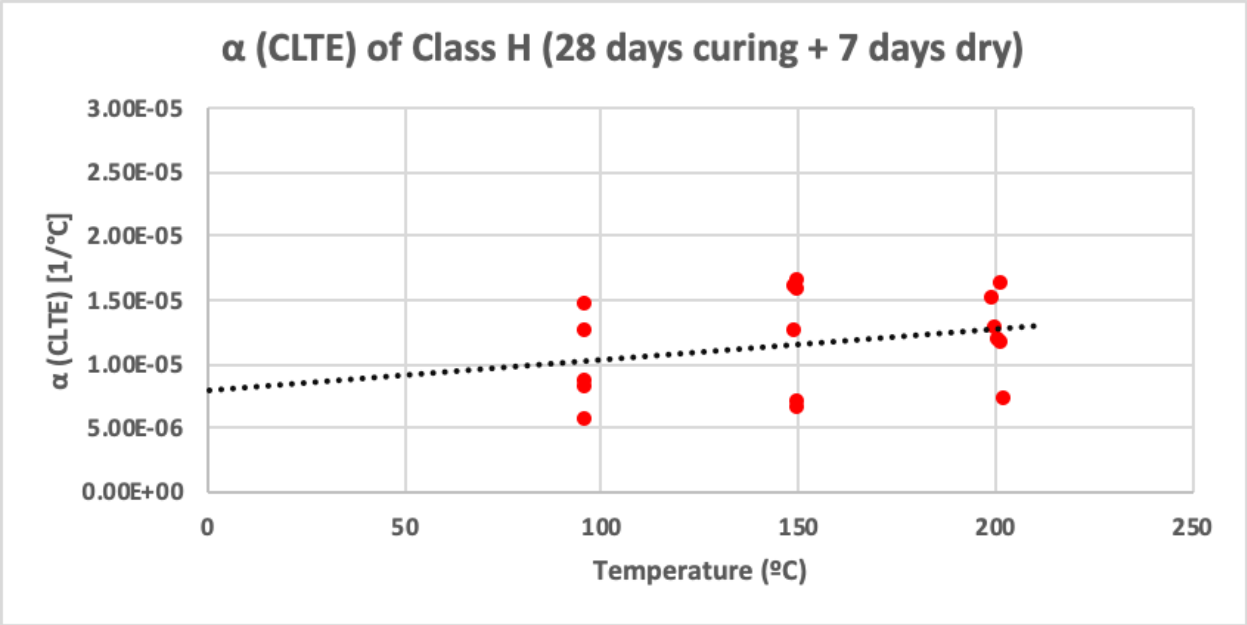

Figure 51 : CLTE values measured for Class H (28 days curing time) – no cyclic testing

5.3.2.3 Class C (28 days curing + 7 days dry)

CLTE values for neat Class C cement are presented in Figure 52. In contrast to Class G, or even Class H, the CLTE values of Class C samples are show a highest inconsistency. Some of the values for both 100 ºC (200 ºF) and 150 ºC (300 ºF) are around 8E-06 [1/ºC] to 1E-05 [1/ºC] and some go up to ~1.8E-05 [1/ºC]). However, the exposure to 200 ºC (400 ºF) shows most of the CLTE values around 8E-06 [1/ºC].

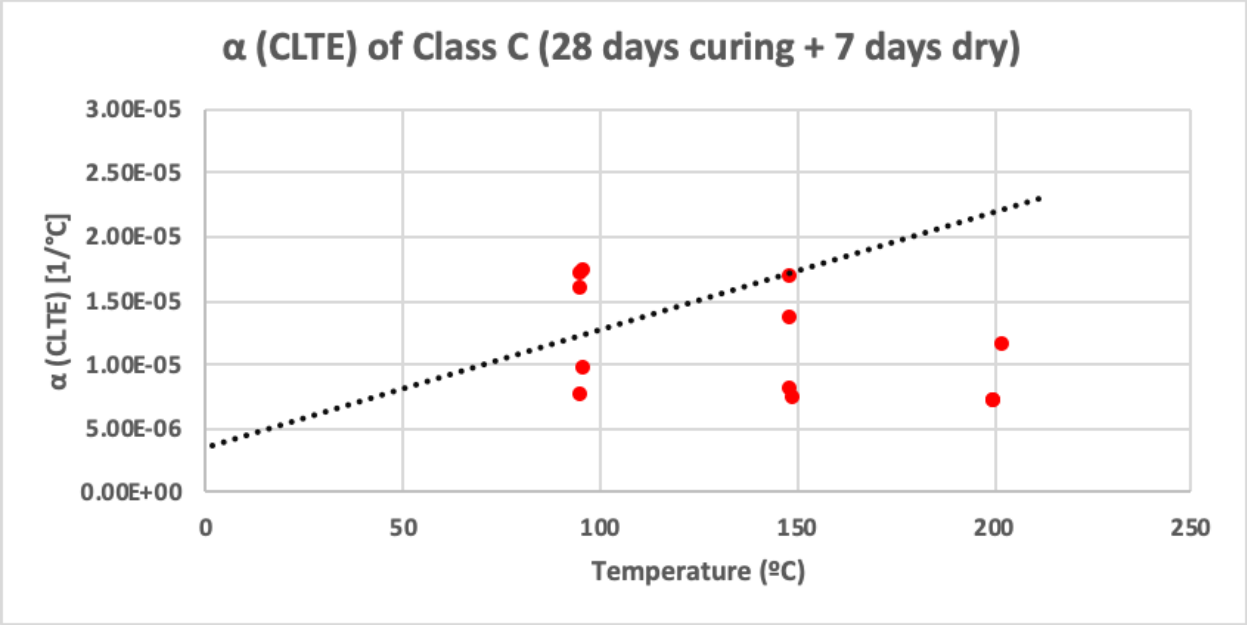

Figure 52: CLTE values measured for Class C (28 days curing time) – no cyclic testing

5.3.2.4 Class G + 40% Silica (28 days curing + 7 days dry)

Class G + 40% Silica is a mixture which, as mentioned previously, is commonly used in high-temperature high-pressure (HPHT) cement applications. The reason behind the usage of silica is the prevention of the cement's retrogression at HPHT conditions, by producing additional compressive strength (Loiseau, 2014).

The CLTE values measured in this test vary for each temperature in which the samples are exposed, as shown in Figure 53. CLTE values of 2E-05 [1/ºC] to 2.5E-05 [1/ºC] are more prominent when the testing temperature is around 100°C (200 ºF), whereas CLTE values around 1E-05 [1/ºC] to 1.5E-05 [1/ºC] are measured when the samples are exposed to 150°C and 200°C (300 ºF and 400 ºF).

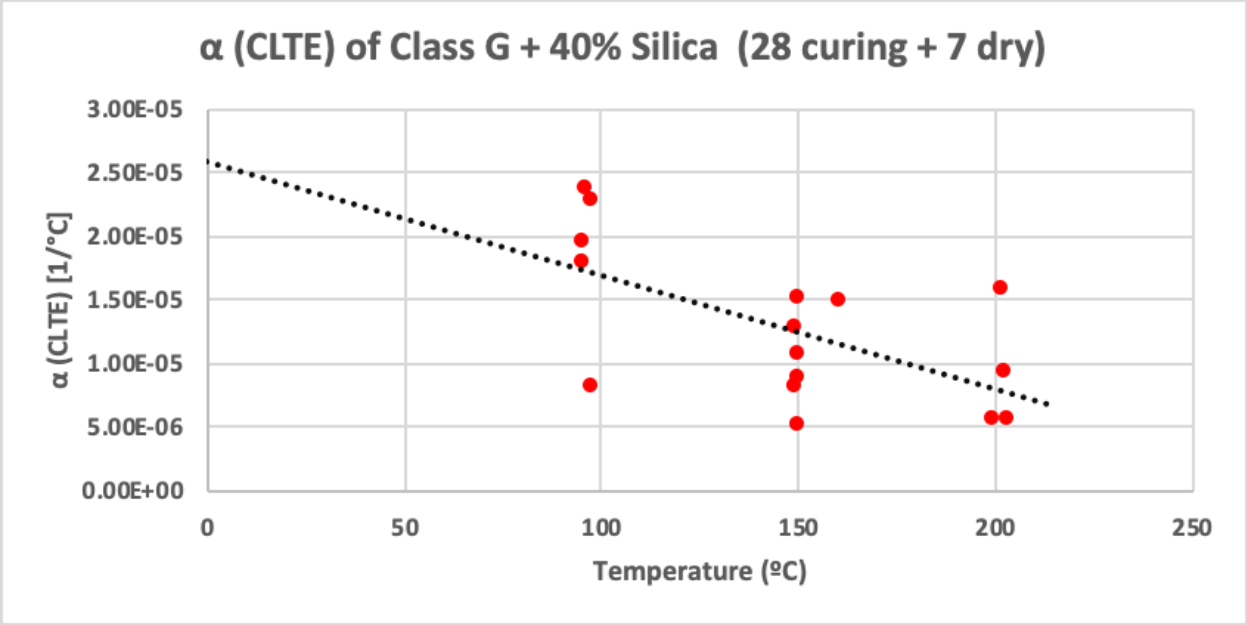

Figure 53: CLTE values measured for Class G + 40% silica (28 days curing time) – no cyclic testing

Same as the neat Class G results, the higher the temperature, the lower CLTE values are perceived. However, and despite some similarity in CLTE values, some of them differ from the ones obtained by Loiseau (2014), which used the same mixture. However, curing conditions differ from both studies. This, in addition on how inconsistent CLTE values are with just 28 days cured, give an idea in how important this factor can be in the determination of the CLTE.

5.3.3 One-year curing time versus short curing time

After calculating CLTE values for samples with 28 days curing time, and following a non-cyclic testing, the idea of curing time as an important factor in the determination of the coefficient of linear thermal expansion, is increasing. The non-cyclic test is helpful in determining that, even with the same mixture preparation and curing conditions, some CLTE values were different, which is not the expected result. Moreover, based on the CLTE results of Cement Class G + 5% Sand,

which was cured for one year; and the difference between the Class G + 40% Silica, from the values provided Loiseau (2014), a comparison following curing time is performed. Rincon (2022) showed how some mechanical properties of the cement vary depending on the curing time. Moreover, Rincon (2023) demonstrated the impact of curing time in one of the thermal properties, such as thermal conductivity, in some Class H composites. The longest curing time showed a better thermal conductivity with constant values in contrast with the samples cured for shorter time.

In this comparison, two mixtures are prepared, each following two different curing-times to visualize the difference, if something, in CLTE values. The mixtures prepared are neat Class H cement, cured for 14 days and one year, and Class G + 10% MB, cured for 21 days and one year. Therefore, a short-term curing time versus long-term curing time evaluation is effectuated.

5.3.3.1 Class H cement – 14 days curing time

Neat Class H was prepared and cured for fourteen days prior test. The CLTE values obtained for this mixture with this curing condition are shown in Figure 54.

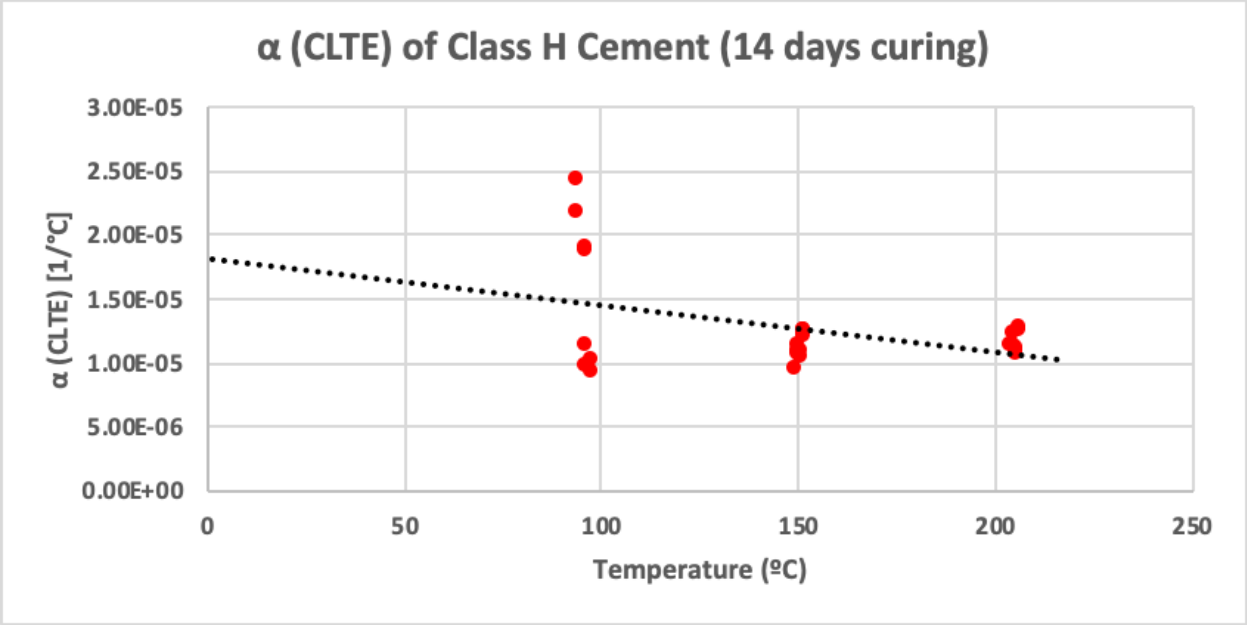

Figure 54: CLTE values measured for Class H (14 days curing time)

From above, it can be noticed how the values were really inconsistent when tested at 100 ºC (200 ºF), varying between 1E-05 [1/ºC] and up to 2.5E-05 [1/ºC]. Nonetheless, some values are in the same range with the values obtained when the temperature of testing is 150 ºC (300 ºF) and 200 ºC (400 ºF), which go in a shorter range, from 1E-05 [1/ºC] to 1.3E-05 [1/ºC].

5.3.3.2 Class H cement – one-year curing time

The same mixture is prepared and, this time, cured for one year. The CLTE values obtained are shown in Figure 55.

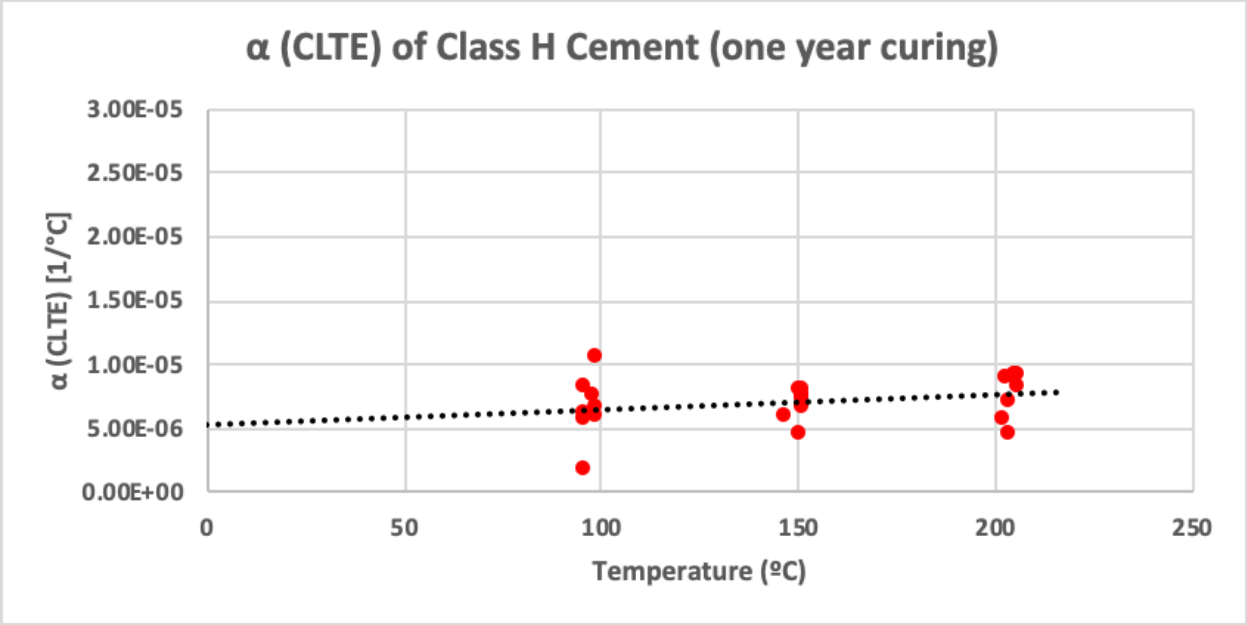

Figure 55: CLTE values measured for Class H (one-year curing time)

The values measured during this experiment are in a range between 5E-06 [1/ºC] to 1E-05 [1/ºC], with most of them laying around 8E-06 [1/ºC]. The inconsistency which is noticed at 100 ºC (200 ºF) for the sample cured for shorter period of time is not shown with this sample cured for longer time.

5.3.3.3 Class G + 10% MB cement – 21 days curing time

The second mixture prepared to make a comparison between curing times was Class G + 10% MB. In this case, the first curing time is 21 days. The results, which are shown in Figure 56, showed a lot of variation, especially at 100 ºC (200 ºF), with some values going from 5E-06 [1/ºC] and up to 1.5E-05 [1/ºC]. Moreover, when exposed to higher temperatures such as 150 ºC (300 ºF) and 200 ºC (400 ºF), the values are getting closer, with values between 1E-05 [1/ºC] to 1.3E-05 [1/ºC].

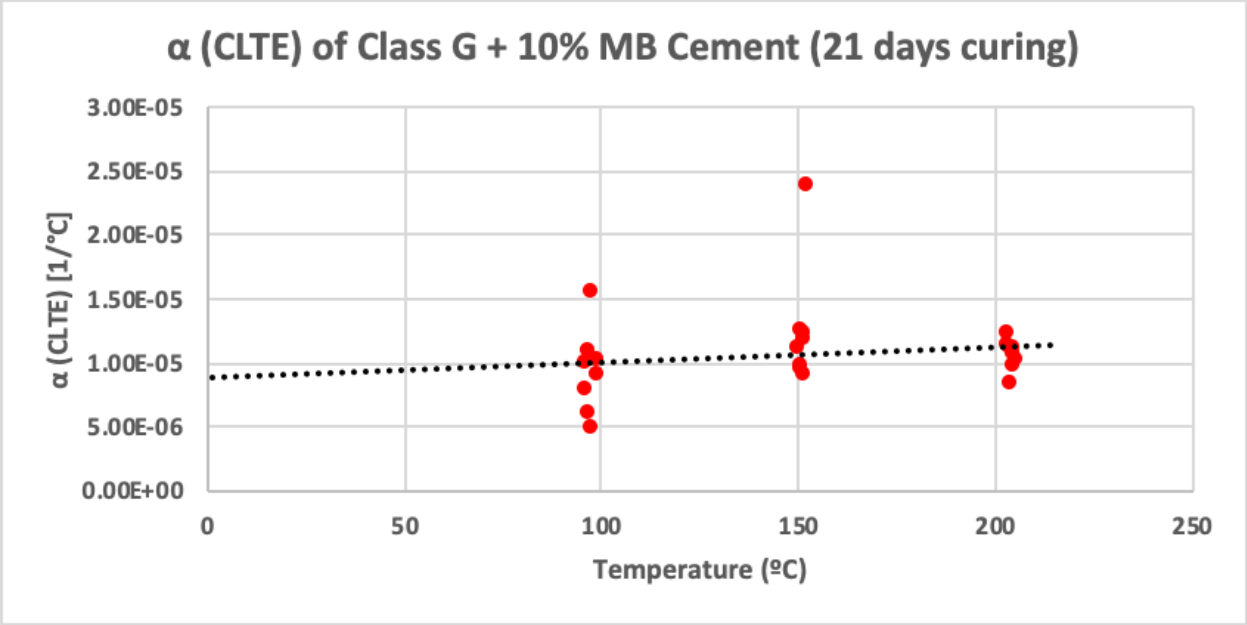

Figure 56: CLTE values measured for Class G + 10% MB (21 days curing time)

5.3.3.4 Class G + 10% MB cement – one-year curing time

Lastly, the same mixture of Class G + 10% MB, but cured for one year, is tested. From Figure 57, it can be noticed how the values of CLTE are closer, with most of them around a range of 5E-06 [1/ºC] to 9E-06 [1/ºC]. Additionally, the CLTE values were smaller than the values obtained on the sample with the shorter curing time.

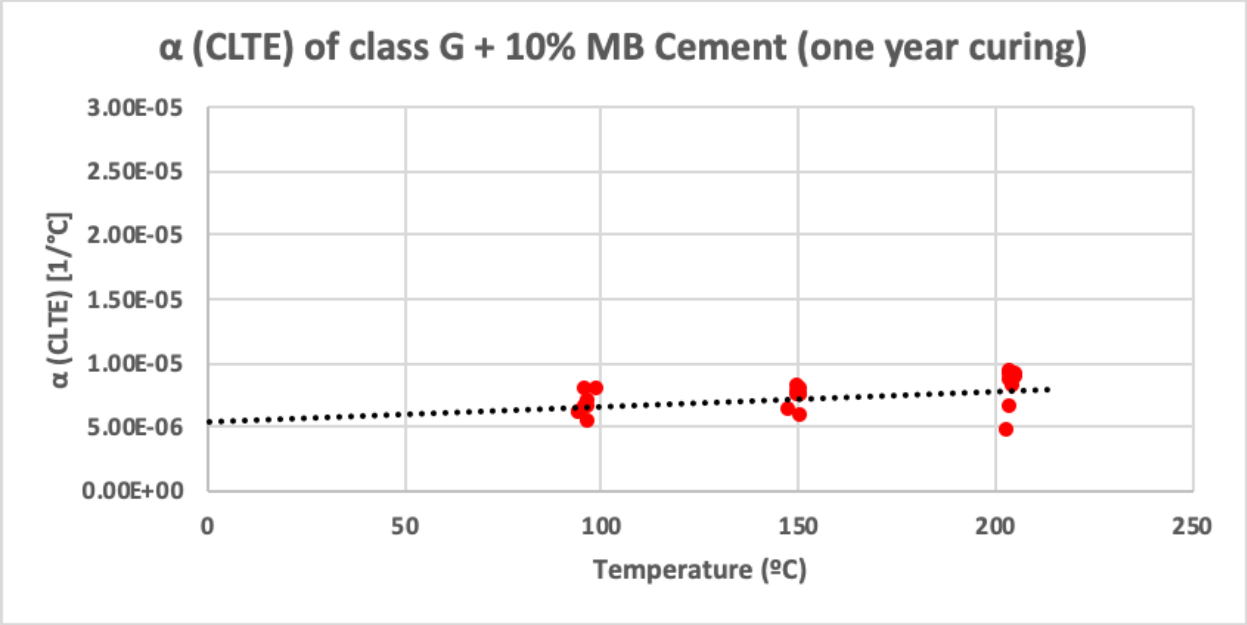

Figure 57: CLTE values measured for Class G + 10% MB (one-year curing time)

From above, it is perceived how important curing time is when it comes to CLTE for cement composites. When the samples with short curing time are tested, some inconsistency is noticed. However, this inconsistency is not visible for the samples cured for one year. The ranges of values CLTE values gets closer and constant for the three different temperatures of testing. Additionally, the CLTE values are lower in samples cured for longer periods of time rather than those obtained when cured for short periods.

5.3.4 Long-term curing time

Once the curing time effects on CLTE calculations are noticed, the next approach is to measure CLTE values for long-term curing time. In this case, three samples with three years curing time are measured. The results are described in the following.

5.3.4.1 Class C cement – three-years curing time

The first mixture is Class C. The CLTE values go from 1E-05 [1/ºC] to 1.25E-05 [1/ºC]. Figure 58 shows these values and, additionally, a consistency can be seen for all the temperatures of testing.

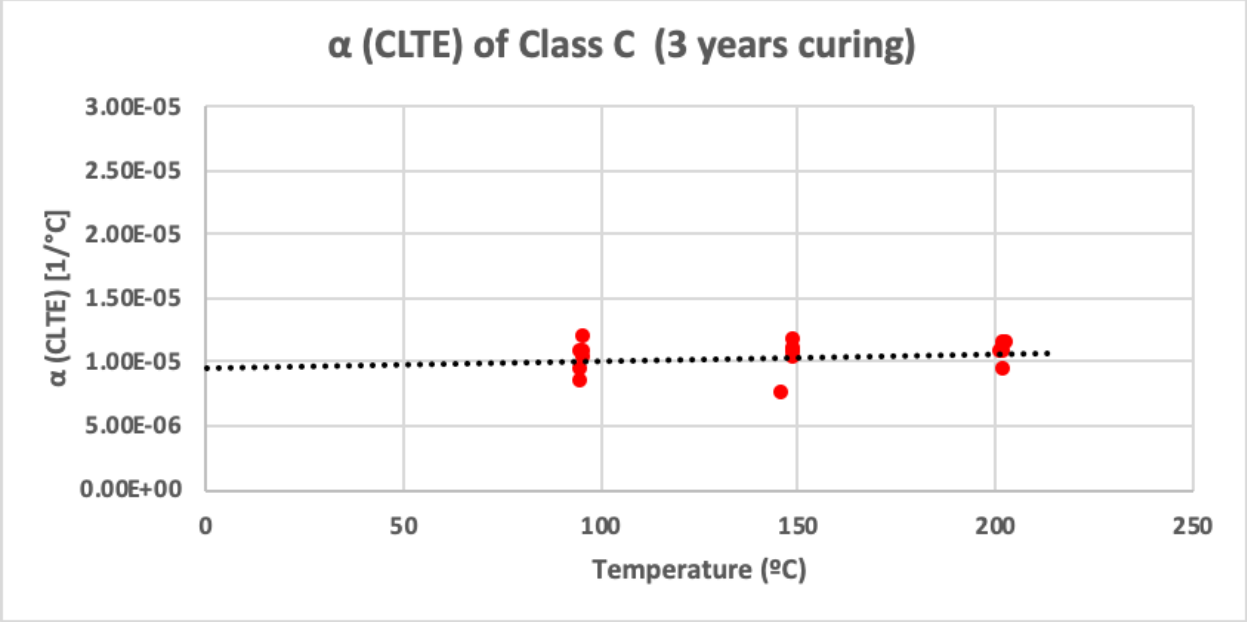

Figure 58: CLTE values measured for Class C (three-years curing time)

The results performed with this sample are also interesting since a Class C mixture, but cured just for 28 days, is presented in this investigation. Those CLTE values are outperformed by these, which just reinforces the idea of curing time as an important factor.

5.3.4.2 Class 50% C + 50% H cement – three-years curing time

The second mixture cured for three years and tested, is Class 50% C + 50% H. The CLTE values were mostly around 1E-05 [1/ºC] for the three temperatures of testing, as seen in Figure 59.

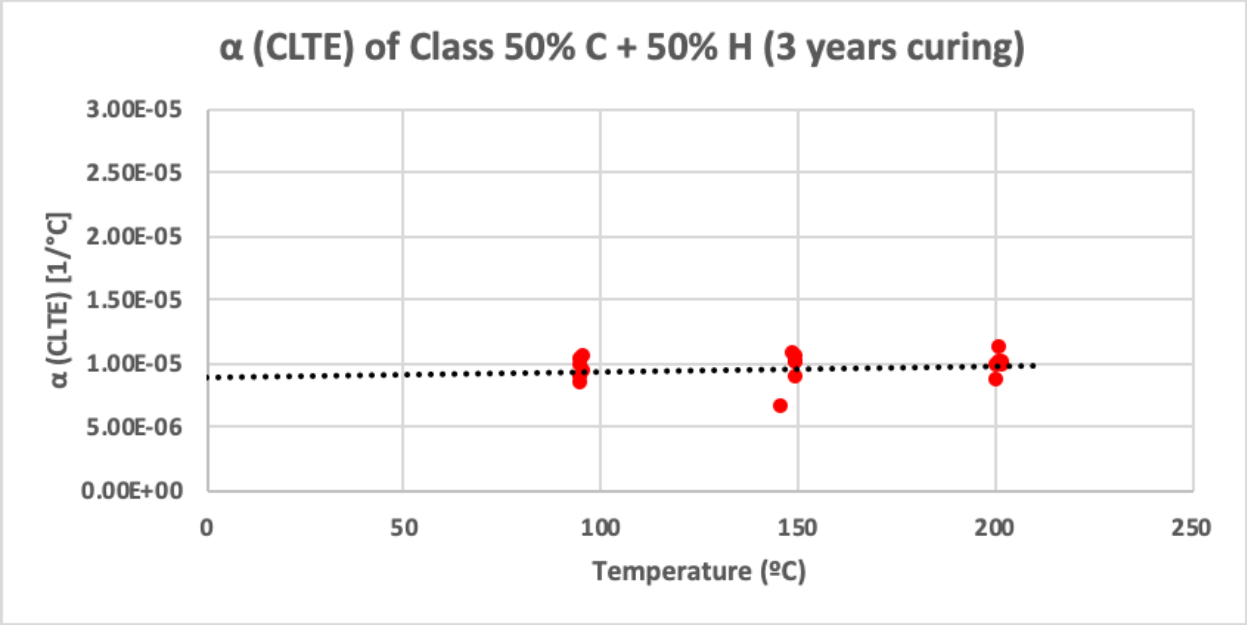

Figure 59: CLTE values measured for Class 50% C + 50% H (three-years curing time)

5.3.4.3 Class C + 10% Bentonite cement – three-years curing time

The last sample tested is Class C + 10% Bentonite. Figure 60 shows the CLTE values obtained, with mostly around 1E-05 [1/ºC] for the three temperatures of testing.

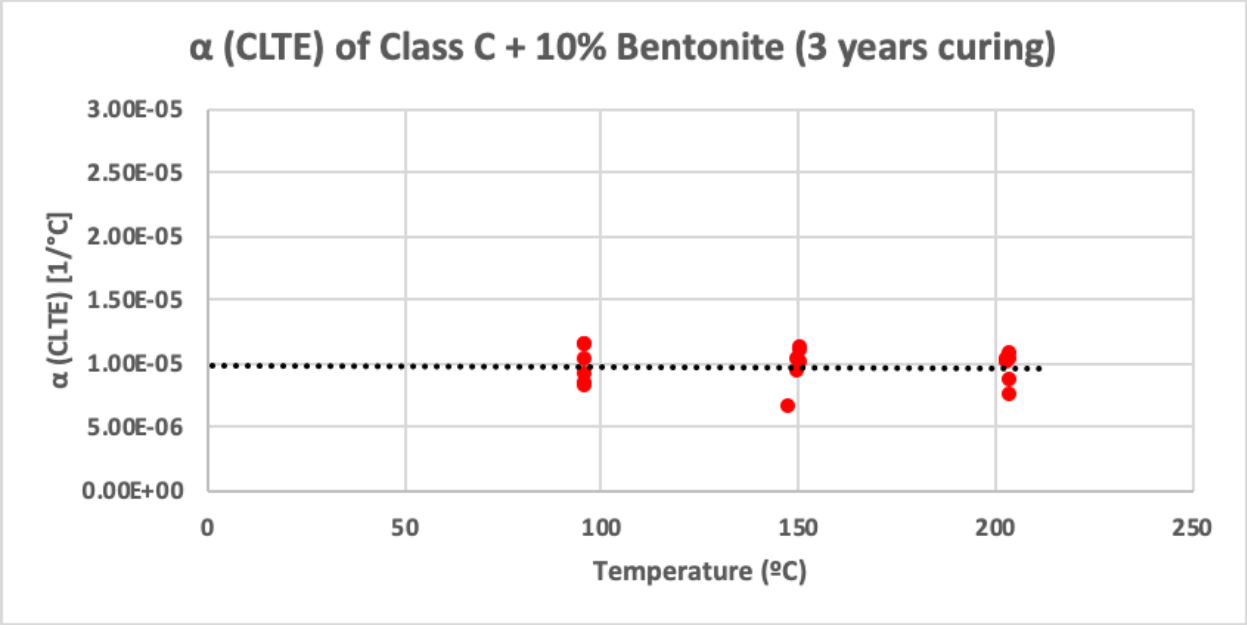

Figure 60: CLTE values measured for Class C + 10% Bentonite (three-years curing time)

From the three samples, similar CLTE values can be observed, independently of the temperature of testing and mixture. Furthermore, it can be demonstrated that curing time is an important factor to consider when it comes to CLTE measurements for cement composites. Further results from cement composites will be done in the next chapter.

Chapter 6. DISCUSSIONS

Some important discussions can be drawn after the investigations performed with the novel apparatus. First, the reliability shown by the equipment is something indispensable for the CLTE calculations. From the literature, it is known that measurements for coefficient of linear thermal expansion are usually performed with more complicated equipments or techniques. The apparatus uses a shadowing technique followed by some laser beams which display the length measurements, and a heat controller which provides the desired high-temperatures with the help of some resistors. The equipment developed at The Well Integrity Laboratory is more practical with also providing reliable results. Additionally, some of the experimentations via other equipments or techniques may take larger periods of time. In this case, one-hour experiments are sufficient to deliver good CLTE results for the materials tested, which went from metals and non-metallic elements to rocks and cement composites.

The results obtained for metallic and non-metallic materials with this apparatus were in accordance to results previously measured by different authors in the literature. Table 4 displays a comparison between some CLTE values found in different literature and values obtained with the novel apparatus for metallic and non-metallic elements, with the % of error between the values gathered by the equipment and the existing literature. It is important to mention that the % of error shown in the Table was calculated from the average of each CLTE range of values provided by the authors, and the measurements obtained with the equipment. Therefore, some of the % error values could be high despite CLTE values being close or same between existing literature and measurements performed with the novel apparatus. For example, Martelli et al. (2013) provided

values of 5E-06 to 1.5E-05 for the CLTE of Stainless Steel, while the results measured by the novel equipment were 1.5E-05. The values measure and the values provided by the author are in accordance. However, and since the error is calculated from the average, the % of error was a 45% despite having similar CLTE values. Nonetheless, most of the % errors calculated between the average CLTE values from previous literature and values obtained from the apparatus are below 10%, showing the reliability of the equipment.

Table 4: Comparison of CLTE values from literature and CLTE values measured with the novel equipment for metallic elements and non-metallic element with % of error

Author	Material	CLTE value (1/ºC)	CLTE measured with the novel equipment (1/ºC)	Error %
Hidnert and Krider (1952)	Aluminum	2.38 x10^{-05} to 2.67 x10^{-05}	2.1 to 2.4 x10^{-05}	10.89%
Yogaswara and Eljabbar (2018)		2.29 x10^{-05} to 2.30 x10^{-05}		1.96%
Shrivastava et. al (2020)		2.32 x10^{-05} to 2.55 x10^{-05}		7.60%
Dunn (2016)	Brass	1.8 x10^{-05}	1.6 to 1.9 x10^{-05}	2.78%
Shrivastava et. al (2020)		1.86 x10^{-05} to 21.1 x10^{-05}		11.84%

The Engineering Toolbox (2023)		1.86×10^{-05} to 1.9×10^{-05}		6.91%
Lewis (1994)	Steel	1.06×10^{-05} to 1.14×10^{-05}	$1 \text{ to } 1.2 \times 10^{-05}$	0 %
Tomilina (2012)		1.3×10^{-05}		15.38%
Martelli et al. (2013)	SS 304	5×10^{-06} to 1.5×10^{-05}	$1.3 \text{ to } 1.6 \times 10^{-05}$	45%
Shrivastava et. al (2020)		1.3×10^{-05} to 1.6×10^{-05}		0%
Okaji and Imai (1984)	Carbon Steel (bar gauge)	1.09×10^{-05}	$1 \text{ to } 1.3 \times 10^{-05}$	5.50%
Kahraman (2007) Fatima et al. (2015)	Carbon Steel (A36)	1.17×10^{-05}		1.71%
				1.71%
Wpengine (2022)	Glass Fiber	5.4×10^{-06}	5×10^{-06}	7.41%

Moreover, some linear trends for the metals were noticed during these investigations. Xie et al. (2018) presented a study in which metallic elements are expected to have a linear relationship between CLTE and temperature. This is noticed in all the metals tested with this equipment. For the glass fiber, which was the non-metallic material tested, the CLTE values are in the range of values found in different literatures. This probes that the equipment is not just good when

measuring metallic samples but also other materials. A comparison for the CLTE values measured for the metallic and non-metallic materials is shown in Figure 61.

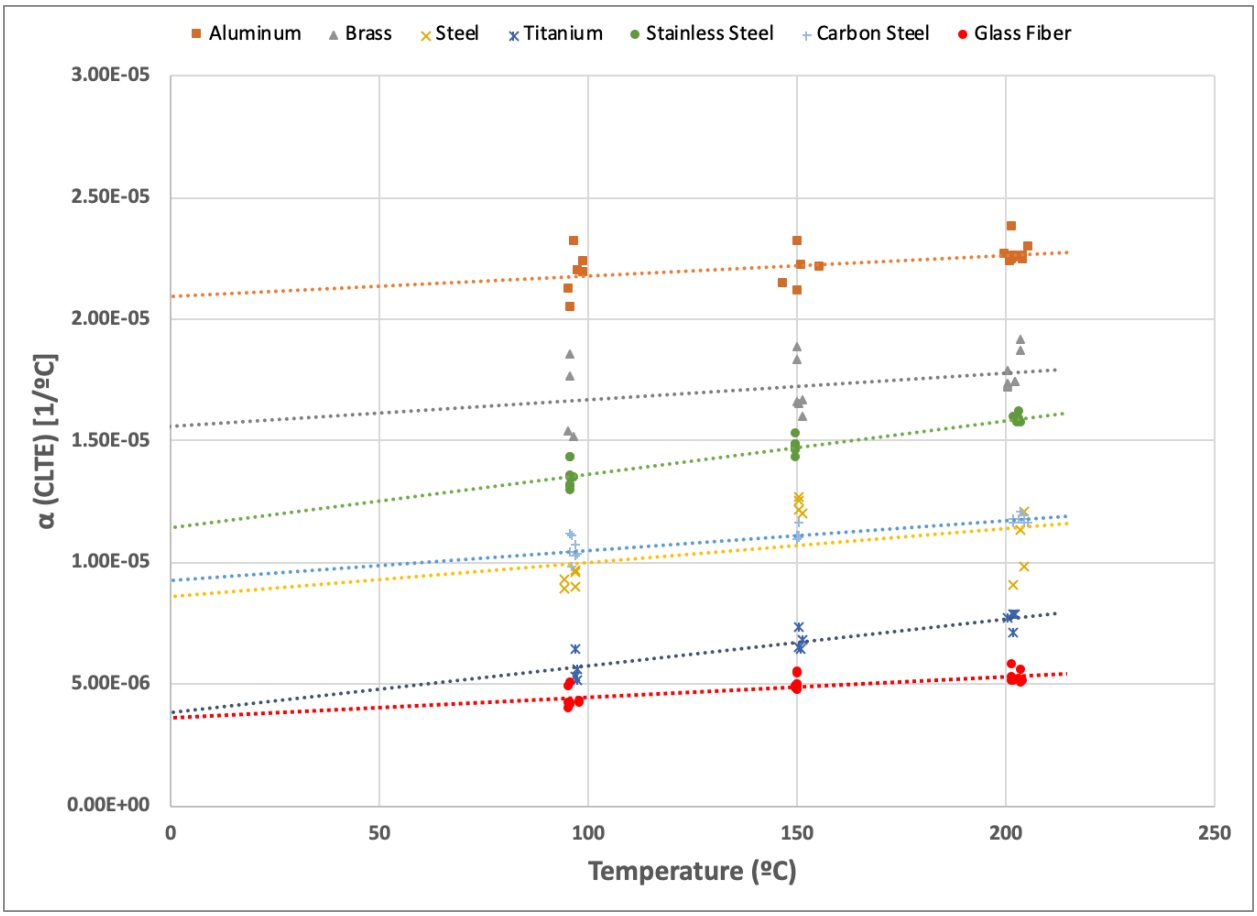

Figure 61: CLTE comparison of all metallic and non-metallic elements tested with the novel apparatus

Some interesting results were also noticed for the rocks and the cement composites. The limitations of the apparatus, previously mentioned in this investigation, in addition to the macro-investigation which did not involve mineral expansion or rock properties, make the measurements in the rock a reference rather than an exact determination. However, some results for some rocks where in accordance to the literature. For example, sandstone, which CLTE values were in a similar range in comparison with values presented by The Engineering Toolbox (2003). Sandstone and

Sandstone Bandera showed similarities in the values of CLTE, which, according to Somerton (1981), could be associated with the presence of quartz, that can control their expansion behavior. Table 5 displays a comparison between results obtained in previous investigations with the CLTE values generated by this equipment. As mentioned previously, the % of error is calculated from the average obtained from the range of CLTE values calculated by the different authors versus the average obtained from the range of CLTE values measured via the novel equipment, which could lead to high % of error despite having similar results. This is noticed, for example, when comparing the Sandstone Bandera values with the values provided by Somerton (1981). Somerton (1981) provided a value of 1.2E-05, whereas the novel equipment measured values in a range between 7E-06 and 1E-05, which is a value close to the CLTE value provided by the author. However, and since the % of error comes from an average, the error between the two investigations is as high as 29%. Nonetheless, it can be seen how the values are close to the values obtained by the different authors, especially with the differences in approaches followed in the investigation, as well as the limitations of the novel apparatus and the complexity of the rocks which could lead to a difference in results.

Table 5: Comparison of CLTE values from literature and CLTE values measured with the novel equipment for rocks with % of error

Author	Rock	CLTE value [1/ºC]	CLTE measured with the novel equipment [1/ºC]	Error %
Feng (2020)	Sandstone	1.84×10^{-05}	8.5×10^{-6} to 1×10^{-05}	49.73%

The Engineering Toolbox (2023)		1.16 x10^{-05}		20.26%
Myer and Rachiele (1981)	Granite	8.75 x10^{-6} to 1.6 x10^{-05}	5 x10^{-6} to 1 x10^{-05}	39.39%
Dwivedi bet al. (2008)		7 x10^{-6} to 1.4 x10^{-05}		28.57%
Somerton et al. (1981)	Sandstone Bandera	1.2 x10^{-05}	7 x10^{-6} to 1 x10^{-05}	29.17%
Popov et al. (2012)		1.09 x10^{-05} to 1.22 x10^{-05}		25.76%
Popov et al. (2012)	Carbonaceous	4.8 x10^{-06} to 6.3 x10^{-06}	3.5 x10^{-06} and 5 x10^{-06}	23.42%

Moreover, and as shown in Figure 62, all the rocks show a linear trend, in which the CLTE value increases with the temperature. This is important when trying to characterize some rocks, such as granite, which is the type of rock that is mostly present in geothermal applications, in which temperatures are really high.

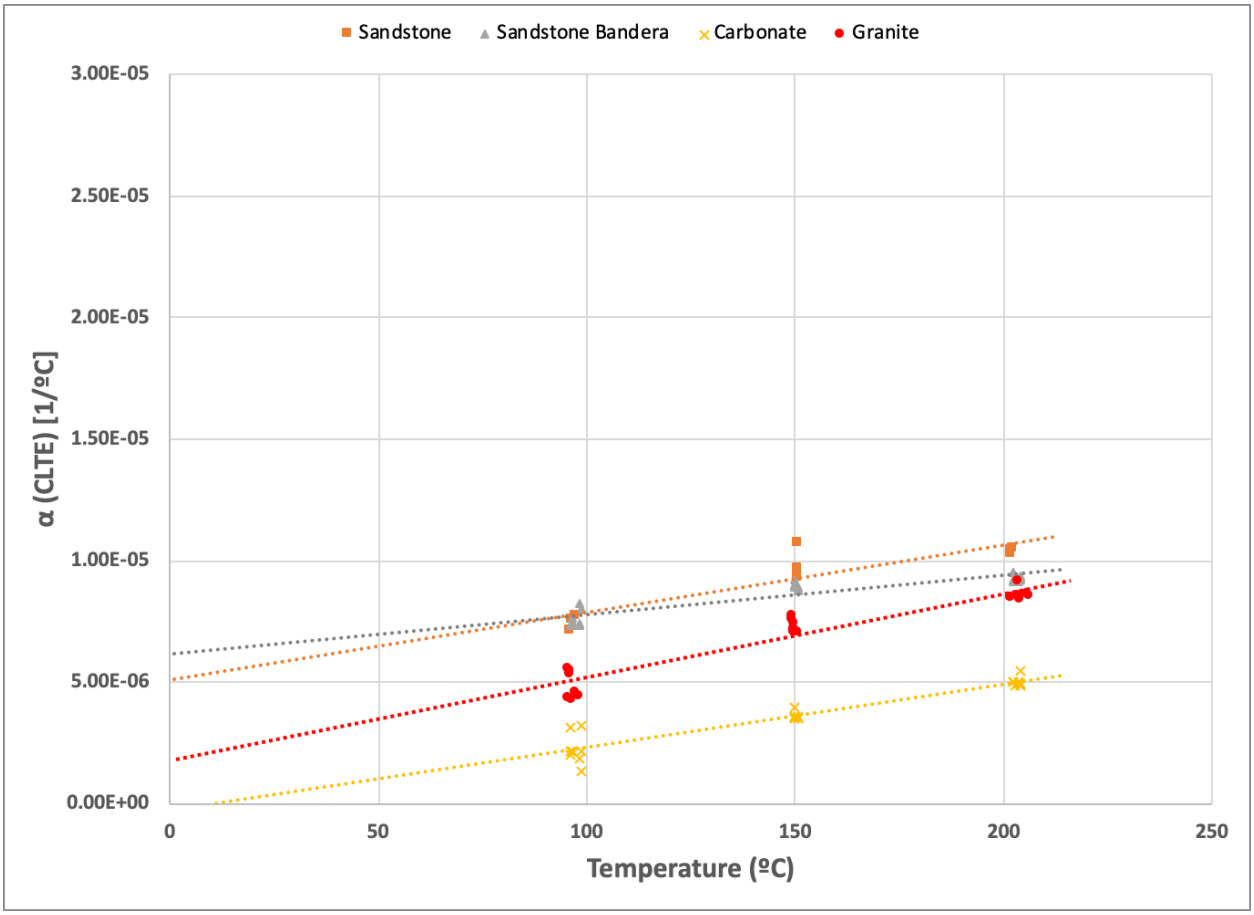

Figure 62: CLTE comparison of rocks tested with the novel apparatus

For cement composites, different scenarios were evaluated and performed to measure the coefficient of linear thermal expansion. Initially, some of the cement samples were assessed and compared with some literature to determine the range in which CLTE values are present. As previously discussed in the chapter 2, few investigations are found when it comes to this thermal expansion for cement composites. In addition to this, these investigations were not performed systematically, leading to a difference in processes followed when curing the samples, or even different mixtures tested for thermal expansion. Therefore, Table 6 displays some of the mixtures found in the literature with some of the samples tested with the apparatus with a similar mixture

for comparison. It is important to highlight that some of the processes of curing followed by the authors may vary from the curing process followed using this novel apparatus, hence some of the CLTE values may differ when comparing them.

Table 6: Comparison of CLTE values from literature and CLTE values measured with the novel equipment for cement composites with % of error

Author	**Cement sample**	**CLTE value [1/ºC]**	**CLTE measured with the novel equipment [1/ºC]**	**Error %**
Ghabezloo et al. (2009)	Class G at HT	$2x10^{-05}$ to 4 $x10^{-05}$	5 $x10^{-06}$ to 2 $x10^{-05}$	58.33%
Tomilina et al. (2012)	Class G + Silica	9 $x10^{-06}$ to 1.3 $x10^{-05}$	5 $x10^{-05}$ to 2.5 $x10^{-05}$	36.36%
Loiseau (2014)	Class G + 40% Silica (cured at 20.7 MPa and HT)	8.8 $x10^{-06}$		70.45%
	Neat Class H	9.1 $x10^{-06}$	5 $x10^{-06}$ to 1 $x10^{-05}$	17.58%
Jimenez et al. (2017)	Class H cured at 60 ºC for 7 days	~4.3 $x10^{-06}$ to 1.1 $x10^{-05}$		1.96%

As shown in Table 6, the % of error of most of the samples is very high. This was expected, not only because of what was previously explained (the % of error is taken from the average of the range of CLTE values from both the authors and the measurements performed in this investigation), but also due to the differences of processes followed when curing the samples despite comparing same mixtures (Class G, Class G + Silica, Class H). Therefore, and in order to provide effective CLTE values, this investigation followed a systematic experimentation, which took curing time and cyclic testing into consideration. First, the overview, which provided some good CLTE data and a glimpse of the importance that curing time has. Second, the cyclic test, which was one of the objectives when preparing four different recipes and curing them for 28 days, to perform CLTE measurements. The scope was not just to identify the importance of curing, but also to determine if there is any dissimilarity when testing under non-cyclic settings. The results obtained where quite surprising, due to the fact that the results obtained for all the samples prepared for the four mixtures had variances despite following the same curing conditions and non-cyclic testing. The variations found in CLTE values for cement composites could be attributed to the hydration still ongoing during heating cycles. Furthermore, and as well as rocks, cement composites are porous materials and air could be trapped within the porous media, which may result in the variations.

Moreover, Class G + 40% Silica, which was one of the mixtures prepared to create a comparison of CLTE values between these results and the ones provided by Loiseau (2014). The inconsistency in the values obtained, which were from 2E-05 [1/ºC] to 2.5E-05 [1/ºC] when the testing temperature around 100°C (200 ºF), and 1E-05 [1/ºC] to 1.5E-05 [1/ºC] when testing to higher temperatures were made. The reason behind the differences perceived could be also related with

the curing time used for the two different investigations. Furthermore, the next step was to make a comparison between samples taking curing time as reference.

Short-term curing time samples against long-term curing time samples was performed, and the results gave an insight on the importance behind this factor. Long curing time periods could also help to avoid any hydration process that may lead to CLTE as stated above. Whereas the results obtained by the short-term cured samples demonstrated a lot of variances, especially when exposed to high temperatures for the first time, the long-term cured samples showed constant CLTE values in all the three different high-temperatures of exposure. Figure 63 compares the CLTE values obtained for two cement mixtures cured for short and long term.

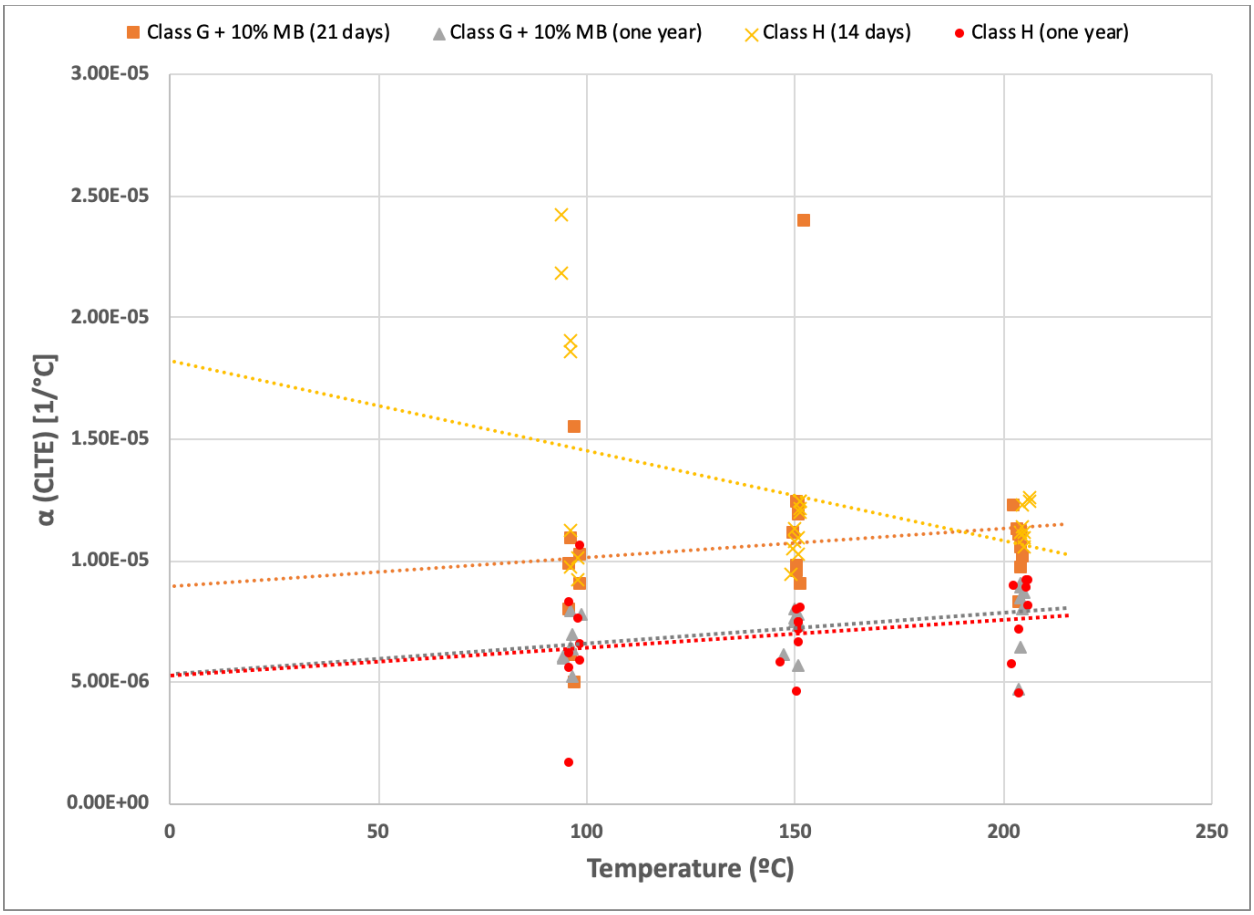

Figure 63: CLTE comparison of short curing time vs long curing time cement tested with the novel apparatus

From the Figure above, it can be seen how constant the CLTE values get when the curing time is higher despite the temperature. In addition, more scattering can be detected in samples with shorter periods of time. This was later corroborated when some samples cured for three years were also tested, and the CLTE values showed a high consistency under high temperatures exposures. The samples tested, despite the difference in mixture and temperature of exposure, showed CLTE values in the same range. The trend also showed that temperature does not have big impact on cement composites when curing time is bigger, rather when the cement is cured for shorter periods of time, in which depending on other factors, the CLTE may be bigger or smaller and without a specific trend.

Moreover, it was also noticed that, CLTE values are smaller when cured for longer period. Figure 64 shows the CLTE values measured for the different cement composites and the decrease in the values when the curing time is bigger.

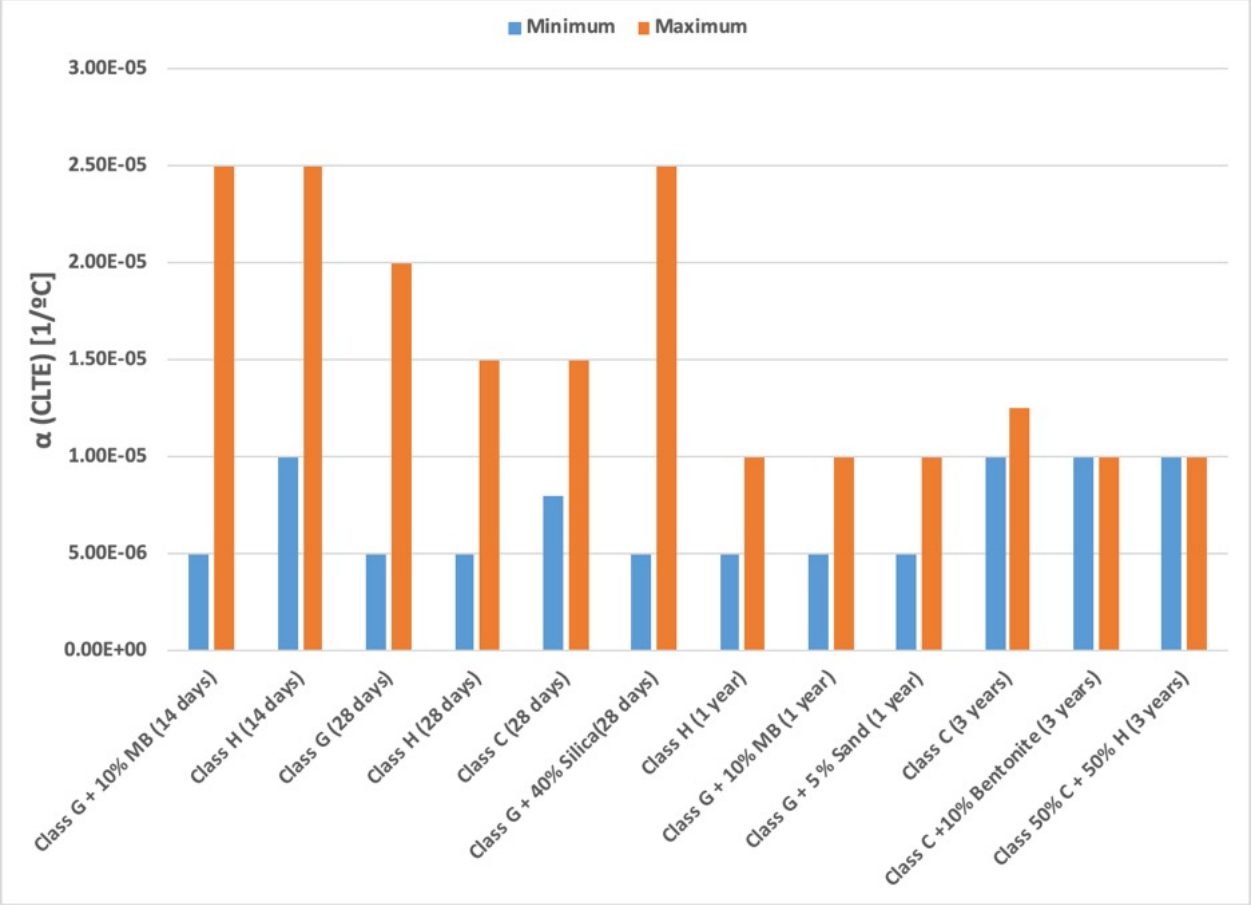

Figure 64: CLTE values of samples depending on their curing time

It is noticed a decrease in the CLTE values and range for each sample when cured for longer curing periods. Furthermore, Abid et al. (2023) concluded that thermal properties of cement composites, such as thermal expansion, evolve with time, becoming more consistent after certain curing time.

Figure 65 illustrates the samples cured for short time. It is noticed that all of these samples display a negative trending, with higher inconsistencies and wide spread CLTE values.

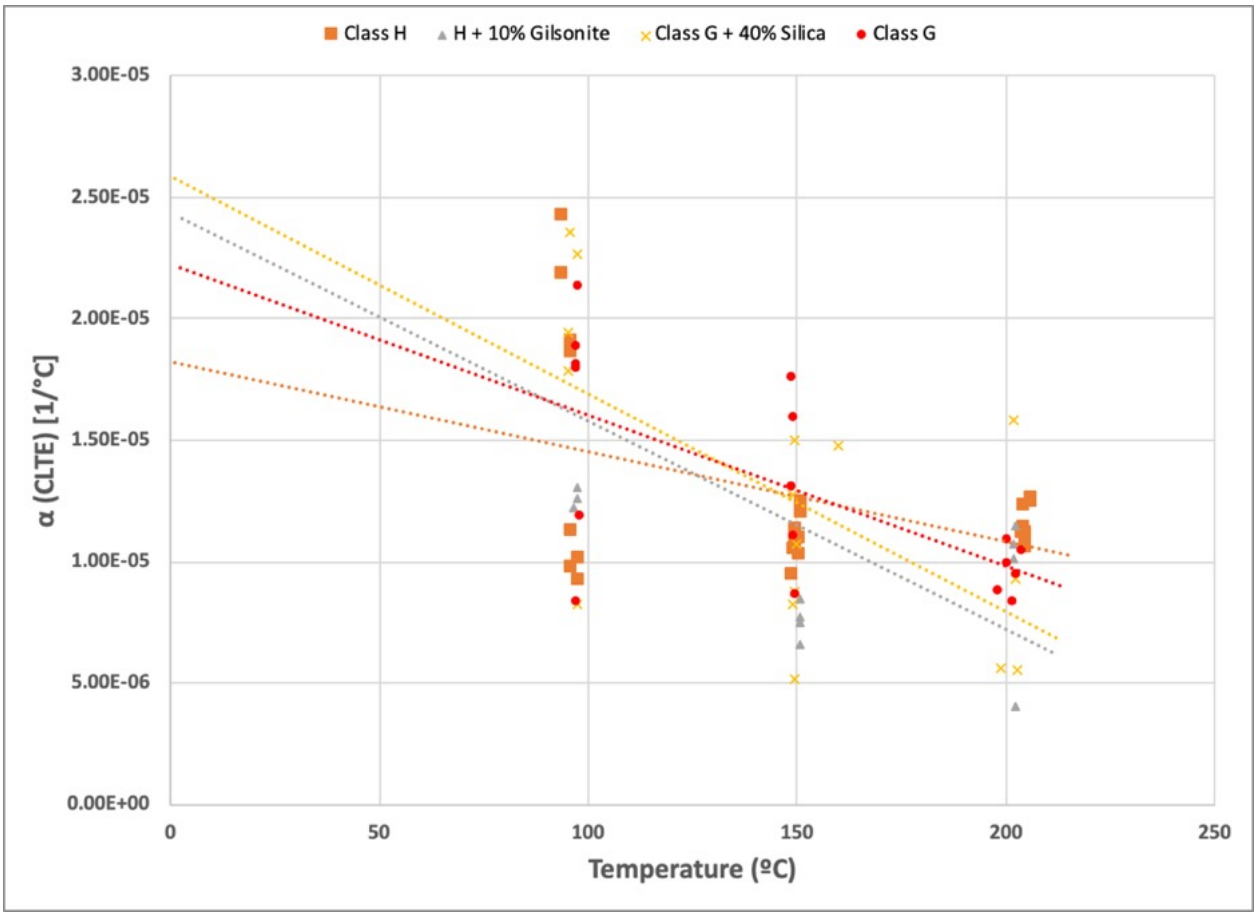

Figure 65: CLTE values measured for oilwell cements cured for short time

Lastly, Figure 66 displays the CLTE values measured for two different metals, two cement composites and a rock, creating a comparison between them and showing the importance of measuring this property. The metals displayed are carbon steel and stainless steel, which are often used in oil and gas and geothermal operations for casing, whereas the rock displayed is granite which is encountered in some geothermal operations. Neat Class H, which serves as a control sample, is also displayed in both short and long curing time.

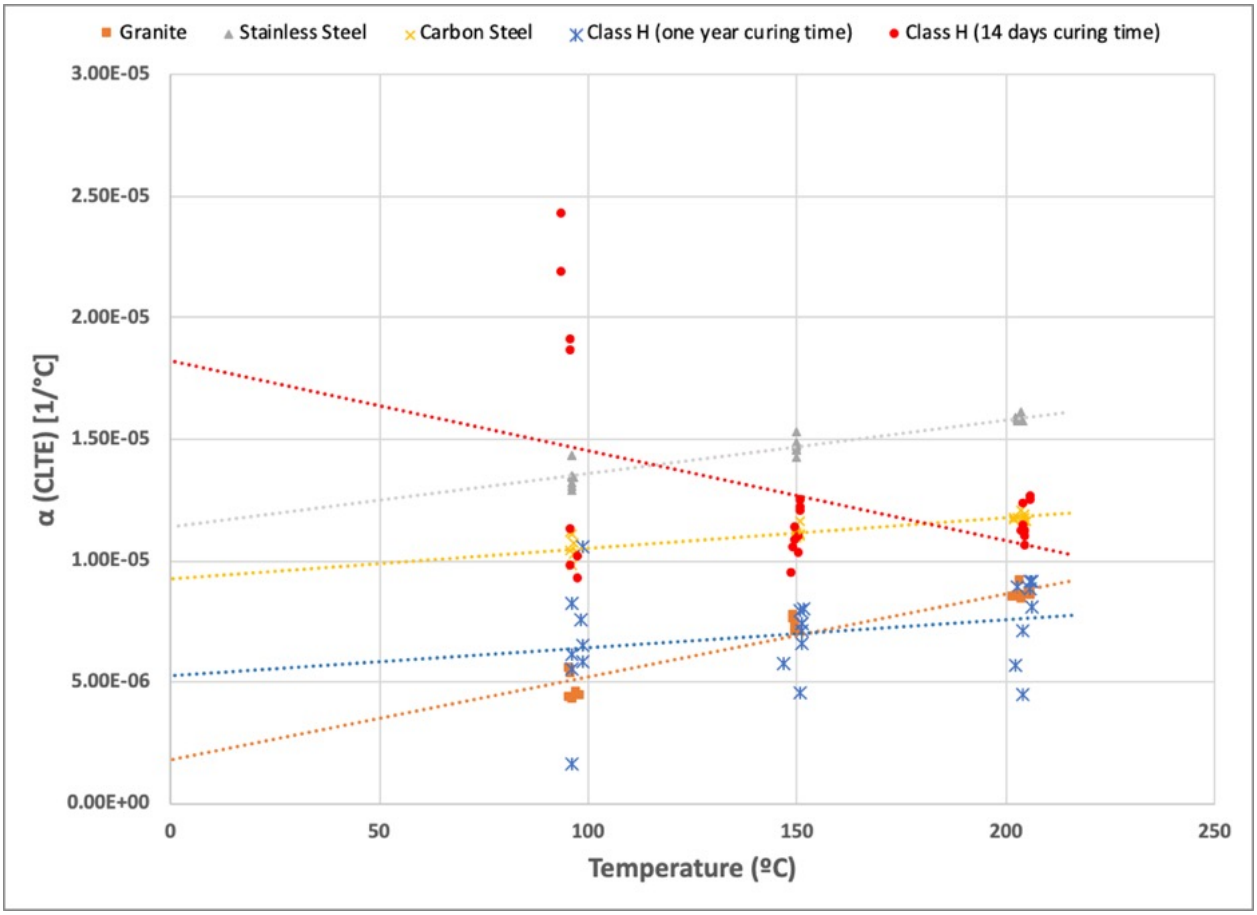

Figure 66: CLTE values measured for metallic elements, cement and rock

The Figure above highlights the importance of measuring the CLTE to better understand the behavior of these elements when operating downhole. It is noticed how the cement thermal expansion is bigger when curing time is short, and closer to the thermal expansion of some metallic elements such as the carbon steel. However, some of these values are wide away from the metallic element, which could lead to a problem in the operation due to the difference in expansion for both casing and cement. Moreover, when curing time is longer, the CLTE for cement gets lower and

consistent despite the temperature. Additionally, the values get closer to the CLTE values obtained for the rock, leading to a constant expansion in both the rock and cement.

The effects of the thermal expansion are illustrated in Figure 67 and Figure 68, in which two different stresses that affect both the casing and cement sheath are simulated for three oilwell cement composites with different CLTE values, following the equations provided by Ugwu (2010). Table 7 displays the input variables used for the simulated scenario, in which some cement properties, carbon steel casing properties and formation properties are assumed. The cement with the low CLTE has a value of 1E-05 [1/ºC], whereas the medium CLTE value for the cement corresponds to 1.5E-05 [1/ºC] which is an increment of 50% of the low CLTE vale. The high CLTE value for the cement is 2.5E-05 [1/ºC], which corresponds to an increment of 150% of the initial low CLTE.

Table 7: Input variables and values for stresses simulation, after Ugwu (2010)

Variables	**Value**
Casing inner radius (r_a)	6.366 in
Casing outer radius (b)	7 in
Cement sheath outer radius (c) or (r_c)	8.5 in
Inner / annulus pressure (p_i)	15,000 psi
Formation pressure (p_f)	3,000 psi
Mean radius (r_m)	6.683 in
Radius of cement sheath (r_c)	8.5 in

Casing thickness (t_s)	0.634 in
Temperature of flowing fluid (t_w)	200 ºF
Formation Temperature (t_f)	212 ºF
Outer casing wall temperature (t_2)	200 ºF
Cement properties	
Variables	**Value**
Poisson ratio (v_c)	0.42
CLTE (α_c)	Varies depending on cement used (1E-05 [1/ºC] to 2.5E-05 [1/ºC])
Young modulus (E_c)	690,000 psi
Radius (r_c)	8.5 in
DT (delta of temperature) (Δt_2)	12 ºF
Compressive strength	8000 psi
Tensile strength	3000 psi
Casing properties (carbon steel)	
Variables	**Value**
Poisson ratio (v_s)	0.3
CLTE (α_s)	1.3E-05 [1/ºC]
Young modulus (E_s)	29,000,000 psi
Radius (r_s)	0
DT (delta of temperature) (Δt_1)	12 ºF
Formation properties	

Variables	Value
Poisson ratio (v_f)	0.49
CLTE	0
Young modulus (E_f)	4,000,000 psi

In order to calculate the tangential and radial stresses, the inner contact and outer contact need to be determined. Inner contact (Pc_1) can be defined as the pressure divided by the confining stress due to the inner pressure and it is represented in Equation 3 as follows:

Equation 3: Inner contact equation, recovered from Ugwu (2010)

$$Pc_1 = \frac{[(1 + v_s)r_a\alpha_s\Delta t_1] - [(1 + v_c)r_c\alpha_c\Delta t_2] + \frac{P_i r_a}{E_s}[\frac{r_m}{t_s}(1 - v_s^2) - (v_s + v_s^2)}{\frac{r_c}{E_c}\left[(1 - v_c^2)\frac{b^2 + c^2}{c^2 - b^2} - (v_c + v_c^2)\right] + \frac{r_a}{E_s}\left[\frac{r_m}{t_s}(1 - v_s^2) - (v_s + v_s^2)\right]}$$

Where, r_a is casing inner radius, b is casing outer radius, c or r_c is cement sheath outer radius, p_i is inner / annulus pressure, r_m is mean radius, r_c is radius of cement sheath, and t_s is the casing thickness for some of the general dimensions of casing and cement. For the cement properties, v_c, α_c, E_c, Δt_2, correspond to Poisson ratio, thermal expansion coefficient, young modulus and delta of temperature, respectively. And lastly, v_s, α_s, E_s and Δt_1 are Poisson ratio, young modulus, thermal expansion coefficient and delta of temperature, respectively, for the carbon steel casing.

Outer contact (Pc_2) is represented in the following Equation 4:

Equation 4: Outer contact equation, recovered from Ugwu (2010)

$$Pc_2 = \frac{\frac{P_f(3v_f^2 + v_f - 2)}{E_f} - [(1 + v_c)\alpha_c \Delta t_2]}{\frac{(1 - v_c - 2v_c^2)}{E_c} - \frac{(1 - v_c - 2v_f^2)}{E_f}}$$

Where p_f is the formation pressure, and E_f and v_f are the young modulus and Poisson ratio, respectively, for the formation. Whereas for the cement, v_c, α_c, E_c, Δt_2, correspond to Poisson ratio, thermal expansion coefficient, young modulus and delta of temperature, respectively.

Once the inner and outer contact have been obtained, the tangential and radial stresses can be calculated. First, the tangential stresses (σ_θ) are defined as follows in Equation 5:

Equation 5: Tangential stresses equation, recovered from Ugwu (2010)

$$\sigma_\theta = Pc_1 \frac{b^2}{c^2 - b^2}\left[1 + \frac{c^2}{r^2}\right] - Pc_2 \frac{c^2}{c^2 - b^2}\left[1 + \frac{b^2}{r^2}\right]$$

Where, Pc_1 and Pc_2 are the inner and outer contact, respectively. And, b and c are the inner radius (casing outer radius) and outer radius of cement sheath. Figure 67 shows the effects of the variations in the CLTE of cement on the tangential stresses, which affects the components on the well.

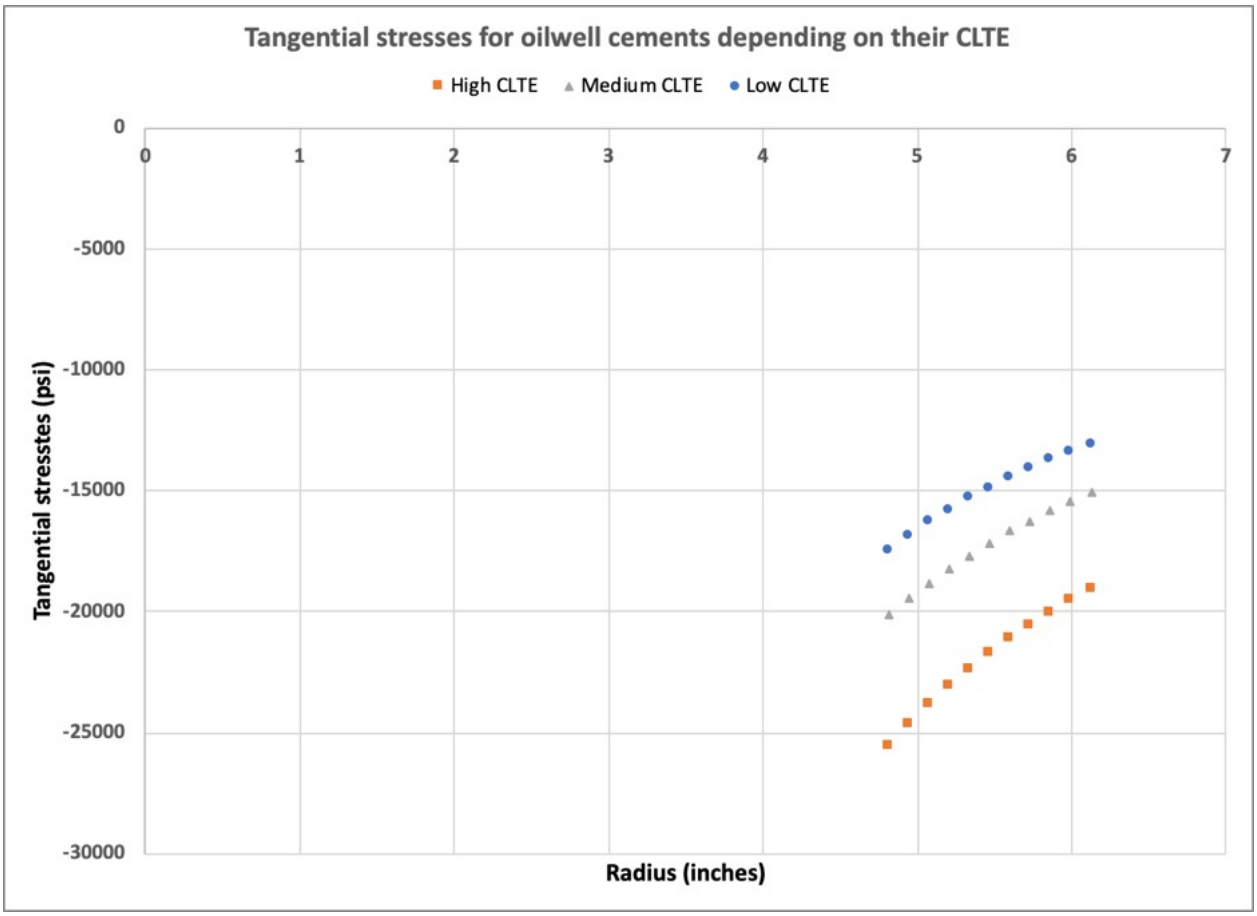

Figure 67: Tangential stresses depending on the CLTE value of oilwell cement

It can be noticed that, the higher the CLTE of the cement, the higher negative tangential stress (compression), which, as previously mentioned, could create some troubles in the integrity of the casing. Moreover, when the cement has a CLTE of 1.5E-05 [1/ºC], the tangential stresses increase 15% in comparison with the stresses provided by the cement with a low CLTE (1E-05 [1/ºC]). However, when the cement has a higher CLTE (2.5E-0 [1/ºC]), which represents an increment in 150% of the CLTE a cement with low coefficient, the tangential stresses may increase up to 46%, when comparing both cements.

On the other hand, radial stresses (σ_r) can be calculated using the formula displayed in Equation 6.

Equation 6: Radial stresses equation, recovered from Ugwu (2010)

$$\sigma_r = Pc_1 \frac{b^2}{c^2 - b^2}\left[1 - \frac{c^2}{r^2}\right] - Pc_2 \frac{c^2}{c^2 - b^2}\left[1 - \frac{b^2}{r^2}\right]$$

Where, Pc_1 and Pc_2 are the same inner and outer contact, respectively. And, b and c are the inner radius (casing outer radius) and outer radius of cement sheath. Figure 68 shows the effect of the CLTE of cement on the radial stresses that affect casing and cement sheath.

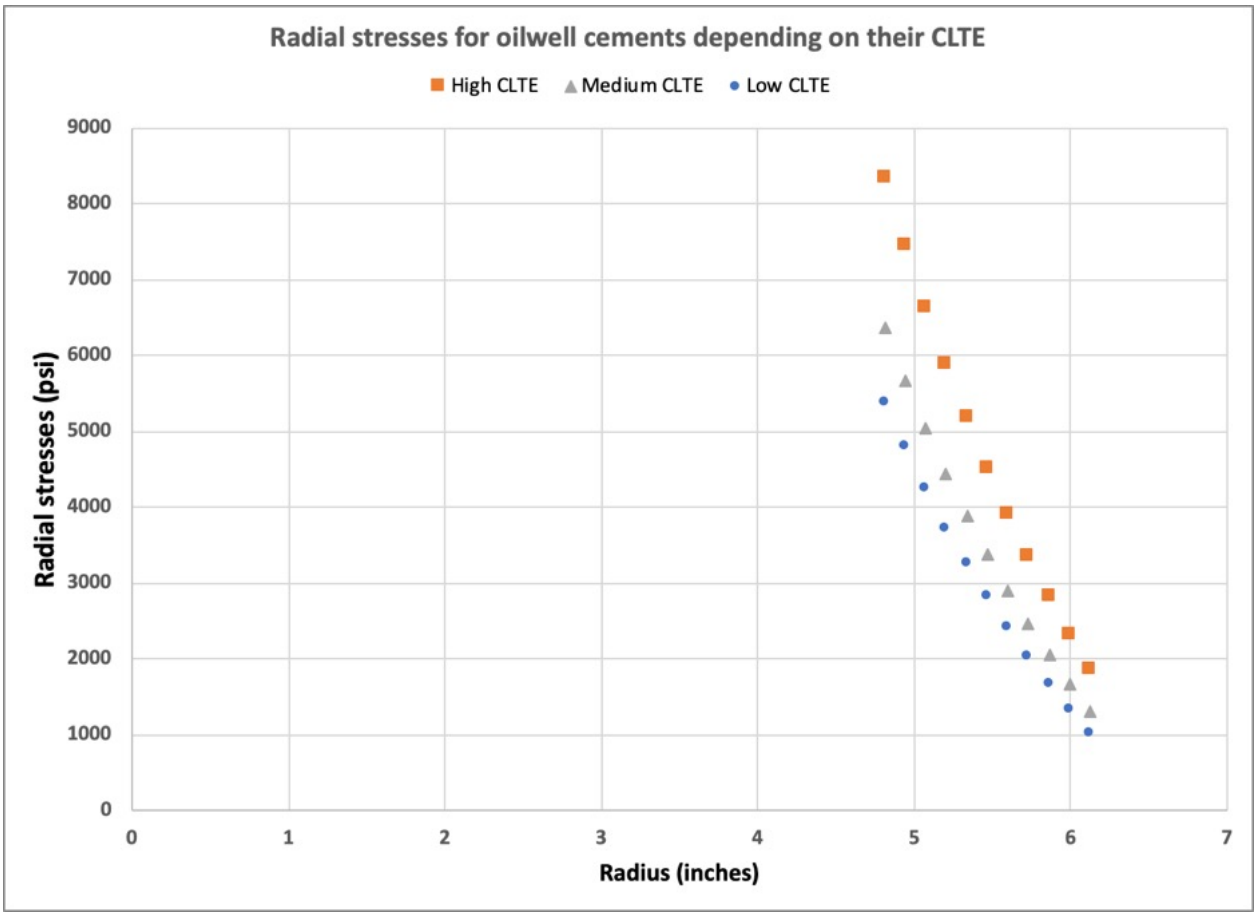

Figure 68: Radial stresses depending on the CLTE value of oilwell cement

It can be noticed how impactful a higher CLTE can be, leading to a higher radial stress in comparison with cements with lower CLTE which deliver lower radial stresses in the system. For these stresses, a cement with a CLTE of 1.5E-05 [1/ºC], which represents a CLTE 50% higher than the value of a cement with low coefficient (1E-05 [1/ºC]), could increase the stresses in a range between 18 to 27% depending on the radius, when comparing both cement composites. In a worst scenario, if a cement possesses a higher CLTE such as 2.5E-05 [1/ºC], which now represents a 150% increment in the CLTE of a cement with a low coefficient (1E-05 [1/ºC]), the increment of the radial stresses generated could be in a range between 54% to 83% depending on the radius, when comparing these with the stresses provided by the cement with the lowest CLTE.

Moreover, it is important to mention that the cement composites that provided the higher CLTE values in this investigation, where the samples cured for a short period, which also provided a lot of variation and scattering. Therefore, the effects in the stresses could be even worse or more difficult to characterize. The samples that delivered the lowest CLTE values in this investigation, despite their mixture, were the samples cured for longer periods of time, which also showed a high consistency independently of the temperature of exposure. This allows a better understanding of the stresses present in the well, which also are lower than the possible stresses that a cement with higher CLTE could generate.

Chapter 7. CONCLUSIONS

This research shows an extensive and dedicated investigation in the thermal property of linear thermal expansion by using a novel apparatus for different materials, rocks and cement composites. The following conclusions can be drawn:

- Thermal expansion, which is a thermal property present in different materials, which go from metals, to cement composites and rocks, is an important factor when it comes to well integrity due to the many effects it may have in both the casing and in the cement sheath.
- A novel apparatus was built at the Well Integrity Laboratory, with the main function of calculating this thermal property in its linear representation. The apparatus measures and collects the length and temperature, the two physical properties needed for coefficient of linear thermal expansion calculations.
- The apparatus provided fast measurements in comparison with other equipments or techniques, such as thermomechanical analysis, dilatometry or interferometry. Additionally, it measures cylindrical-shaped samples, allowing those samples to be testes for other mechanical properties, and making the linear expansion analysis better. In addition, temperatures up to 200 ºC (400 ºF) were achieved during this investigation.
- In this investigation, more than 300 experiments were performed for metallic and non-metallic materials, as well for rocks and cement composites.
- CLTE values obtained by using this equipment showed a strong relationship with the values present in diverse literature. Metal elements were also used for calibration purposes due to their known coefficients of linear thermal expansion.

- A linear trend is visible for all the CLTE measurements in metallic elements. This aligns with studies performed by Xie et al. (2018).
- Carbon steel showed smaller CLTE values than stainless steel, and similar to pure steel. However, titanium showed smaller values then the three types of steel measured.
- Glass fiber had smaller CLTE values than the metallic elements measured with the novel equipment, and is in accordance with the literature.
- Measurements in rocks were performed. However, certain limitations when testing rocks, which were mentioned above, are present while using this equipment. The limitations from the apparatus, in addition to the complexity of the rocks, makes these values an approximation to real values, which, as stated by Feng et al. (2020), may vary depending on factors such as anisotropy, size of the grains, degree of bonding, etc.
- From the CLTE values obtained for rocks, a linear trend can be noticed, in which the higher the temperature of exposure, the higher CLTE values obtained.
- All the rocks presented CLTE values under 1E-05 [1/ºC], in which carbonate was the rock with the lowest values from all (up to 5E-06 [1/ºC] when exposed at 200 ºC).
- The apparatus was also used to measure CLTE for cement composites in a systematic investigation. Current data is very scarce regarding this thermal property, although is something relevant for well integrity purposes, both in oil and gas and in geothermal applications. In this investigation up to ten different mixtures, with different curing conditions and testing procedures were measured for CLTE purposes.
- The CLTE results obtained for cement composites showed some variety in values. These variations could be related with some ongoing cement hydration during heating cycles.

Moreover, the air trapped in cement's porous media, as well as curing time could lead to CLTE variations.

- Non-cyclic test was performed for four mixtures, in which same curing conditions and testing procedures were followed. The CLTE results showed a variation in each one of the samples measured, in contrary with the initial thoughts in which the results would be similar due to the same conditions in each individual sample.
- Curing time highlighted as one of the properties of cement that affect this thermal property. Whereas short-term cured samples showed high inconsistencies and variations in CLTE values, the long-term cured samples showed smaller values, with a shorter range and higher consistency despite the different high temperatures of testing. As previously mentioned, this is supported by studies performed by Abid et al. (2023) in which is stated that thermal properties evolve with time, leading to a consistency when longer curing time in cement composites occur. Additionally, Long-time cured samples showed similar CLTE values despite the mixture.
- The effects of thermal expansion in both casing and cement are important and need to be understood. The different values of CLTE of cements could affect the different stresses present in the well. Higher CLTE values create higher compression tangential stresses and higher radial stresses, whereas cements with lower CLTE values have less impact.

REFERENCES

1. AASHTO T336-15 (2019) Standard method of tests for the coefficient of thermal expansion of hydraulic cement concrete, AASHTO

2. Abid, K., Sharma, A., Ahmed, S., Srivastava, S., Toledo Velazco, A., & Teodoriu, C. (2022). A review on geothermal energy and HPHT packers for geothermal applications. *Energies*, *15*(19), 7357.

3. Abid, K., Velazco, A. T., Teodoriu, C., & Amani, M. (2023, June). Investigations on Cement Thermal Properties with Direct Application to Underground Energy Storage. In *ARMA US Rock Mechanics/Geomechanics Symposium* (pp. ARMA-2023). ARMA

4. *AEO2023*. (2023). https://www.eia.gov/outlooks/aeo/pdf/AEO2023_Narrative.pdf

5. American Petroleum Institute. (2016). *Annular Casing Pressure Management for Onshore Wells*, Recommended Practice 90-2; RP 90-2.

6. Antii M-L, Babushkin O,Shen Z, Nygren Mand Warren R. (1999). *Key Eng. Mater.* 164–165 279–82

7. ASM International Handbook Committee, & Davis, J. R. (1998). Metals Handbook Desk Edition. 2nd Edition (2nd ed.). CRC Press.

8. Bachu, S., & Bennion, D. B. (2009). Experimental assessment of brine and/or CO2 leakage through well cements at reservoir conditions. *International Journal of Greenhouse Gas Control*, *3*(4), 494-501.

9. Bajpai, P. (2018). Biermann's Handbook of Pulp and Paper: Volume 1: Raw Material and Pulp Making (3rd ed.). Elsevier.

10. Bittorf Ch, Matthies S, Priesmeyer H G and Wagner R 1999 *Intermetallics* 7 251–8

11. Bowman AL, Krikorian NH and Neveson NG. (1972). *American Institute of Physics Conf. Proc. No 3—Thermal Expansion* (New York: American Institute of Physics) pp 119–30

12. BP, & Dale, S. (2022). *bp Energy Outlook: 2022 edition*. https://www.bp.com/content/dam/bp/business-sites/en/global/corporate/pdfs/energy-economics/energy-outlook/bp-energy-outlook-2022.pdf

13. Bu, Y., Chang, Z., Du, J., Liu, D. (2017). Experimental study on the thermal expansion property and mechanical performance of oil well cement with carbonaceous admixtures. Royal Society of chemistry 7, 29240–29254.

14. Cooper, H. W., & Simmons, G. (1977). The effect of cracks on the thermal expansion of rocks. *Earth and Planetary Science Letters*, *36*(3), 404-412.

15. Corporation, H. H. (2024). *Principle of Thermomechanical Analysis (TMA): Hitachi High-Tech Corporation*. Hitachi High-Tech Corporation. https://www.hitachi-hightech.com/global/products/science/tech/ana/thermal/descriptions/tma.html

16. Cverna, F. (Ed.). (2002). *ASM Ready Reference: Thermal properties of metals*. Asm International.

17. Dincer, I.; Ezzat, M.F. (2018). Geothermal Energy Production. In *Comprehensive Energy Systems*; Elsevier: Amsterdam, The Netherlands, pp. 252–303.

18. DiPippo, R. (Ed.). (2016). *Geothermal power generation: Developments and innovation*. Woodhead Publishing.

19. Dudley, B. (2017). *BP Energy Outlook—2017 Edition*; British Petroleum: London, UK.

20. Dunn, B. D. (2016). *Materials and processes: for spacecraft and high reliability applications* (Vol. 10, pp. 978-3). Switzerland: Springer.

21. Dwivedi, R. D., Goel, R. K., Prasad, V. V. R., & Sinha, A. (2008). Thermo-mechanical properties of Indian and other granites. *International Journal of Rock mechanics and mining Sciences*, *45*(3), 303-315.

22. Fatima, S., Khan, M., Jaffery, S. H. I., Ali, L., Mujahid, M., & Butt, S. I. (2016). Optimization of process parameters for plasma arc welding of austenitic stainless steel (304 L) with low carbon steel (A-36). *Proceedings of the Institution of Mechanical Engineers, Part L: Journal of Materials: Design and Applications*, *230*(2), 640-653.

23. Feng, Z., Qiao, M., Dong, F., Yang, D., & Zhao, P. (2020). Thermal expansion of triaxially stressed mudstone at elevated temperatures up to 400°C. *Advances in Materials Science and Engineering*, *2020*, 1–8. https://doi.org/10.1155/2020/8140739.

24. Ghabezloo, S., Sulem, J., & Saint-Marc, J. (2009). The effect of undrained heating on a fluid-saturated hardened cement paste. *Cement and Concrete Research*, *39*(1), 54-64.

25. Hahn T A. (1998). Cindas Data Series on Material Properties, Volume I-4—Thermal Expansion of Solids ed R E Taylor (Materials Park, OH: ASM International) ch 6, pp 181–92.

26. Hidnert, P., & Krider, H. S. (1952). Thermal expansion of aluminum and some aluminum alloys. *Journal of research of the national bureau of standards*, *48*(3), 209-220.

27. Hidnert, P., & Souder, W. H. (1950). *Thermal expansion of solids*(Vol. 486). US Government Printing Office.

28. Hidnert, P. & Sweeney, W. T. (1928). Thermal expansion of magnesium and some of its alloys. *Bureau of Standards Journal of Research*, *1*(5), 771. https://doi.org/10.6028/jres.001.029

29. Hulen, J. B., & Wright, P. M. (2001). *Geothermal energy: clean sustainable energy for the benefit of humanity and the environment*. Energy & Geoscience Institute, University of Utah

30. Industrial Metal Supply Corporation. *Differences between carbon steel & stainless steel*. (2022, May 24). https://www.industrialmetalsupply.com/blog/carbon-steel-vs-stainless-steel#:~:text=The%20thermal%20expansion%20coefficient%20for,generally%20less%20than%20stainless%20steel.

31. ISO 11359-1 Standard. Plastics — Thermomechanical analysis (TMA) -Part 1: General principles, ISO

32. ISO 11359-2 Standard. Plastics — Thermomechanical analysis (TMA) -Part 2: Determination of coefficient of linear thermal expansion and glass transition temperature, ISO

33. Iyer, J., Lackey, G., Edvardsen, L., Bean, A., Carroll, S. A., Huerta, N., ... & Cerasi, P. (2020). A Review of International Field Experience with Well Integrity at Carbon Utilization and Storage Sites.

34. James, J. D., Spittle, J. A., Brown, S. G. R., & Evans, R. W. (2001). A review of measurement techniques for the thermal expansion coefficient of metals and alloys at elevated temperatures. *Measurement science and technology*, *12*(3), R1.

35. Jimenez, W. C., Pang, X., Urdaneta, J. A., Sørensen, E., Lende, G., & Nimane, S. (2017, October). Thermo-mechanical properties of annular sealants—A path to optimized wellbore integrity and economics. In *SPE Kuwait Oil and Gas Show and Conference* (p. D031S011R006). SPE.

36. Kagel, A., Bates, D. & Gawell, K. (2005). A guide to geothermal energy and the environment. GEOTHERMAL ENERGY ASSOCIATION. https://doi.org/10.2172/897425.

37. Kahraman, N. (2007). The influence of welding parameters on the joint strength of resistance spot-welded titanium sheets. *Materials & design*, *28*(2), 420-427.

38. Kaldal, G. S., & Þorbjörnsson,O. I. (2016). Thermal expansion of casings in geothermal wells and possiblemitigation of resultant axial strain. In *European geothermal congress*.

39. Kim S, Kim JH, Lee JK and Jarng SS. (1997). *J.Mater.Sci. Lett.* 16 1753–6

40. Kroeger, F. R. & Swenson, C. A. (1977). Absolute linear thermal-expansion measurements on copper and aluminum from 5 to 320 K. *Journal of Applied Physics*, *48*(3), 853-864. https://doi.org/10.1063/1.323746

41. Lavrov, A., et al., (2016). Impact of Voids on Mechanical Stability of Well Cement, in: Energy Procedia. Elsevier Ltd, pp. 401–410. https://doi.org/10.1016/j.egypro.2016.01.041.

42. Leendertz J A. (1970). *J. Phys. E: Sci. Instrum.* 3 214–18

43. Lewis, A. (1994). Measurement of length, surface form and thermal expansion coefficient of length bars up to 1.5 m using multiple-wavelength phase-stepping interferometry. *Measurement Science and Technology*, *5*(6), 694.

44. Liu, Z. K., Shang, S. L. & Wang, Y. (2017). Fundamentals of Thermal Expansion and Thermal Contraction. Materials, 10(4), 410. https://doi.org/10.3390/ma10040410

45. Loiseau, A. (2014). Thermal Expansion of Cement and Well Integrity of Heavy Oil Wells. SPE-171066-MS.

46. Lokberg O J, Malmo J T and Slettemoen G A. (1985). *Appl. Opt.* 24 3167–72

47. Lund, J. W. (2000). World status of geothermal energy use overview 1995-1999. In Proceedings of the World Geothermal Congress 2000, Kyushu-Tohoku, Japan, 28 May–10 June 2000.

48. Luo, H., & Hu, W. (2021, October). Evidence of overpressure at the base of huge landslide. In *IOP Conference Series: Earth and Environmental Science* (Vol. 861, No. 6, p. 062045). IOP Publishing.

49. Martelli, V., Bianchini, G., Natale, E., Scarpellini, D., & Ventura, G. (2013). A novel interferometric dilatometer in the 4–300 K temperature range: thermal expansion coefficient of SRM-731 borosilicate glass and stainless steel-304. *Measurement Science and Technology*, *24*(10), 105203

50. McKinstry H A, Huang C Y and McKinstry S T. (1998). *Cindas Data Series on Material Properties, Volume I-4—Thermal Expansion of Solids* ed R E Taylor (Materials Park, OH: ASM International) ch 7, pp 193–206

51. Meyers, S. L. (1951). Thermal expansion characteristics of hardened cement paste and of concrete. In *Highway Research Board Proceedings* (Vol. 30).

52. Miyake T, Oodake I. and Petek H. (1999). *Surf.Sci.*427–428 39–43

53. Moore, J., McLennan, J., Pankow, K., Simmons, S., Podgorney, R., Wannamaker, P., ... & Xing, P. (2020, February). The Utah Frontier Observatory for Research in Geothermal Energy (FORGE): A Laboratory for characterizing, creating and sustaining enhanced geothermal systems. In Proceedings of the 45th Workshop on Geothermal Reservoir Engineering. Stanford University.

54. Moya, D., Aldás, C., & Kaparaju, P. (2018). Geothermal energy: Power plant technology and direct heat applications. *Renewable and Sustainable Energy Reviews*, *94*, 889-901.

55. Myer, L., & Rachiele, R. (1981). LABORATORY INVESTIGATIONS OF THERMOMECHANICAL PROPERTIES OF STRIPA GRANITE. PART I: APPARATUS. PART II: APPLICAION AND RESULTS.

56. Nelson, E.B. and Guillot, D. 2006. *Well Cementing,* second edition, Sugar Land: Schlumberger.

57. NORSOK. (2013). Norsok Standard D-010 Well Integrity in Drilling and Well Operations; *NORSOK*.

58. Nugroho, W. A., Hermawan, S., Lazuardi, B. H., & Mirza, R. (2017, October). Drilling problems mitigation in geothermal environment, case studies of stuck pipe and lost circulation. In *SPE Asia Pacific Oil and Gas Conference and Exhibition* (p. D031S004R004). SPE.

59. Okaji, M. and Imai, H. (1984). A practical measurement system for the accurate determination of linear thermal expansion coefficients. *Journal of Physics E: Scientific Instruments*, *17*(8), 669-673. https://doi.org/10.1088/0022-3735/17/8/011

60. Okaji M and Imai H. (1983). High-resolution multifold path interferometers for dilatometric measurements *J. Phjs. E: Sci. Instrum.* 16 1208-13

61. Okaji M and Yamada N. (1999). *ThermalConductivity 24—Thermal Expansion 12* ed P S Gaal and D A Apostolescu (Lancaster, PA: Technomic) pp 336–43

62. Okaji M,Yamada N and Moriyama H. (2000). *Metrologia* 37. 165–71

63. Phi, T., Elgaddafi, R., Al Ramadan, M., Ahmed, R., & Teodoriu, C. (2019, November). Well integrity issues: Extreme high-pressure high-temperature wells and geothermal wells a review. In *SPE Thermal Integrity and Design Symposium* (p. D031S007R001). SPE.

64. Pierce, K. G., Livesay, B. J., & Finger, J. T. (1996). *Advanced drilling systems study* (No. SAND95-0331). Sandia National Laboratories (SNL), Albuquerque, NM, and Livermore, CA (United States).

65. *Plastics | ASTME228 | Prospector*. (n.d.). https://plastics.ulprospector.com/properties/ASTME228

66. *Plastics | ASTME831 | Prospector*. (n.d.). https://plastics.ulprospector.com/properties/ASTME831

67. Popov, Y., Parshin, A., Abashkin, V., & Miklashevskiy, D. (2012, June). Instrument for measurements of linear thermal expansion coefficient of rocks. In *ARMA US Rock Mechanics/Geomechanics Symposium* (pp. ARMA-2012). ARMA.

68. Reinsch, T., Dobson, P., Asanuma, H., Huenges, E., Poletto, F., & Sanjuan, B. (2017). Utilizing supercritical geothermal systems: a review of past ventures and ongoing research activities. *Geothermal Energy*, *5*(1), 1-25.

69. Rincon, F., Abid, K., Arbad, N., & Teodoriu, C. (2022). A comprehensive analysis of class H cement Unconfined Compressive Strength using cubical and cylindrical samples. *Journal of Petroleum Science and Engineering*, *215*, 110692.

70. Rincon, F., Abid, K., & Teodoriu, C. (2023). Effect of gilsonite on mechanical and thermal properties of class H cement. *Gas Science and Engineering*, *110*, 204896.

71. Ruffino G. (1984). Compendium of Thermophysical Property Measurement Methods vol 1, ed K D Maglic, A Cezairliyan and V E Peletsky (New York: Plenum) ch 18, pp 689–706.

72. Shapely. (2011). Renewable Energy Overview. Available online: http://butane.chem.uiuc.edu/pshapley/Environmental/L8 /index.html.

73. Shortall, R., Davidsdottir, B., & Axelsson, G. (2015). Geothermal energy for sustainable development: A review of sustainability impacts and assessment frameworks. *Renewable and sustainable energy reviews*, *44*, 391-406.

74. Shrivastava, A., Lambade, V., & Chaudhuri, P. (2020). *Measurement of thermal expansion for stainless steel 304, copper, aluminium and brass by push rod dilatometry*. Technical report, Institute for Plasma Research, Bhat, Near Indira Bridge, Gandhinagar, 2020. IPR/TR-603.

75. Somerton, W. H., Janah, A. H., & Ashqar, P. I. (1981, June). Thermal expansion of fluid saturated rocks under stress. In *SPWLA Annual Logging Symposium* (pp. SPWLA-1981). SPWLA.

76. Teodoriu, Catalin, Bello, Opeyemi, Vasquez, R. R., Melander, Ryan M., and Yosafat Esquitin. "Cementless Well Construction Opens the Full Control on Well Integrity for the Life of the Well." (2021). Paper presented at the SPE Annual Technical Conference and Exhibition, Dubai, UAE. doi: https://doi-org.ezproxy.lib.ou.edu/10.2118/206052-MS.

77. The Engineering ToolBox, (2023). Thermal Expansion - Linear Expansion Coefficients. [online] Available at: http s://www.engineeringtoolbox.com/linear-exp ansion-coeff icients-d_95.html.

78. The Nickel Institute. (2024). https://www.nickelinstitute.org/media/1842/types304and304lstainlesssteelsforlowtemperatureser vice_328_.pdf

79. Tomilina, E. M., Chougnet-Sirapian, A., & Aboutourkia, W. (2012, June). New thermally responsive cement for heavy oil wells. In *SPE Canada Heavy Oil Conference* (pp. SPE-157892). SPE.

80. Torbergsen, H.E., Haga, H.B., Aadnøy, B.S., Sæby, J., Johnsen, S., Rausand, M., Lundeteigen, M.A. (2012). An Introduction to Well Integrity. *Prepared Joint Project Between Members of the Norwegian Oil and Gas Association's Well Integrity Forum (WIF) and Professors at NTNU and Uis*.

81. Touloukian Y S, Kirby R K, Taylor R E, and Desai P D. (1975). Thermophysical Properties of Matter, Volume 12—Thermal Expansion, Metallic Elements and Alloys (New York: IFI–Plenum)

82. Ugwu, I. O. (2010). *Cement fatigue and HPHT well integrity with application to life of well prediction* (Doctoral dissertation, Texas A & M University).

83. United Nations. (n.d.). *Population | United Nations*. https://www.un.org/en/global-issues/population#:~:text=Our%20growing%20population&text=The%20world's%20population%20is%20expected,billion%20in%20the%20mid%2D2080s.

84. Velazco, A. T., Abid, K., & Teodoriu, C. (2023). Themral Expansion Investigation of Oilwell Cements Using Novel Appratus. In *48th Workshop on Geothermal Reservoir Engineering. Stanford: Stanford University*.

85. Velazco, A. T., Abid, K., Tellez, M. L. R., & Teodoriu, C. (2024). Measuring Cement Thermal Expansion Coefficient and Its Impact Towards Geothermal Well Construction.

86. Walters, J.; Thorhallsson, S.; Wood, E. *Zonal Isolation for Geothermal Wells*; International Partnership for Geothermal Technology: Keflavik, Iceland, 2012.

87. WEC. (2016). *World Energy Resources 2016*; World Energy Council: London, UK. Williams, C.F.; Reed, M.J.; Mariner, R.H. (2008). *A Review of Methods Applied by the U.S.*; U.S. Geological Survey: Reston, VA, USA.

88. Wolterbeek, T. K. T., & Hangx, S. J. T. (2023). The thermal properties of set Portland cements–a literature review in the context of CO2 injection well integrity. *International Journal of Greenhouse Gas Control*, *126*, 103909.

89. Wpengine. (2022, June 24). *Why fiberglass fabric?* JPS Composite Materials. https://jpscm.com/why-fiberglass/#:~:text=The%20average%20linear%20thermal%20expansion,cm%2Fcm%2F%C2%B0C.

90. Xie, J., & Liu, Y. (2008, May). Analysis of Casing Deformations in Thermal Wells. In *Abaqus Users' Conference, RI*.

91. Xie, J., Yan, JB. (2018). Tests and Analysis on Thermal Expansion Behaviour of Steel Strand used in Prestressed Concrete Structure under Low Temperatures. Int J Concr Struct Mater 12, 5. https://doi.org/10.1186/s40069-018-0236-9.

92. Yang, S; Kim, N; Kim, J, Park; J, Kim. (2003). Experimental Measurement of Concrete Thermal Expansion), Journal of the Eastern Asia Society for Transportation Studies Vol. 5. (pp. 1035 - 1048).

93. Yogaswara, Y. & Latief, F. D. E. (2018). The Development of Experimental Sets for Measuring Linear Thermal Expansion Coefficient of Metal Using Digital Video-Based Single Slit Diffraction Method. *Jurnal Penelitian & Pengembangan Pendidikan Fisika*, *4*(2), 141-152. https://doi.org/10.21009/1.04211

94. Zeng X and Elsayed-Ali HE. (1999). *Surf.Sci.*422L977–82

95. Zhang, M., & Bachu, S. (2011). Review of integrity of existing wells in relation to CO2 geological storage: What do we know? *International Journal of Greenhouse Gas Control*, *5*(4), 826-840.

96. Zoet, A., Bowyer, J., Bratkovich, D. S., Frank, M. A. T. T., & Fernholz, K. A. T. H. R. Y. N. (2011). Geothermal 101: The basics and applications of geothermal energy. *Dovetail Partners Inc.: Minneapolis, MN, USA*.